SEDIMENTOLOGY AND RESERVOIR POTENTIAL OF THE LOWER AMARANTH MEMBER SOUTHWESTERN MANITOBA

A Thesis

Presented to the University of Manitoba

in Partial Fulfillment of the

Requirements for the Degree of

Master of Science

in the

Department of Geological Sciences

Winnipeg, Manitoba 1987

ISBN 0-315-51675-5

SEDIMENTOLOGY AND RESERVOIR POTENTIAL OF THE LOWER AMARANTH MEMBER SOUTHWESTERN MANITOBA

BY

BEVERLY J. HANSEN

A thesis submitted to the Faculty of Graduate Studies of the University of Manitoba in partial fulfillment of the requirements of the degree of

MASTER OF SCIENCE

DEDICATION

This study is dedicated to the handful of early Manitoba geologists and stratigraphers who first identified and described the subsurface of the northeastern Williston Basin ... Lillian Kerr, Hugh McCabe, Andy Baillie and Don Stott.

ABSTRACT

The Jurassic Lower Amaranth Member is the lowermost unit of the Amaranth Formation, southwestern Manitoba. The Lower Amaranth Member is composed of greenish-gray, very fine-grained subarkose and interbedded reddish-brown siltstone. Commercial hydrocarbon production was first obtained from this interval in 1980 with the discovery of the Waskada Field. In this study, the stratigraphy, sedimentology, and diagenesis were examined to determine the depositional environment, reservoir potential, and an exploration model. The study area extends from Township 1-3, Range 25-29 WPM.

The basal 20-25 metres of the Lower Amaranth Member is composed of several repeated fining-upward sequences comprised of a basal (1-4 metre thick) ripple-laminated, glauconitic, very fine-grained subarkose grading upward to lenticular bedded mudstone, siltstone, and subarkose overlain by siltstone with nodular anhydrite. The glauconitic, very fine-grained subarkose is distributed as a series of interfingering units, where 2-4 subarkose intervals are present at most well locations. A second sequence dominated by coarse-grained sublitharenite fining-upward to parallel-bedded and cross-bedded, medium-grained subarkose is developed locally.

The Lower Amaranth Member was deposited on a low-energy tidal flat along the northeastern flank of the Williston Basin. Sedimentation was associated with periodic inundation and exposure of the tidal flat where the very fine-grained subarkose represent tidal creek deposits and coarse-grained sequences represent tidal channels.

The very fine-grained subarkose is the reservoir facies. Pre-existing porosity in the coarser-grained facies has been occluded by anhydrite cement. The optimum porosity (20-25%) and permeability are found in the central Waskada Field associated with a higher energy regime near the Waskada dome. The primary intergranular porosity is modified by pore-filling dolomite and expandable, mixed-layer clay minerals. Porosity and permeability decrease (2-10%, <1 millidarcy) outward from the central Waskada Field associated with an increase in silt and clay matrix (up to 10%).

Oil has migrated into structurally high, porous carbonates of the underlying Mississippian sequence. In the absence of an effective seal, oil has migrated into the overlying Lower Amaranth where it is trapped stratigraphically by the variation in porosity and by the overlying Amaranth siltstone.

TABLE OF CONTENTS

ILLUSTRATIONS

CHAPTER 1: INTRODUCTION

1.1 Introductory Statement

The Lower Amaranth Member is the lowermost unit of the Amaranth Formation, a sequence of interbedded, red-brown mudstones; siltstones; and greenish-gray, very fine-grained subarkose found in the subsurface of Manitoba. No evidence of the age of the Lower Amaranth Member is known. Consequently, it has been dated relative to the adjacent strata. In this study, the Lower Amaranth Member is recognized as middle Jurassic in age (Section 2.3).

Studies of the Lower Amaranth have historically been hindered by the lack of outcrop and subsurface data. Although several regional stratigraphic studies of Western Canada have considered the Lower Amaranth Member, only three studies have discussed the detailed sedimentology of the sequence. These include the early work by Stott (1954) and McCabe (1956) and the more recent study of Barchyn (1982).

Renewed interest in the Lower Amaranth Member has been generated by the recent discovery of oil (1980) at Waskada, Manitoba. This discovery has initiated an exploration and development effort which is currently in progress. The Lower Amaranth Member is the main oil producing interval in the Waskada and Coulter Fields with minor Amaranth production in the Pierson and South Pierson Fields, southwestern Manitoba

(Section 1.3). Approximately 365 wells are presently producing oil from the Lower Amaranth Member with an approximate cumulative production of 6 MMBO (951 M m^3) and remaining established reserves of 13 MBO (2.1 M m^3) (Manitoba Energy and Mines, December 31, 1986).

The increasing availability of well data since the most recent study of Barchyn (1982) has provided an excellent and timely opportunity to examine the Lower Amaranth in greater detail. A study of the sedimentology and diagenesis of this sequence can contribute to a better understanding of this reservoir and the development of a viable model for further exploration. An understanding of the sedimentology of the Lower Amaranth Member is also important in deciphering the stratigraphic and facies relationships in the northeastern Williston Basin.

1.2 Objectives of Study

The sedimentary rocks of the Lower Amaranth Member were studied for the following purposes:

1. to interpret the depositional environment;

2. to examine reservoir quality, reservoir distribution, and the controls on porosity; and

3. to develop a viable model for further exploration.

1.3 Study Area

The study area is located in the extreme southwestern corner of Manitoba and extends from Township 1 to 3, Range 29 to 25 W1 (Figure 1). It is bound on the west by the Saskatchewan-Manitoba border and on the south by the North Dakota-Manitoba border. The study area includes the Pierson, South Pierson, Coulter, and Waskada Fields (Figure 2 - map pocket). Approximately 750 wells have penetrated the Amaranth Formation in the study area with the greatest density of wells in the producing oil fields.

1.4 Methods of Study

1.4.1 Core Examination

Most of the information for this study was obtained from the detailed examination of cores, petrophysical logs, and thin-section analyses. Approximately 1010 metres of core were examined during April and May, 1985 and selected sections were re-examined for greater detail (Appendix A).

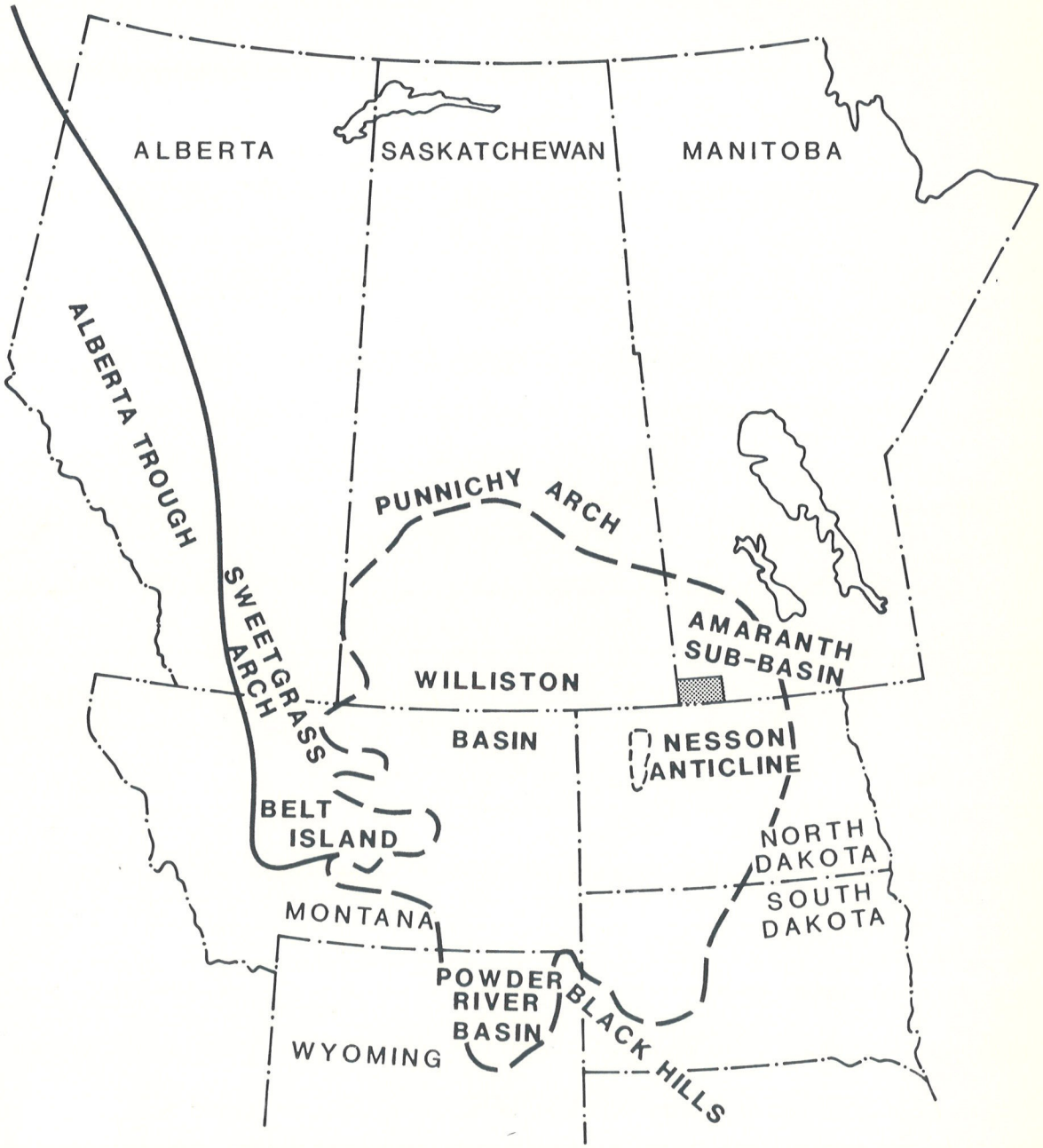

FIGURE 1 : LOCATION OF STUDY AREA AND MAJOR TECTONIC ELEMENTS
(MODIFIED FROM: CARLSON , 1968 ; CHRISTOPHER , 1984)

1.4.2 Petrography

Approximately 93 thin sections were prepared from representative samples of the entire Lower Amaranth Member. Particular attention was given to the very fine-grained subarkose which constitutes the reservoir facies. Selected thin sections were stained with a solution of Alizarin Red S and Potassium Ferricyanide to differentiate carbonate cements and with Sodium Cobaltinitrate to detect potassium feldspar. Grain size and porosity values were estimated from thin-section with the caliper on the polarizing microscope. Porosity values were compared with core analysis.

1.4.3 X-Ray Diffraction Analysis and Scanning Electron Microscopy

Fourteen samples were examined by scanning electron microscopy to observe the morphology and mineralogy of the fine-grained matrix, cements, and various clay minerals. Fourteen bulk samples and eleven clay mineral separations were analyzed by x-ray diffraction (Appendix B). These samples were chosen to include an overview of the study area but were confined primarily to the reservoir facies.

1.4.4 Petrophysical Log Evaluation

The Lower Amaranth Member was identified on petrophysical logs following Stott (1954). Stratigraphic cross-sections were hung on the top of the Lower Amaranth Member which Barchyn (1982) defined as a time stratigraphic marker.

Petrophysical logs from 265 wells were incorporated into cross-sections and isopachous and structural contour maps. A normalized gamma-ray index (NGRI) (log cut-off) was determined in order to correlate and map the distribution of subarkose (potential reservoir) units. An NGRI was calculated following the method of Connolly and Reed (1983):

$$NGRI = \frac{GR\ Log - GR\ Min}{GR\ Max - GR\ Min} = \%$$

where:

GR Log is the maximum API value on the gamma-ray log which corresponds to a subrakose rock observed in the core. GR Log represents the most argillaceous subarkose rock in the Lower Amaranth sequence.

GR Min is the lowest API value on the gamma ray log. GR Min represents the cleanest subrakose rock in the Lower Amaranth sequence.

GR Max is the highest API value on the gamma-ray log. GR Max corresponds to the base shale line.

All cores examined were calibrated to the gamma-ray log and an average NGRI of (67%) was determined for the subarkose units of the Lower Amaranth Member. In the absence of core and/or cuttings, this method was useful in identifying subarkose units on petrophysical logs and mapping their distribution in the subsurface.

1.4.5 Hydrocarbon Production Analysis

Fifteen wells were selected in the Waskada Field based on continual oil production over a one year period. Monthly oil and water production was plotted on a graph and an average production decline rate determined.

ACKNOWLEDGEMENTS

The writer would like to take this opportunity to thank the many people and industry groups who gave generously of their time and resources to make this thesis possible. Dr. Bill Last of the Department of Earth Sciences, University of Manitoba acted as faculty advisor. The advice and support of Dr. Jim Teller, University of Manitoba and Dr. Graham Davies, Calgary, is also gratefully acknowledged.

Financial assistance and laboratory facilities were provided with the aid of Mr. David Wilson and Dr. Volkmar Schmidt by Petro-Canada Exploration. I would particularly like to thank Mr. Chuck Savoie, Petro-Canada Exploration, for his very valuable assistance with thin section preparation and photography. Dr. Kuis Pahlavan, Petro-Canada Exploration, analyzed and interpreted the XRD and Mr. Brian Miller assisted with the SEM.

Texaco Canada provided a two year Geological Research Grant. Canterra Energy, with the assistance of Mr. Craig Lamb and Dr. Grant Bartlett, provided technical support. I would like to thank the drafting department for their advice and patience in drafting the figures and maps. Additional funding was provided by Mr. Jack Hall, Omega Hydrocarbons, in the form of a research grant.

The Petroleum Branch, Manitoba Energy and Mines, provided access to core, well logs, photocopying facilities, and base maps. I would especially like to acknowledge the staff of the Petrological Laboratory for their patience and assistance in moving core.

The writer would like to thank the many geologists who offered advice and discussion during the course of this study. These include Mr. Dan Barchyn, Tundra Oil and Gas, Winnipeg; Dr. Hugh McCabe, Manitoba Energy and Mines, Winnipeg; Mr. Voker Braun, Shell Canada Ltd., Calgary; Dr. Dennis Meloche, Petro-Canada Exploration; and Mr. Paul Johnson, Chevron Canada Resources. I would particularly like to thank Mr. Steve Halabura, formerly of Manitoba Energy and Mines, for sharing his ideas and great enthusiasm for Williston Basin geology! Lastly, I would like to thank my family and friends for their encouragement and support.

CHAPTER 2: REGIONAL GEOLOGY

2.1 Geological Setting

2.1.1 Geology of Southwestern Manitoba

Southwestern Manitoba is located on the extreme northeastern rim of the Williston Basin (Figure 1). Basinward thickening of sediment and continual basin subsidence has resulted in the formation of a sedimentary wedge which dips to the southwest (McCabe, 1959). Three major lithological units compose the sedimentary sequence; Paleozoic rocks which consist of carbonates and evaporites, an overlying Mesozoic unit composed of terrigenous clastics and interbedded carbonates and evaporites, and an Cenozoic sequence composed of terrigenous clastics with minor carbonates and evaporites (McCabe, 1959).

The Mesozoic and Paleozoic sequences are separated by a marked angular unconformity which represents a period of erosion from late Mississippian to early Jurassic time (Stott, 1954). Erosion resulted in the removal of progressively older units to the northeast of the province. Paleozoic strata are truncated by the Amaranth Formation which onlaps rocks of Mississippian to Ordovician age (Figure 3) (McCabe, 1959).

Southwestern Manitoba has been characterized by minor basinward tilting (southwest), a slow continual rate of basin subsidence, and structural

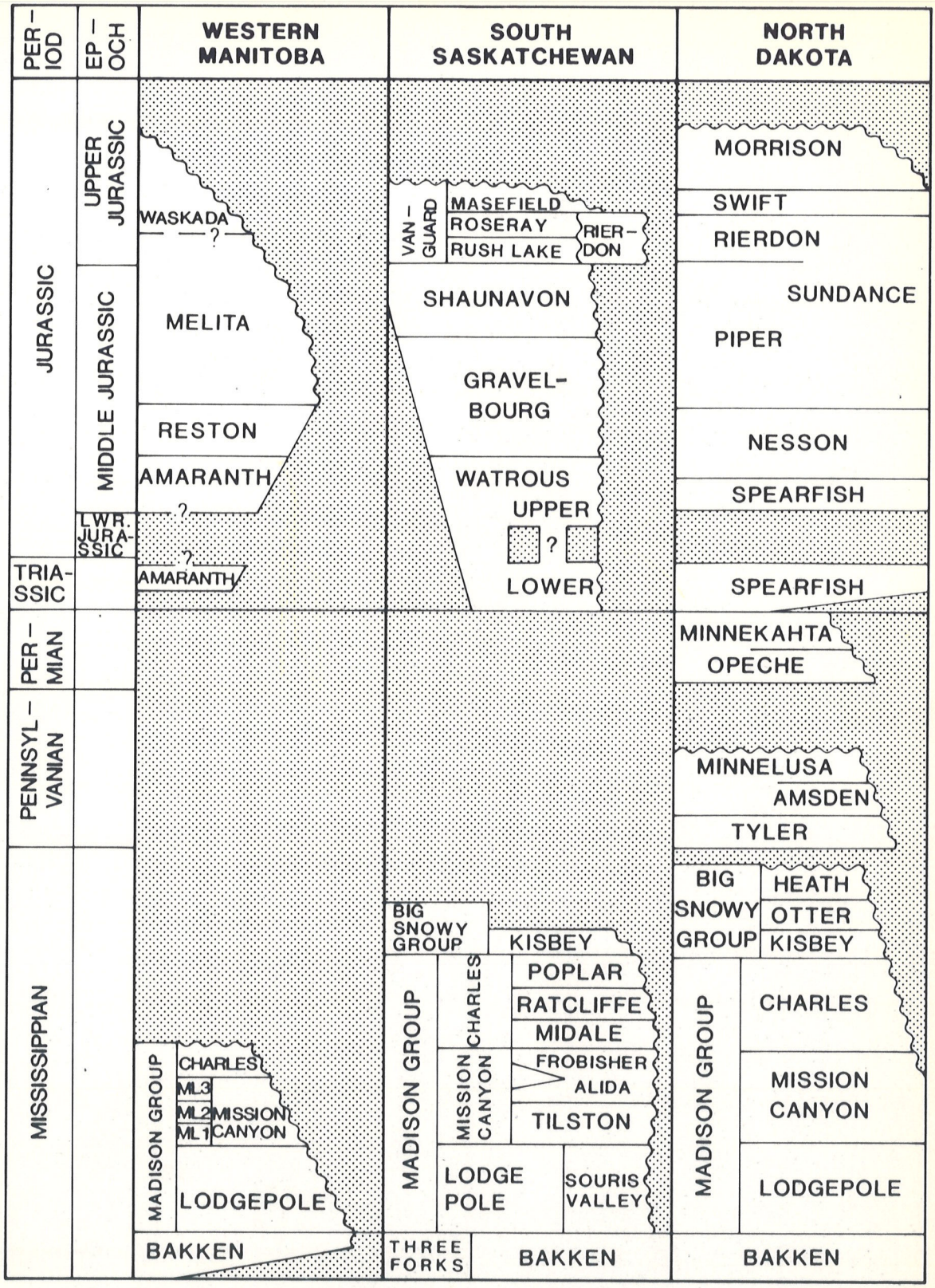

FIGURE 3 : STRATIGRAPHIC NOMENCLATURE CHART
(MODIFIED AFTER: DEPARTMENT OF MINERAL RESOURCES, REGINA, SASKATCHEWAN)

disturbance associated with multi-stage salt solution and removal of the Devonian Prairie (evaporite) Formation and subsequent collapse of the overlying strata. Major stages of salt solution in the Williston Basin occurred during Devonian, Mississippian to Jurassic, and Cretaceous time (De Mille et al, 1964). Salt solution-type structures were noted by McCabe (1959) and Rodgers (1986) in the Waskada area and by Halabura (in press) in the Pierson Field. In these areas, salt solution and collapse have resulted in the development of anticlinal features which form significant structural-stratigraphic hydrocarbon traps (Chapter 6).

2.1.2 Williston Basin Morphology

During the Jurassic, the Williston Basin was separated from the Alberta Trough by the Sweetgrass Arch and bordered on the north-northeast by the Punnichy Arch in southern Saskatchewan and the Precambrian Shield to the east in Manitoba (Figure 1) (Christopher, 1984). This vast epeiric sea (Williston Basin) assumed several configurations from late Paleozoic to early Cretaceous time. During Amaranth time, the basin became two distinct elements; a northeasterly-trending trough (sub-basin) extending from northern Wyoming and South Dakota into southwest Manitoba forming the Amaranth embayment or sub-basin, and a second trough extending northwest from the depositional centre of the Williston Basin in North Dakota - northern Montana into southern Saskatchewan (Schmidt, 1953; Stott, 1954; Christopher, 1984). Several escarpments,

Paleozoic erosional remnants, and a prominent ridge along the Saskatchewan-Manitoba border further restricted normal marine circulation (Stott, 1954; Christopher).

A structural contour map of the post-Paleozoic erosional surface was constructed to illustrate the topography of the basin prior to Lower Amaranth deposition (Figure 4 - map pocket). The unconformity surface dips gently basinwward to the southwest with no evidence of structural closure. This structural contour map shows a valley and ridge or "cuesta" topography which is likely the result of erosion by a southwesterly trending paleodrainage system (Martin, 1966).

2.1.3 Amaranth Sedimentation

The Jurassic period was characterized by at least four transgressive-regressive cycles. Each successive transgressive pulse extended progressively further eastward across Western Canada. Amaranth sediments were deposited during the extensive middle Jurassic transgressive-regressive cycle where seas flooded the Williston Basin as far east as Manitoba (Stott, 1954).

The Lower Amaranth Member was deposited in a mud flat environment as part of a vast episode of red bed sedimentation (Barchyn, 1982) Clastic sediments of the basal Amaranth were derived from the Precambrian Shield to the north and east and from Paleozoic red-bed se-

quences exposed at the basin margin (Stott, 1954; McCabe, 1956; Poulton, 1982). Culmination of clastic sedimentation and increasing basin salinity resulted in precipitation of the shallow marine evaporites of the Upper Amaranth Member (Stott, 1954).

Regression of the middle Jurassic sea resulted in exposure and erosion of the Amaranth along the basin margin in southwestern Manitoba (Stott, 1954). The overlying Jurassic Reston Formation was deposited during the second marine transgressive-regressive cycle. The Reston is composed of a basal shale, a middle marine carbonate, and an upper oolitic limestone which represents shallowing upward, normal-marine sedimentation (Stott, 1954).

2.2 Stratigraphy

2.2.1 Historical Development of Nomenclature

The term Amaranth Formation was first suggested by Kirk (1929) for the reddish-brown siltstones and dolomitic shales found near the town of Amaranth, Manitoba (Figure 5). Wickenden (1945) later traced this sequence from the type locality into the subsurface and formally defined the Amaranth Formation at the Commonwealth Manitou No. 2 (2-9-8-26 W1) and the Neepawa Salt Company No. 2 (14-15-9-3 W1) wells in southwestern Manitoba. The Amaranth Formation was informally subdivided by Stott

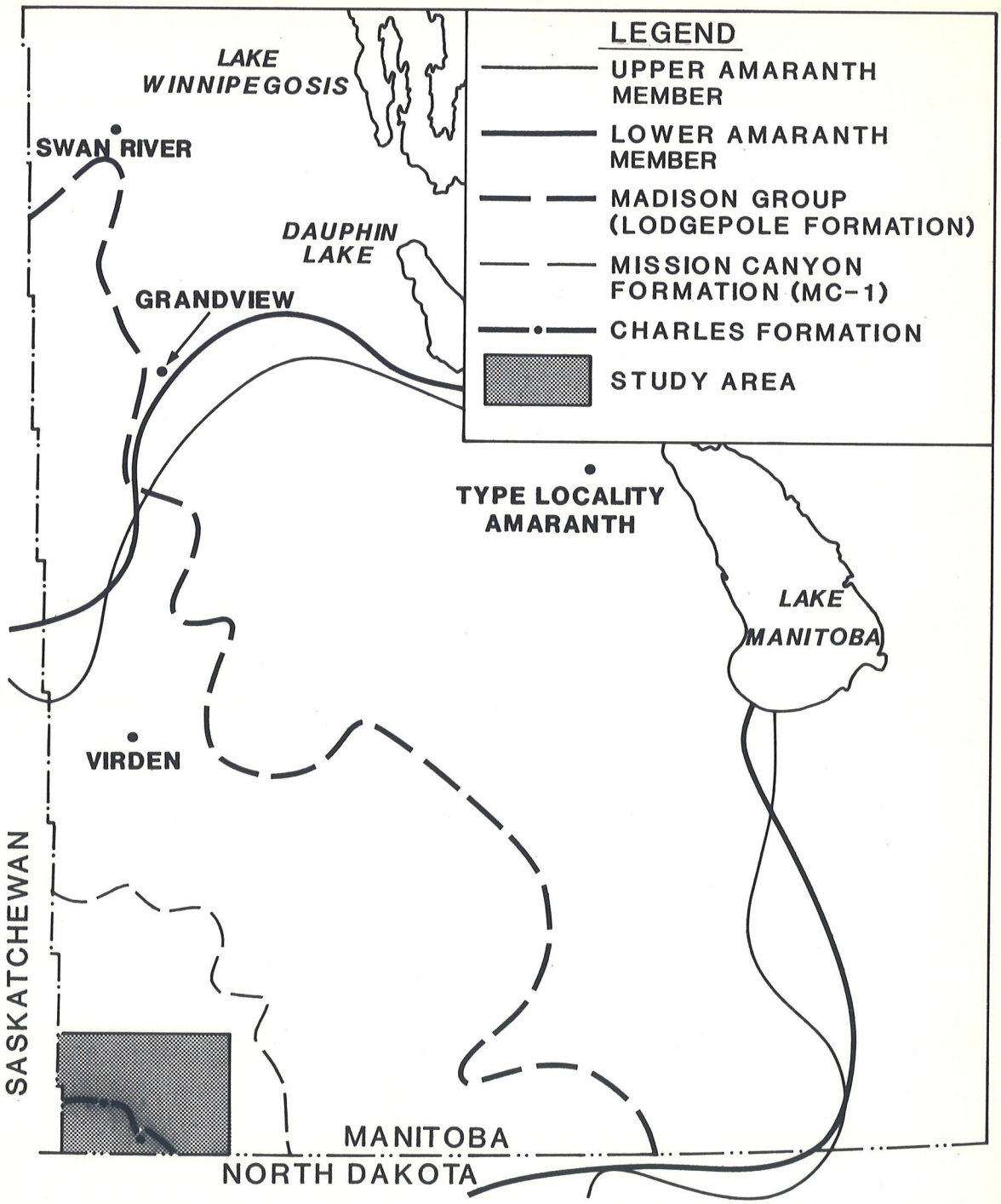

FIGURE 5 : SUBCROP OF AMARANTH AND MISSISSIPPIAN FORMATIONS SOUTHWESTERN MANITOBA
(MODIFIED FROM STOTT, 1954; McCABE, 1967; MANITOBA ENERGY AND MINES,1976)

(1954) into the upper Amaranth unit and the lower Amaranth unit (Figure 6). Stott (1954) based this subdivision on the presence of two distinct lithological units (Figure 6); an upper anhydrite and a lower clastic sequence. McCabe (1956) and Barchyn (1982) later referred to these "units" as the Lower Amaranth and Upper Amaranth Formations.

The stratigraphic subdivisions used in this study follow Stott (1954). However, in compliance with the rules of proper stratigraphic nomenclature the upper and lower Amaranth units should have member status. Although the terms Lower Amaranth Formation and Upper Amaranth Formation are used by industry and are well entrenched in the literature, for the purpose of clarity and regional correlation the informal terminology Lower Amaranth Member and Upper Amaranth Member will be applied in this thesis.

2.2.2 Definition of the Amaranth Formation, Manitoba

In Manitoba, the Amaranth Formation is composed of a basal red-bed sequence comprised of interbedded shale, siltstone, and greenish-gray, fine-grained sandstone; and an upper interbedded anhydrite and carbonate (McCabe, 1956). The Amaranth Formation overlies Paleozoic carbonates and evaporites and underlies the Jurassic Reston Formation (Figure 3) (Stott, 1954).

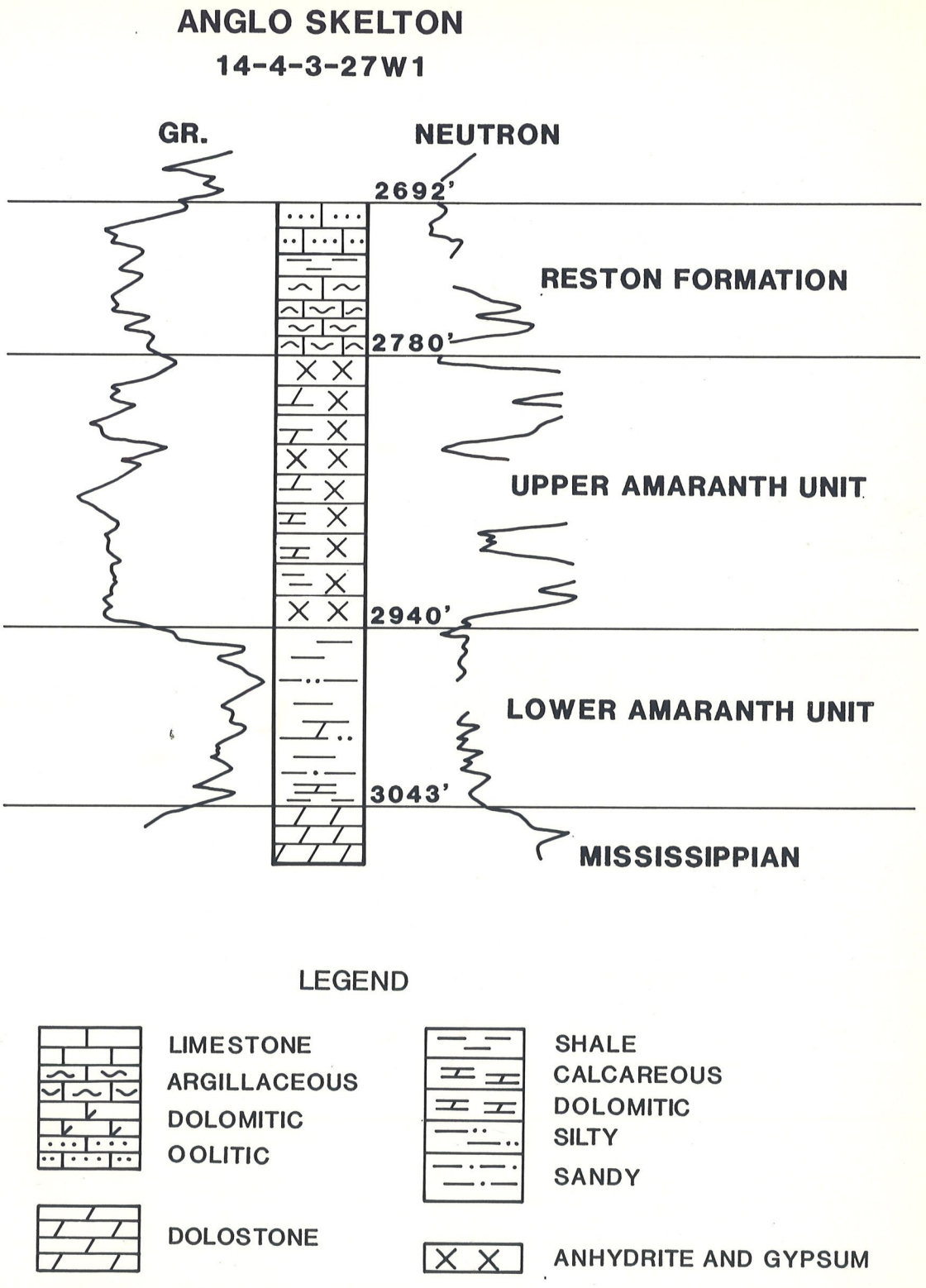

FIGURE 6 : STRATIGRAPHIC SUBDIVISIONS, MANITOBA
(MODIFIED FROM STOTT, 1954, 1955)

The Amaranth Formation is stratigraphically equivalent to the Jurassic Watrous Formation of Saskatchewan (Stott, 1954; Hadley and Milner, 1953) and the Triassic upper Spearfish and Jurassic lower Nesson Formations of North Dakota (Figure 3) (Stott, 1954; Ziegler 1955). Imlay (1947) correlated Spearfish outcrop in the Black Hills of South Dakota and Wyoming to the Amaranth Formation of Manitoba.

The base of the Amaranth Formation is easily identified in core by the unconformable contact between the red-brown siltstones of the Amaranth Formation and the underlying Paleozoic carbonates and evaporites. On petrophysical logs, the boundary is marked by a sharp decrease in the neutron log count, a marked increase in resistivity, a general decrease in porosity (BHCS-CNL-FDC) and a decrease in the API reading on the gamma-ray log (Figure 6).

The top of the Amaranth Formation is distinguished in core by the contact between the anhydrite of the Upper Amaranth Member and a thin shale and/or argillaceous carbonate of the Reston Formation (Stott, 1954, McCabe, 1956). Stott (1954) identified an unconformable contact between the Amaranth and Reston Formations. However, no expression of this unconformity was identified in Saskatchewan (Stott, 1954). On petrophysical logs this contact is defined by an decrease in the API reading on the gamma-ray log and an increase in the neutron count (Stott, 1954) (Figure 6).

2.2.3 The Lower Amaranth Member, Manitoba

The Lower Amaranth Member is composed of an interbedded, reddish-brown, dolomitic siltstone, shale, and fine-grained sandstone (Stott, 1954) with sandstone content increasing to the southwest of the province (Stott, 1954; McCabe, 1956). The boundary between the upper and lower members is gradational (McCabe, 1956). On petrophysical logs, the top of the Lower Amaranth Member is placed at the base of the Upper Amaranth anhydrite (Figure 6). The Lower Amaranth Member appears as a shaly sequence on the gamma-ray log (Stott, 1954).

The thickness of the Lower Amaranth varies from 2-40 metres. It thins markedly in the Wawanesa area and the Daly-Virden district to the north of the province and thickens towards the basin centre to the southwest (Figure 5). The Lower Amaranth Member pinches out near the Grandview-Swan River region (Figure 5) (Stott, 1954; McCabe 1956). The eastern limit of the Lower Amaranth is erosional, as no facies change occurs near the subcrop edge (Stott, 1954) (Figure 5).

2.2.4 The Upper Amaranth Member, Manitoba

In Manitoba, the Upper Amaranth Member average approximately 16 metres in thickness. It is composed of a a massive, white anhydrite with minor interbedded shale, enterolithic anhydrite, and buff-colored dolomite

(Stott, 1954). A basal silty shale is present locally. The Upper Amaranth Member is well defined on petrophysical logs by a low reading on the gamma-ray log and a low neutron count (Stott, 1954). The eastern erosional limit of the Upper Amaranth is illustrated in Figure 5 (Stott, 1954). The Upper Amaranth thins towards the basin centre to the southwest coincident with an increase in dolomite (Stott, 1954).

2.2.5 Lower Amaranth Member - Study Area

In the study area, the Lower Amaranth Member varies in thickness from 25-40 metres with an increase in thickness basinward to the southwest. (Figure 7 - map pocket). Several elongate, subparallel belts of thick Lower Amaranth section are noted on the isopach map and show an overall trend to the southwest-northeast (Figure 7). These thick belts are coincident with paleotopographic lows on the post-Mississippian unconformity surface (Figure 4 - map pocket).

The structural contour map on the top of the Lower Amaranth Member shows a gently sloping surface which dips basinward to the southwest (Figure 8 - map pocket). There is no evidence of structural closure. Structure on the top of the Lower Amaranth Member appears to reflect the post-Paleozoic erosional surface (Figure 4) although, the undulating topography is generally less pronounced. This may indicate that Lower Amaranth sedimentation was insufficient to infill paleotopograph-

ic lows on the unconformity surface, but more likely indicates salt solution and collapse throughout Amaranth and post-Amaranth time.

The Lower Amaranth Member is underlain by the Mississippian Charles anhydrite in the western portion of the study area (Figure 3, Figure 4 - map pocket, Plate 1B), and/or a locally developed detrital zone (Plate 1A). In the eastern portion of the study area, the Lower Amaranth overlies the Mission Canyon Formation (MC-3 and MC-1 Members) (Figure 3, Figure 4 - map pocket, Plate 1C) and/or the locally developed detrital zone.

Barchyn (1982) informally subdivided the Lower Amaranth Member (Twp. 1-3, Rge. 24-25 W1) into an "upper shaly unit" (USU) and a "lower sandy unit (LSU)." Recognition of these units was based on the resistivity characters of the DI-SFL Log (Figure 9). This subdivision was useful in isolating the oil-producing, lower, sandier sequence (Barchyn, pers. comm.). Within the "lower sandy unit" (LSU), Barchyn (1982) identified the "A" and "B" resistivity markers which delineate a laterally extensive sandstone interval (Figure 9).

The "lower sandy unit" is approximately 20 - 25 metres in thickness and is composed of several repeated fining-upward sedimentary sequences (Barchyn, 1982). Each sequence consists of a basal sandstone, which varies in thickness from 1 - 4 metres, and grades upward to a siltstone or interbedded shale and siltstone (Barchyn, 1982). The sandstone of

PLATE 1

Plate 1A

Detrital zone at the Mississippian unconformity.

7-25-2-29W1
999.5 metres

Plate 1B

Anhydrite of the Charles Formation, directly underlying the Amaranth Formation in the western portion of the study area.

12-27-1-28W1

Plate 1C

Lower Amaranth, basal, reddish-brown siltstone and nodular anhydrite (left) overlying (dense-cap) anhydritized and dolomitized porous Mississippian carbonate (right).

15-24-1-28W1
989.4 metres

PLATE 1


A


B


C

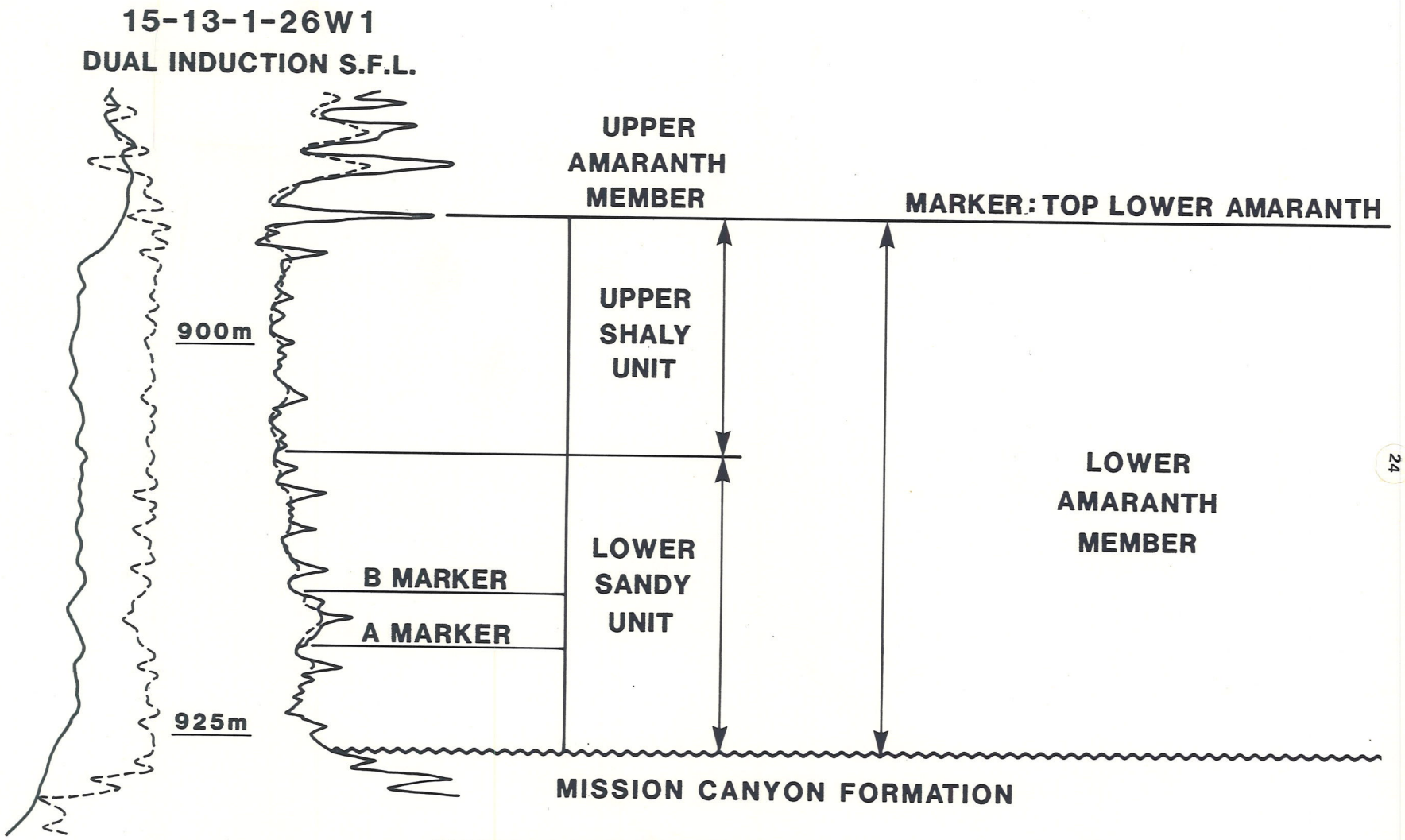

FIGURE 9: STRATIGRAPHIC SUBDIVISIONS
LOWER AMARANTH MEMBER
(AFTER BARCHYN, 1982)

the "lower sandy unit" is the reservoir facies of the Lower Amaranth Member. The "upper shaly unit" averages approximately 15 metres in thickness and is composed of a reddish-brown shale with localized beds of very fine-grained sandstone (Barchyn, 1982; McCabe, 1956).

2.3 Age of the Lower Amaranth Member

2.3.1 Introductory Statement

Wickenden defined the Amaranth Formation of southwestern Manitoba in 1945. However, due to the absence of preserved fossils, no geological age was determined. Since that time, the Lower Amaranth Member has been dated relative to the adjacent strata. The age assignment is controversial and the age discrepancy centres around the following factors:

1. the absence of preserved fossils useful in age dating;

2. the nature of the contact between the Lower and Upper Amaranth Member; and

3. the identification of the Jurassic-Triassic boundary.

In southwestern Manitoba, late Mississippian (dated paleontologically) rocks unconformably underlie the Lower Amaranth Member. Stott (1954)

and Ziegler (1955) have correlated the Upper Amaranth Member to the lower member (Poe Member) of the Nesson Formation, North Dakota (Figure 3). The Poe Member has been dated paleontologically as middle Jurassic. Therefore, the Lower Amaranth Member is middle Jurassic to Triassic in age.

2.3.2 Triassic Age Assignment

The Spearfish Formation of North Dakota unconformably underlies the Nesson Formation (Figure 3). Ziegler (1955) and Dow (1967) subdivided the Spearfish Formation into three members. They correlated the Lower Amaranth Member to the lower Watrous Formation (Member) of Saskatchewan and to the uppermost unit of the Spearfish Formation, the Triassic Saude Member. A middle Jurassic age assignment for the Upper Amaranth and a Triassic age assignment for the Lower Amaranth necessitates an unconformable contact between the Upper and Lower Amaranth Members.

Roscoe and Baar (1972), cited in Christopher (1984), also favored a Triassic age assignment. Based on subsurface correlations which extended from North Dakota northward into Saskatchewan, Roscoe and Barr (1972) suggested that the Permian lower Spearfish Formation was truncated progressively northward by the Triassic upper Spearfish Formation. This unconformity cut across Pennsylvanian and upper Mississippian strata and underlies the lower Watrous Formation of Saskatchewan. Roscoe and Baar noted that the Triassic Saude Member and lower Watrous

Formation (Member) are correlative units. Therefore, the contact between the middle Jurassic upper Watrous and Triassic lower Watrous Formation is unconformable. This unconformity is further supported by physical evidence observed by Carlson (1968) in cuttings and core.

2.3.3 Jurassic Age Assignment

Stott (1954) identified the Jurassic sequence in Manitoba and considered the Amaranth Formation to be the lowermost formation of the Jurassic. Stott (1954) and McCabe (1956) identified a conformable contact in core between the Upper and Lower Amaranth Members. Accepting a middle Jurassic age for the Upper Amaranth Member and a conformable contact between the upper and lower members implies a Jurassic age assignment to the Lower Amaranth and a post-Paleozoic unconformity which represents a hiatus of late Mississippian to Jurassic time. Barchyn (1982) also supported a Jurassic age assignment for the Lower Amaranth and a conformable contact between the lower and upper members. He based this on the presence of a depositional sequence indicative of a transition from a terrestrial to marine to restricted marine environment, a sequence commonly deposited during a single transgressive-regressive event.

Stott (1954, 1955) suspected that the Lower Amaranth Member had been correlated to rocks incorrectly included in the upper part of the Spearfish Formation. He suggested that the Spearfish Formation was

Triassic in age and that the Jurassic/Triassic contact within the sequence had not been correctly recognized. Dow (1967) suggested that the Saude Member is diachronous and the Jurassic/Triassic boundary may be found within the Saude Member near the basin margin.

2.3.4 Discussion

To date, this problem figures prominently in the geological literature. Ongoing research emphasizes palynological and chert/phosphate methods of dating (Poulton, 1984). Based on a concensus of available evidence presented in studies of the Amaranth Formation in Manitoba, a Jurassic age is accepted for the Lower Amaranth Member in this study.

CHAPTER 3: DESCRIPTIVE SEDIMENTOLOGY

3.1 Introductory Statement

Interpretation of the depositional environment of a clastic sedimentary sequence involves consistent observation of the features of the rocks. These features include the:

1. bulk mineralogical composition;
2. grain size and textural maturity;
3. thickness and regularity of bedding;
4. type and sequence of sedimentary structures;
5. nature of bedding contacts; and
6. presence or absence of porosity.

The sedimentary rocks of the Lower Amaranth Member were assigned to six lithofacies based on the variation in grain size and sedimentary structures observed in core. The following lithofacies were identified:

A - massive to laminated mudstone to silty mudstone;

B - massive to laminated siltstone to sandy siltstone;

C - massive to ripple-laminated, silty, very fine-grained, lithic subarkose;

D - interlaminated mudstone, siltstone, and fine-grained subarkose;

E - parallel to cross-laminated, medium-grained, lithic subarkose; and

F - massive, coarse-grained, feldspathic sublitharenite.

In the study area, no core was available for examination in the "upper shaly unit." Consequently, these lithofacies were described from the basal 18-25 metres of the Lower Amaranth, coincident with the "lower sandy unit" of Barchyn (1982).

3.2 Terminology

Folk's (1972) classification scheme for terrigenous rocks was applied in this study. Folk's scheme is particularly applicable to the classification of texturally immature rocks such as those of the Lower Amaranth Member (Figure 10). The Goddard-Rock-Color chart was used to describe color variation. Porosity grades were defined following Choquette and Pray (1970.

3.3 Lithological Sequence - Lower Amaranth Member

The dominate rock-type of the Lower Amaranth Member is an interbedded reddish-brown siltstone and very fine-grained, greenish-gray, silty, subarkose. The basal 20-25 metres (LSU) of the Lower Amaranth Member

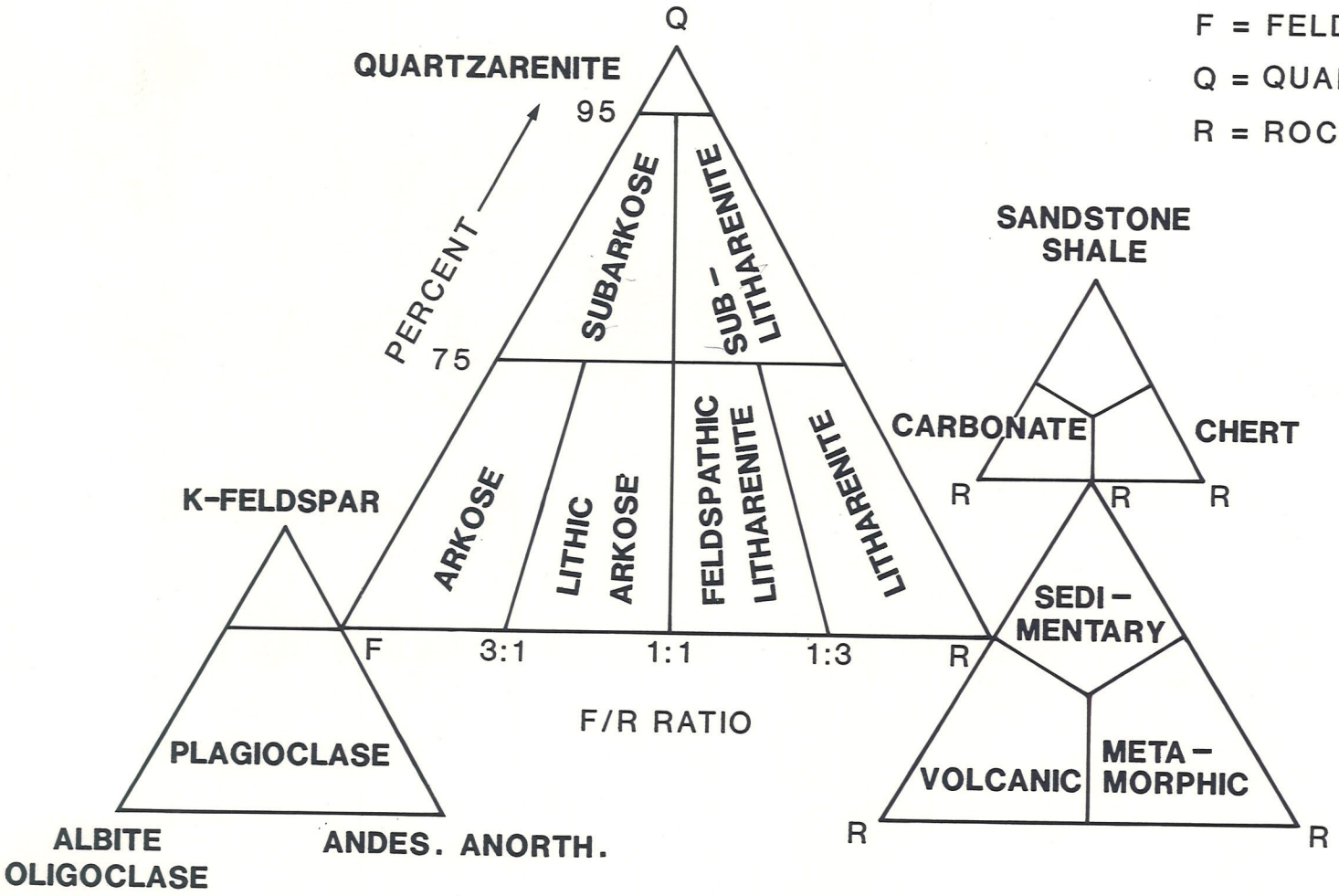

FIGURE10: SANDSTONE CLASSIFICATION SCHEME (FROM FOLK, 1968)

is comprised of several repeated or "stacked" fining-upward sequences which vary considerably in composition. The "upper shaly" unit is composed of siltstone (McCabe, 1956).

The vertical distribution of these "stacked" sequences is best illustrated in the Omega Waskada (8-26-1-26 W1) well (Figure 11). This is a typical core from the Waskada Field which shows five fining-upward sequences in the basal LSU dominated by the very fine-grained, silty, subarkose and Lithofacies Sequences II - IV (Figure 12).

Each fining-upward sequence commonly consists of a basal, silty, fine-grained subarkose unit (Lithofacies C) which varies in thickness from 1-4 metres. This basal subarkose fines upward to reddish-brown siltstone (Lithofacies B) or interlaminated to wavy-bedded mudstone, siltstone, and subarkose (Lithofacies D) (Figure 12 - II, III, IV). Several fining-upward sequences in the Lower Amaranth Member are much coarser-grained, dominated by coarse-grained sublitharenite (Lithofacies F) and parallel-laminated to cross-laminated, medium- grained subarkose (Lithofacies E) (Figure 12 - I). In addition, several of the sequences (Figure 12 - V, VI) are composed of fine-grained, subarkose rocks with coarsening upward sub-cycles and considerable lithological variation over a 1-2 metre interval. The resulting sequences can be very complex but overall fining-upward in character. Each sequence averages 8 metres in thickness and is bounded by a sharp and/or

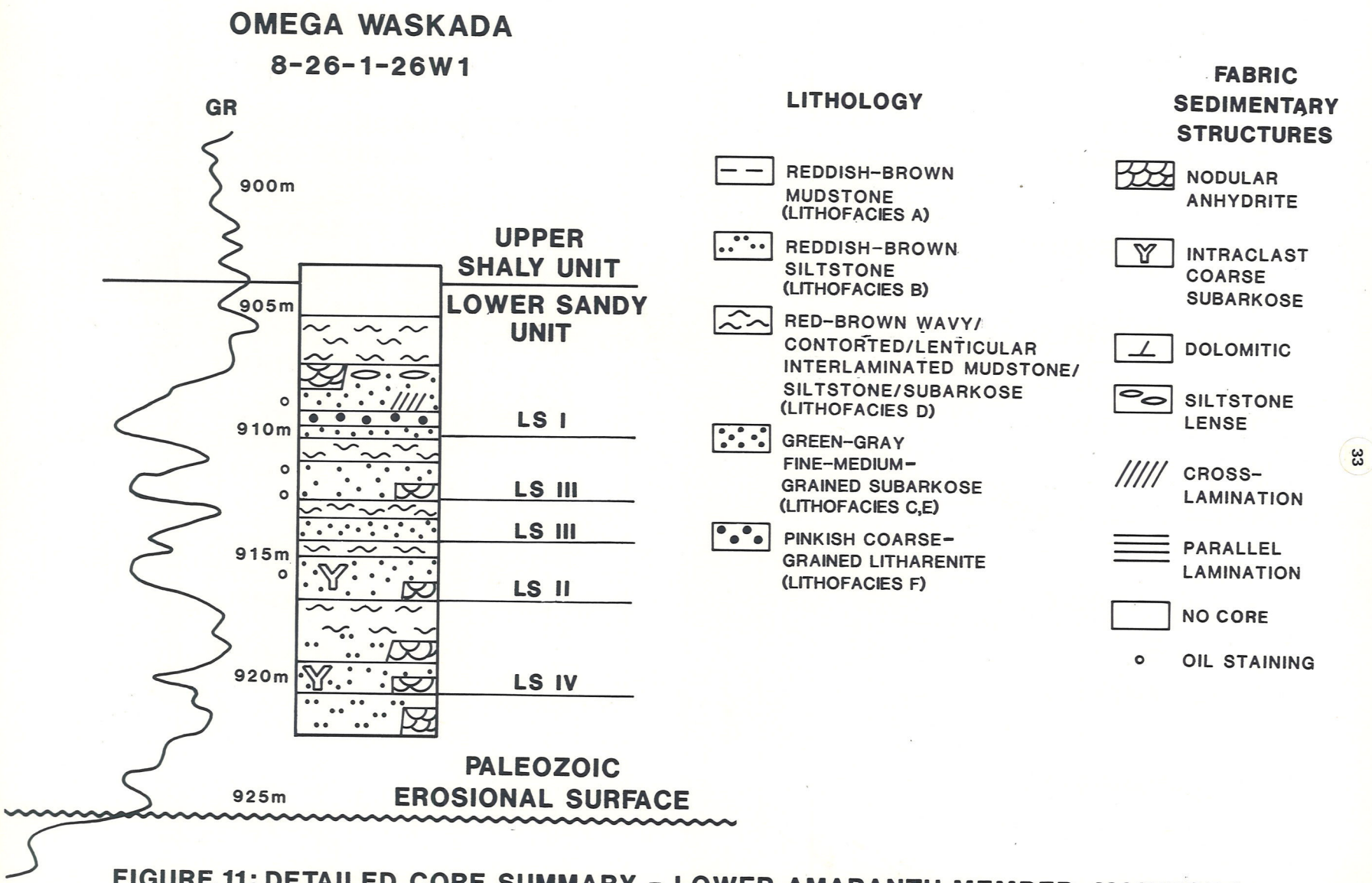

FIGURE 11: DETAILED CORE SUMMARY - LOWER AMARANTH MEMBER, MANITOBA

LITHOLOGY

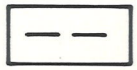
REDDISH-BROWN MUDSTONE
(LITHOFACIES A)

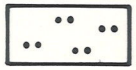
REDDISH-BROWN SILTSTONE
(LITHOFACIES B)


RED - BROWN WAVY/CONTORTED/
LENTICULAR INTERLAMINATED
MUDSTONE/SILTSTONE/SUBARKOSE
(LITHOFACIES D)


GREEN-GRAY FINE-MEDIUM-
GRAINED SUBARKOSE
(LITHOFACIES C,E)


PINKISH COARSE-
GRAINED LITHARENITE
(LITHOFACIES F)


NODULAR ANHYDRITE

FABRIC
SEDIMENTARY
STRUCTURES


INTRACLAST
COARSE SUBARKOSE

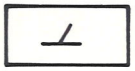
DOLOMITIC


SILTSTONE LENSE


CROSS-LAMINATION


PARALLEL LAMINATION


NO CORE

EROSIONAL CONTACT

GRADATIONAL CONTACT

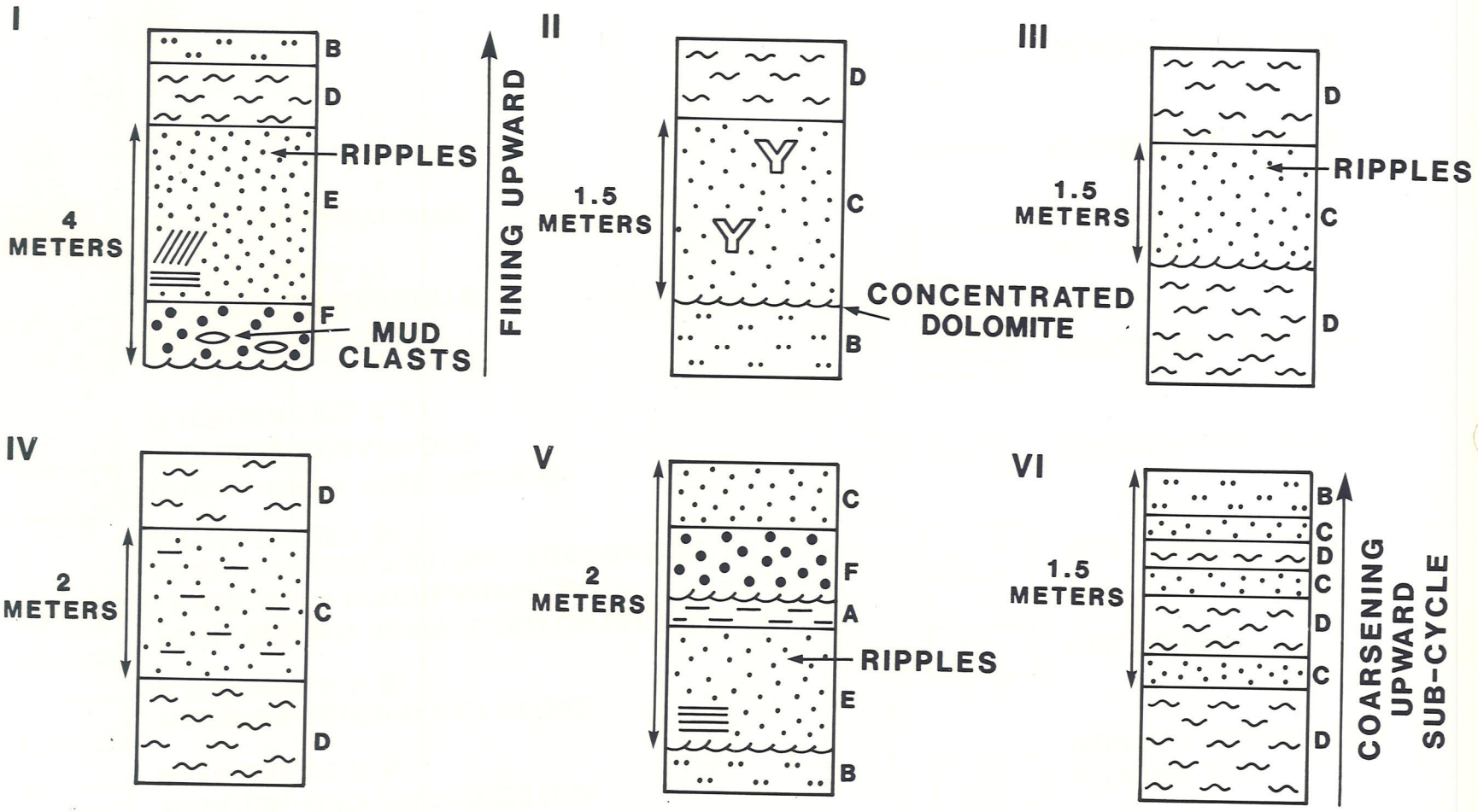

FIGURE 12 : LITHOFACIES SEQUENCE "LOWER SANDY UNIT" - LOWER AMARANTH MEMBER

scoured basal contact. The fining-upward unit appears to constitute one deposition event.

3.4 Description of Lithofacies

3.4.1 Lithofacies A - Massive to Laminated, Mudstone to Silty Mudstone

Lithofacies A is composed of a dark reddish-brown (5 YR 3/4) to grayish-red (5 R 4/2), massive to laminated mudstone with localized patches of greenish-gray mudstone (Plate 2A, 2B). The siltstone component (10%) is present as randomly distributed silt-sized grains and pods or as siltstone lenses and/or swirly laminae. Local occurrences of floating, well-rounded, quartz grains and nodular anhydrite are also present. Lithofacies A is frequently dolomitic (Section 5.2.1).

3.4.2 Lithofacies B - Massive to Laminated Siltstone to Sandy Siltstone

Lithofacies B is composed of a yellowish-brown (10 YR 6/2) to pale red (5 R 6/2) siltstone to sandy siltstone. Lithofacies B is the most common rock type within the Lower Amaranth Member (Plate 2C - 2E). The fine to medium-grained, sandy component (10%) is present as randomly dispersed grains or as sandstone lenses (Plate 2E). This siltstone is dolomitic (Section 5.2.2).

PLATE 2

Plate 2A

Core photograph of mottled, reddish-brown mudstone with irregular laminae of greenish mudstone (arrow). The greenish color is probably the result of iron reduction (diagenetic bleaching) (Lithofacies A).

12-27-2-28W1
960 metres

Plate 2B

Core photograph of mottled, reddish-brown mudstone and anhydrite. This core sample shows a spherical patch of greenish mudstone (Lithofacies A).

3-29-1-27W1
940.3 metres

Plate 2C

Core photograph of interlaminated siltstone and mudstone. Note the irregular, wavy laminae (arrow) and the marked variation in color saturation. Color intensity appears to increase with a decrease in grain size (Lithofacies B).

11-30-1-25W1
912.9 metres

Plate 2D

Core photograph of reddish-brown siltstone showing mudcracks (Lithofacies B).

2-20-1-26W1
927.2 metres

Plate 2E

Core photograph of siltstone with lenses or pods of very fine-grained sandstone. Nodular to mozaic anhydrite is also shown (arrow) (Lithofacies B).

14-5-2-28W1
990 metres

PLATE 2

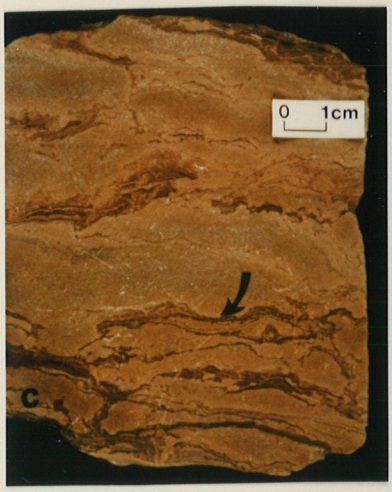

Bedding characteristics range from massive to millimetre-thick, wavy, contorted to discontinuous laminae composed of mudstone or very fine-grained sandstone (Plate 2C, 2E). The lamination of the rocks often appears disturbed (or bioturbated). This type of disrupted lamination is commonly described as a "chaotic" texture. Mud cracks are present associated with local concentrations of biotite along the mud crack surfaces (Plate 2D). Mud cracks were not well preserved and it was difficult to associate them with a specific stratigraphic horizon. In the Coulter Field, abundant tarry residual oil is also present along mud cracks planes (Figure 2). These is no clear evidence of burrow structures or fossil remains.

Nodular anhydrite is common in Lithofacies B and varies from isolated nodules to coalesced masses of anhydrite known as "chicken-wire" structure (Maiklen et al, 1969) (Plate 1C, 2E). Minor large subangular clasts of purple anhydrite are also present in this lithofacies. The purple clasts are similar in composition to the underlying Charles evaporite and commonly found near the post-Paleozoic erosion surface. Very fine-grained, angular to subrounded dolomite is concentrated in lenses associated with well-rounded, floating, quartz grains (Plate 3A). "Floating", quartz grains are common throughout this lithofacies but more so in the Pierson and Coulter Fields (Figure 2 - map pocket).

PLATE 3

Plate 3A

Core photograph of siltstone with minor swirly, laminated mudstone. The arrow shows well rounded "floating", quartz grains which are aeolian in origin. Detrital dolomite (a) is also present (Lithofacies B).

11-19-3-28W1
971 metres

Plate 3B

Core photograph of reddish-brown siltstone with fracturing (arrow). These fractures are filled with residual hydrocarbon (Lithofacies B).

2-14-3-28W1
950 metres

Plate 3C

Photomicrograph of sandy siltstone showing lenses of fine-grained quartz (q) which have been preferentially cemented by anhydrite (a). The reddish hematite pigment is associated with the finer-grained siltstone (Lithofacies B).

16-18-3-28W1
962 metres

Plate 3D

Photomicrograph under x-nichols. Same as Plate 3C.

16-18-3-28W1
962 metres

Plate 3E

Core photograph of very fine-grained, silty subarkose with irregular laminae of siltstone and lenses of well-rounded, "floating" quartz grains (top arrow). The bottom arrow indicates fine-grained, detrital dolomite probably aeolian in origin (Lithofacies C).

11-30-1-25W1
908.6 metres

PLATE 3

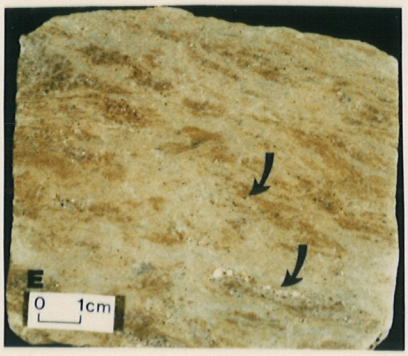

Plate 3F

Core photograph of very fine-grained, glauconitic, silty subarkose. This subarkose is massive with no evidence of sedimentary structures or fossil remains (Lithofacies C).

2-20-1-26W1

Subhorizontal micro-fractures are present in several cores (Plate 3B). Fracturing may be due to the coring process. However, in some cores fractures are filled with residual oil.

This siltstone lithofacies shows good primary micro-intergranular porosity and secondary micro-intercrystalline porosity (Section 5.2.2). The coarser-grained sandstone lenses within this lithofacies are commonly cemented with anhydrite (Plate 3C, 3D).

3.4.3 Lithofacies C - Massive to Ripple-Laminated, Silty, Very Fine-Grained, Lithic Subarkose

Lithofacies C is composed of a massive to ripple-laminated, silty, very fine-grained, lithic subarkose which varies in color from light gray (N7) to light olive gray (5 GY 6/1) and pale red (5 R 6/2) (Plate 3E - 4B). This lithofacies contains 15% feldspar, 8% lithic grains, as well as trace amounts of chert, hematite, and 1% glauconite (Section 5.2.3) (Plate 4A - 4E).

Although this subarkose is generally massive, millimetre to centimetre thick pods and lenses of dark gray, silty material are often present (Plate 3E). Ripple-lamination is preserved in approximately 10% of the core examined. Pinkish, coarse-grained, sandstone clasts are common to this lithofacies particularly in the Waskada area (Plate 4F). The clasts are angular and irregular in shape. There is some evidence of a

PLATE 4

Plate 4A

Photomicrograph of fine-grained, silty subarkose showing the mineralogical composition. The subarkose is composed primarily of quartz (q) with up to 15% feldspar. Potassium feldspar is stained yellow in color. The grains are mainly subangular (Lithofacies C).

14-5-2-28W1
991.42 metres

Plate 4B

Photomicrograph (x-nichols) of very fine-grained subarkose illustrating a sutured, quartz grain common to this lithofacies. This quartz grain was probably derived from a metamorphic source rock (Lithofacies B).

1-13-1-26W1
916 metres

Plate 4C

Photomicrograph of very fine-grained subarkose showing a bimodality to rock texture. These medium to coarse-grained "floating" quartz (q) are aeolian in origin (Lithofacies C).

1-13-1-26W1
915.4 metres

Plate 4D

Photomicrograph of a porous, fine-grained, silty subarkose. The arrow shows glauconite. The blue color indicates porosity. Quartz (q) (Lithofacies C).

9-26-1-26W1
913 metres

Plate 4E

Photomicrograph of silty, very fine-grained subarkose. Anhydrite cement (a) is preferentially infilling porosity which is present within coarser-grained lenses. Hematite is associated with the siltstone.

9-1-1-26W1
920 metres

PLATE 4

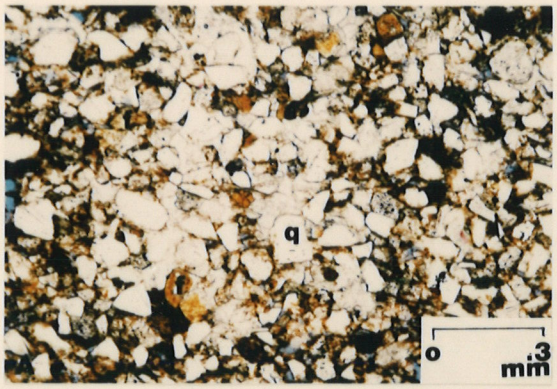

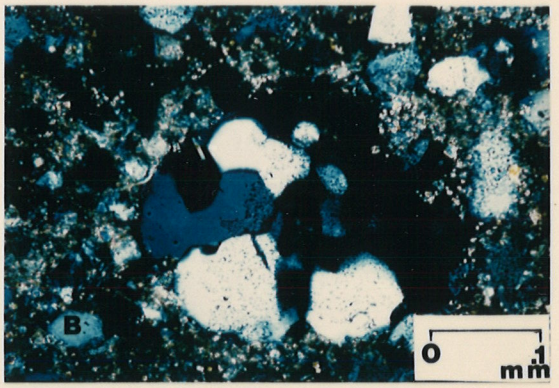

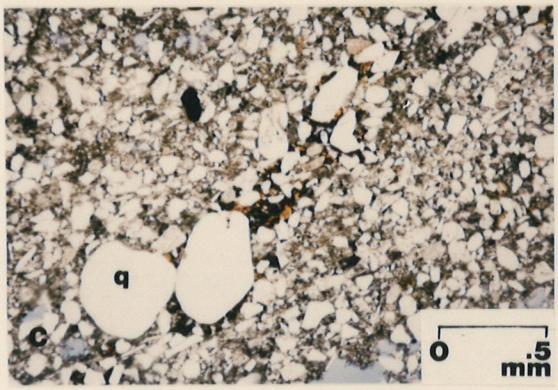

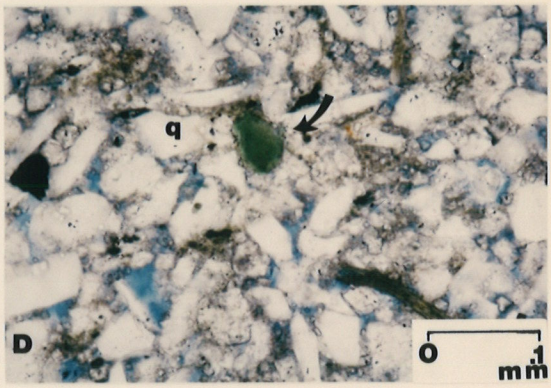

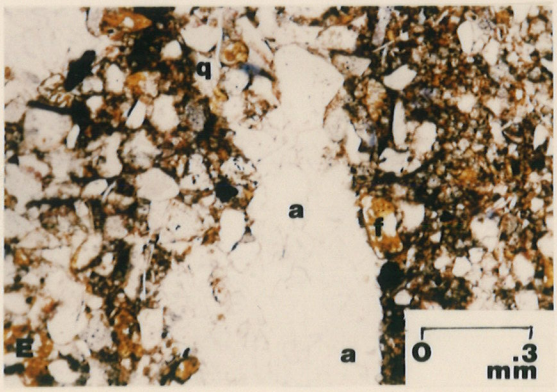

Plate 4F

Core photograph of greenish, very fine-grained, silty subarkose with a turbated appearance. The arrows show interclasts of coarse-grained, pinkish subarkose.

3-34-1-26W1
911.5 metres

disruption of laminae in the host sediment associated with these clasts where laminae appear to be dragged downward.

Subrounded, randomly dispersed, dolomite grains are present in this lithofacies often associated with well-rounded, medium-grained, "floating", quartz grains. The dolomite and floating quartz are also concentrated in lenses (Plate 3E). There are no fossil remains in this lithofacies but minor fecal pellets are present.

Lithofacies C may vary from a very, silty subarkose with very, poor porosity to a very, clean, friable rock with excellent primary intergranular porosity. Where present, the matrix is usually dolomitized (Section 5.2.3). Dolomitization is associated with microintercrystalline porosity. The core in the Coulter and Waskada Fields is commonly oil stained (Plate 5A).

3.4.4 Lithofacies D - Interlaminated Mudstone, Siltstone, Fine-Grained Subarkose

Interlaminated mudstone, siltstone, and fine-grained subarkose is the most common rock unit in the study area. The three constituents of this rock type have been described previously as Lithofacies A, B and C. One distinct feature of this rock type is the marked difference in color saturation. The mudstone laminae are dark reddish-brown (5 YR 3/4), the siltstone are a pale yellowish-brown (10 YR 6/2) to pale red

PLATE 5

Plate 5A

Core photograph of oil stained, fine-grained subarkose (Lithofacies C) common to the south-central Waskada field.

3-18-1-25W1
959 metres

Plate 5B

Core photograph of silty subarkose and an overlying siltstone (Lithofacies B). The arrow shows the contact with the underlying silty subarkose. Note the presence of anhydrite (a).

3-34-1-26W1
921.3 metres

Plate 5C

Core photograph of wavy-lenticular to interlayered mudstone, subarkose, and siltstone, typical of an environment associated with fluctuating current energy. The arrow shows a questionable bioturbation feature (Lithofacies D).

5-5-2-27W1
959 metres

Plate 5D

Core photograph of subhorizontal, wavy-bedded (arrow) to interlayered mudstone, siltstone, and subarkose (Lithofacies D).

16-15-1-28W1
990 metres

Plate 5E

Core photograph of parallel-interlaminated mudstone, siltstone, and subarkose. The arrow shows a sharp contact with the overlying subarkose (Lithofacies D).

3-34-1-26W1
923.5 metres

PLATE 5

A

B

C

D

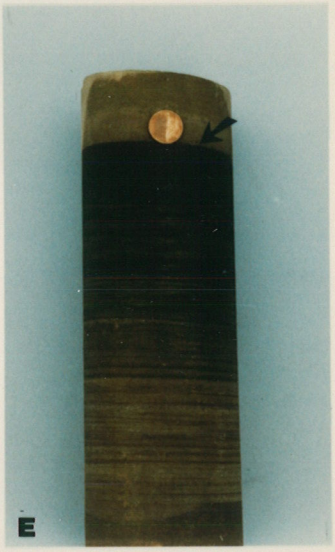

E

(5 R 6/2), and the subarkose are yellowish-gray (5 Y 7/2) to grayish-pink (5 R 4/2) (Plate 5C - 5E).

Parallel to subhorizontal laminae are present and vary from a few millimetres to one centimetre in thickness (Plate 5E). The most common sedimentary feature is wavy to lenticular lamination (Plate 5C, 5D). In approximately 50% of the core examined, interlaminated mudstone, siltstone, and subarkose units have a distinct turbated appearance with only local preservation of laminae. Minor soft-sediment deformation features were also noted. There are no fossil remains and it is difficult to recognize distinct burrow structures.

3.4.5. Lithofacies E: Parallel to Cross-Laminated Medium-Grained, Lithic Subarkose

This lithofacies is composed of a parallel to cross-laminated, fine to medium-grained, lithic subarkose which is light gray (N7) in color (Plate 6A - 7C). This subarkose is composed of quartz (65%) and contains approximately 18% feldspar, 8% opaque grains, and minor chert (Section 5.2.5) (Plate 6D, 7A - 7C). This is a very clean rock. However, where present matrix material is dolomitized (Plate 7C). This rock is usually completely cemented with anhydrite but does show poor to good porosity locally (Plate 6E, 7A, 7B).

Sedimentary structures include, parallel-lamination, high-angle cross-lamination with forsets of approximately 4 centimetres in height, and

PLATE 6

Plate 6A

Core photograph of medium-grained, silty subarkose with parallel-lamination and cross-lamination. The arrow shows the presence of lithic fragments outlining the primary structures (Lithofacies E).

2-20-1-26W1
935.8 metres

Plate 6B

Core photograph of medium-grained subarkose with parallel-lamination. The arrow shows unidirection ripple-lamination. The contact with the overlying siltstone is sharp (Lithofacies E).

3-34-1-26W1
922.3 metres

Plate 6C

Core photograph of medium-grained subarkose with low-angle cross-lamination (Lithofacies E).

2-20-1-26W1
930 metres

Plate 6D

Photomicrograph of medium to fine-grained subarkose showing the mineralogical composition and texture. The rock is composed primarily of quartz. Potassium feldspar is stained yellow in color. The blue coloring indicates porosity (Lithofacies E).

2-20-1-26W1
929 metres

Plate 6E

Photomicrograph of medium-grained subarkose of core sample 6A (under x-nichols). Note the subrounded to rounded, quartz grains and chert. Poikilotopic, anhydrite cement has occluded the pre-existing porosity (Lithofacies E).

2-20-1-26W1
924.6 metres

PLATE 6

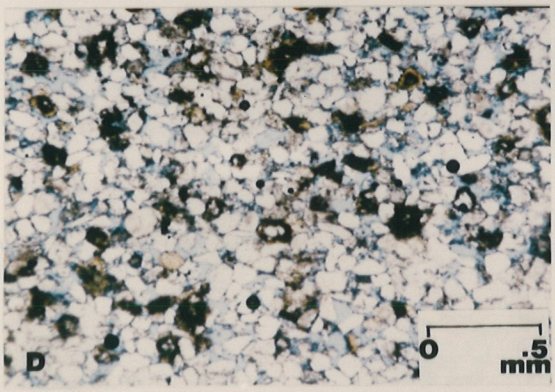

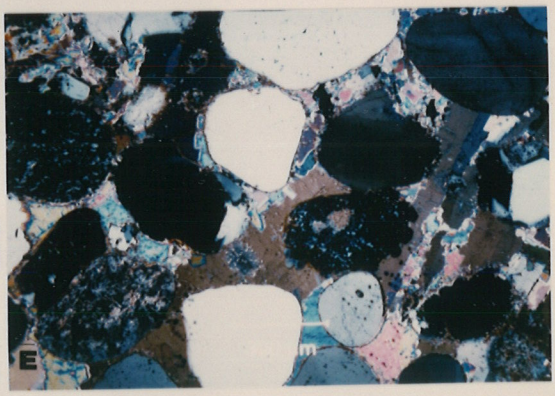

PLATE 7

Plate 7A

Photomicrograph of medium-grained subarkose. The arrow shows hematite grain coatings around quartz (q) grains. Note the presence of anhydrite cement which occludes any pre-existing porosity (Lithofacies E).

2-20-1-26W1
929 metres

Plate 7B

Photomicrograph showing (arrow) hematite grain coatings and the presence of hematite along cleavage planes (Lithofacies E).

2-20-1-26W1
929 metres

Plate 7C

Photomicrograph (x-nichols) of medium-grained subarkose showing fairly coarse-grained zebraic chalcedony. Note the dolomitized matrix (Lithofacies E).

16-1-2-26W1
909.8 metres

Plate 7D

Core photograph of a corase-grained, felspathic sublitharenite. The arrow indicates the presence of mud rip-up clasts probably derived from the underlying unit (Lithofacies F).

2-20-1-26W1
927.2 metres

Plate 7E

Photomicrograph of coarse-grained sublitharenite (quartz grain - q) showing a dolomitized mud clast (arrow). Note the presence of anhydrite cement (a) which occludes any pre-existing porosity (Lithofacies F).

13-32-2-25W1
972 metres

PLATE 7

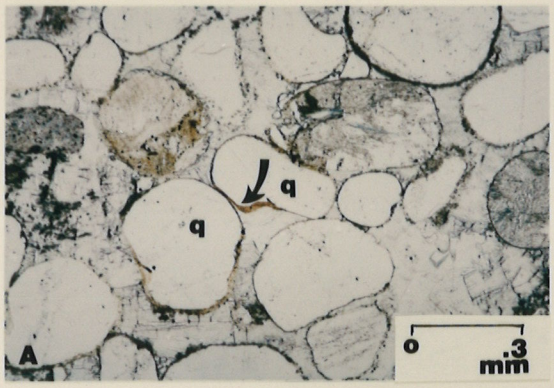

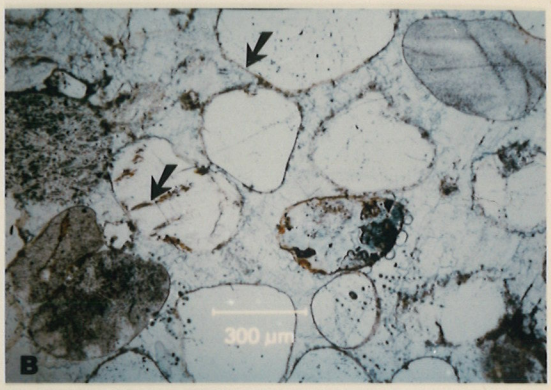

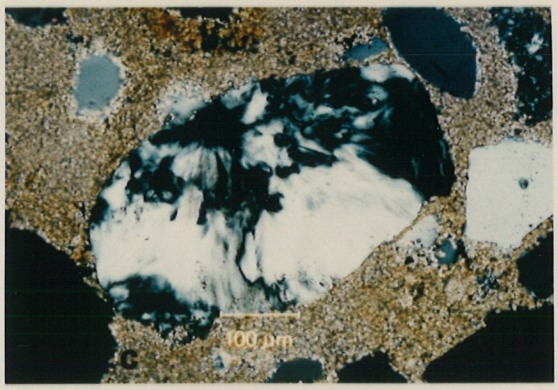

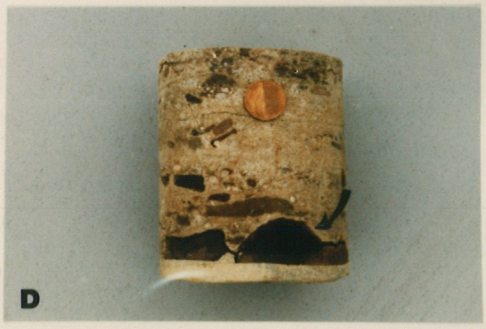

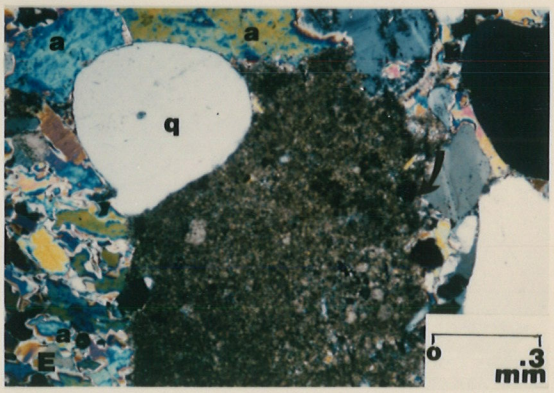

ripple-lamination with forsets of approximately 1.3 centimetres in height (Plate 6A, 6B, 6C).

3.4.6 Lithofacies F - Massive Coarse-Grained, Feldspathic Sublitharenite

Massive, coarse-grained, feldspathic litharenite is rare in the study area (Plate 7D). The rock is commonly gray to grayish-orange-pink (5 YR 7/2) to pale red (10 R 6/2) in color. The rock is composed of quartz (65%) and also contains 5-18% feldspar and 15% chert (Section 5.2.6). Well-rounded anhydrite and reddish-brown mud clasts are common (Plate 7D). The mud clasts have been preferentially dolomitized (Plate 7E). The rock is completely cemented with anhydrite and appears tight (Plate 7E).

3.5 Vertical Lithofacies Sequence of the "Lower Sandy Unit"

3.5.1 Lithofacies Sequence (LS) I

Lithofacies Sequence I (Figure 12-I) is the coarser grained sequence found in the Lower Amaranth Member. This sequence is present in only five of the cores examined (e.g., 2-20-1-26 W1; 6-25-1-26 W1; 14-32-1-25 W1). LSI is comprised of a basal (4 metre thick) subarkose unit which is composed of Lithofacies F (coarse-grained sublitharenite - Plate 7D) fining upward to Lithofacies E (medium-grained subarkose - Plate 6A). Lithofacies E shows some of the best preserved sedimentary

structures in the Lower Amaranth section. The subarkose fines upward to Lithofacies D and/or B (Plate 2C, 5C). Lithofacies Sequence I is characterized by an erosional basal contact with evidence of scour and rip-up clasts derived from the underlying mudstone.

3.5.2 Lithofacies Sequence (LS) II, III, IV

These three units (Figure 12-II, III, IV) are very similar in composition and represent the most common fining-upward sequences of the Lower Amaranth Member. Lithofacies Sequence II is composed of a basal 1.5 metre thick glauconitic, silty subarkose (Lithofacies C) which fines upward to Lithofacies D and/or B. The subarkose of Lithofacies Sequence II is characterized by pinkish, coarse-grained subarkose clasts (Plate 4F). Lithofacies Sequence III is composed of a silty subarkose with preserved ripple-lamination and fines upward to Lithofacies D. Lithofacies Sequence IV contains a basal, glauconitic, silty subarkose with siltstone lenses. This basal subarkose also fines upward to Lithofacies D (Plate 3E). The base of each unit varies from an erosional contact with a lag deposit composed of very fine-grained dolomite and well-rounded quartz to a sharp basal contact.

3.5.3 Lithofacies Sequence (LS) V

Lithofacies Sequence V is a complex sequence not particularly common to the Lower Amaranth Member (Figure 12-V). This sequence is a good example of the rapid changes in lithology (over a 2 metre interval) which characterizes the Lower Amaranth Member. Lithofacies Sequence V is composed of a basal ripple-laminated, fine-grained subarkose (Lithofacies C) grading upward to Lithofacies A (mudstone). The reddish-brown mudstone is overlain by Lithofacies F which shows evidence of erosion into the underlying mudstone. The sequence fines upward to Lithofacies C. The basal contact of the entire sequence is erosional.

3.5.4 Lithofacies Sequence (LS) VI

Lithofacies Sequence VI is a 1.5 metre thick sequence which shows an overall fining-upward character with internal coarsening-upward subcycles (Figure 12-VI). In this sequence, Lithofacies C gradually becomes more argillaceous grading upward to Lithofacies D. Lithofacies D gradually becomes sandier coarsening-upward to Lithofacies C and continuing to fine upward to the siltstone of Lithofacies B. This sequence shows a sharp basal contact.

3.6 Distribution of Lithofacies

3.6.1 Introductory Statement

The sandy (grain size) lithofacies (Lithofacies C, E, F) are distinguished on petrophysical logs from the non-sandy (grain size) lithofacies (Lithofacies A, B, D) by a core to gamma-ray log calibration and gamma-ray log cut-off (NGRI - Section 1.4.4). Figures 13-17 (map pocket) show the localized development of Lithofacies F (coarse-grained sublitharenite) and Lithofacies E (medium-grained subarkose) when core is present. These rocks generally represent the basal unit of Lithofacies Sequence I (dark yellow color).

The light yellow color on these maps illustrates the distribution of Lithofacies C (fine-grained, glauconitic subarkose) which represents the basal unit of Lithofacies Sequence II - IV. Lithofacies C is the reservoir facies (Section 5.5). Lithofacies C is distributed as a series of interfingering to laterally extensive units. These interfingering units pinch-out to Lithofacies B (siltstone) and/or interlaminated to wavy-bedded Lithofacies D (mudstone, siltstone, subarkose). These fine-grained subarkose units often correlate to the coarser-grained subarkose units. In general, two to four sandy units are present at any one well location over the entire study area, forming a "sheet"-type distribution.

In cross-section, variation on the unconformity appears to affect the thickness of the Lower Amaranth Member. The thickness of the Lower Amaranth increases from 5-10 metres near paleotopographic lows, coincident with the local development of a basal Lower Amaranth subarkose unit.

3.6.2 Distribution of Sandy Lithofacies (Lithofacies C, E, F)

Figure 13 (map pocket) is a stratigraphic cross-section through the Lyleton-Napinka area (Figure 2 - map pocket) which extends perpendicular to depositional strike. The cross-sections illustrate relatively poor subarkose development in the central study area with an increase in fine-grained subarkose in the Cobra Shell Lyleton wells. An anomalously thick development of subarkose is present in the Imperial Copley (11-18-1-29 W1) well and the Cleary Souris Valley White (5-24-1-29 W1) well. There is a localized deposit of coarse-grained sublitharenite in the 1-9-2-28 W1 well.

Figure 14 (map pocket) extends through the southern portion of the study area (Figure 2 - map pocket) illustrating four to five interfingering to laterally extensive subarkose units. The fine-grained subarkose in the central Waskada Field (6-25-1-26 W1) is a well-sorted, matrix-free rock (Section 5.5) whereas, the Lithofacies C in the Coulter-Lyleton wells is characterized by a high silt content and low permeability (Section 5.5). A local deposit of Lithofacies E and F is

present in the North Amercia Arthur (2-20-1-26 W1) well and the Omega Waskada (6-26-1-26 W1) well. These deposits correlate laterally with fine-grained subarkose units.

The Melita-Waskada Cross-Section (Figure 15) illustrates the sedimentation trends in the eastern portion of the study area (Figure 2 - map pocket). A series of interfingering to laterally extensive subarkose units are present with an increase in subarkose development in the Waskada wells. In the (14-25-1-26 W1) and (11-24-1-26 W1) wells paleotopographic lows on the unconformity effect the thickness of the Lower Amaranth Member which is associated with the local development of a lower subarkose unit.

Figure 16 and 17 (map pocket) illustrate subarkose distribution near the Pierson Field (Figure 2 - map pocket). Figure 16 is a structure cross-section which shows the presence of one to two interfingering subarkose units. Figure 17 runs sub-parallel to regional dip and shows the relative increase in fine-grained subarkose in the Lyleton-Coulter wells. The fine-grained subarkose units in the southern portion of this cross-section area pinch-out to the north into Lithofacies B and the wavy-bedded facies (Lithofacies D).

A total sand isopach map of the Lower Amaranth Member shows the presence of sandy lithofacies throughout the study area forming a sheet-type distribution or geometry (Figure 18 - map pocket). A minimum

thickness of 2 metres of sand is present over the entire study area with 6 to 8 metres of sand present in the southwest. Thick sand development is also noted in some portions of the Pierson Field, the Coulter-Lyleton area and the Waskada Field. Poor sand development occurs to the north and northeast in the study area. There is a correlation between thick sand development, thick total Lower Amaranth (Figure 7 - map pocket) and paleotopographic lows on the unconformity surface (Figure 4 - map pocket).

3.6.3 Distribution of Non-Sandy Lithofacies (Lithofacies A, B, D)

Figures 13-17 (map pocket) show the presence of non-sandy lithofacies throughout the study area. The wavy-bedded facies (Lithofacies D) dominates the eastern portion of the study area (Figure 14) in comparison to rocks in the Coulter Field (Figure 2 - map pocket) which are generally composed of siltstone and/or reworked Lithofacies D. Figure 16 shows the dominance of non-sandy lithofacies in wells in the Pierson Field. Where core data is available, a marked increase in "floating" quartz grains is present in the Pierson and Coulter areas compared to the remainder of the study area.

In general, the basal deposit above the unconformity is a reddish-brown siltstone with nodular anhydrite (Plate 1). Fine-grained subarkose units pinch-out laterally to siltstone and Lithofacies D. Lithofacies change rapidly throughout the study area.

CHAPTER 4: INTERPRETATION OF LITHOFACIES AND DEPOSITIONAL ENVIRONMENT

4.1 Introductory Statement

The study of lithofacies, lithofacies sequences, and sandstone geometry in any clastic depositional system is useful in unravelling the depositional setting. Studies of modern depositional regimes have shown that certain distinct features are characteristic to a particular sedimentary environment. By analyzing similar features in ancient rocks, it is often possible to reconstruct, within reason, the depositional environment of an ancient rock sequence.

The Lower Amaranth Member is a unique sedimentary unit, one that poses several problems when considering the interpretation of a depositional environment. In any rock sequence, the lithology, sedimentary structures, and fossil remains reflect the physical, chemical, and biological processes active at the time of sedimentation. An interpretation of the Lower Amaranth Member is hampered by the absence of preserved fossil remains. This makes it necessary to rely heavily on primary sedimentary structures and the preserved lithofacies sequence. However, in the Lower Amaranth Member only 10% of the cores examined contain preserved sedimentary structures. The remaining cores show extensive mechanical reworking and/or bioturbation of sediment.

Barchyn (1982, 1984) suggested that the Lower Amaranth Member was deposited in a mud flat environment, dominantly continental to marine. Sediment was deposited under shallow marine conditions where sandy beds in the "lower sandy unit" are, in part, fluvial deposits on an emergent mud flat (Barchyn, 1982). Alternatively, winnowing of sediment by wave action in a shallow marine environment may have been the primary depositional process (Barchyn, 1982). The Lower Amaranth represents the initial deposit of a transgressive event and is transitional between the continental environment associated with post-Paleozoic erosion and the shallow marine, hypersaline environment which dominated during precipitation of the Upper Amaranth anhydrite (Barchyn, 1984).

No detailed depositional model is documented in the published literature for the equivalent lower Watrous Formation (member) of Saskatchewan or the Spearfish Formation (Saude Member) of North Dakota. Cummings (1953) suggested that the basal lower Watrous is an aeolian deposit and Dow (1967) interpreted the Spearfish Formation as a continental to playa lake sequence.

In this study, the depositional environment of the Lower Amaranth Member is interpreted as a low-energy, tidal flat setting with a prevailing arid climate. Sediments were deposited on a broad tidal flat situated along the flank of the Williston Basin in a restricted embayment known as the Amaranth sub-basin (Figure 1). This environment was subjected to periodic inundation and exposure of the tidal flat

where sandy beds were deposited in a shallow marine setting (Figure 19). This interpretation is supported by the basin margin setting and the following evidence from cores:

1. The dominance of mudstone; siltstone; and texturally immature, fine-grained subarkose combined with the presence of mildly, erosive, basal contacts of fining-upward sequences indicate that the Lower Amaranth Member was deposited under low energy conditions.

2. The "stacked" or repeated fining-upward sequences of the "lower sandy unit" favor a cyclic marine process as opposed to an ephemeral, terrestrial setting.

3. The presence of locally preserved ripple-lamination (Lithofacies C) which indicates deposition of sediment under shallow-water, low-energy conditions.

4. The presence of wavy to lenticular bedding (Lithofacies D) which is associated with rapidly fluctuating current energy common to tidally influenced environment.

5. Glauconite is a minor but persistent component of the silty subarkose (Lithofacies C). Glauconite is a good indicator of marine sedimentation.

LITHOLOGY

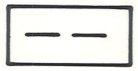
REDDISH-BROWN MUDSTONE
(LITHOFACIES A)

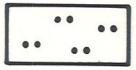
REDDISH-BROWN SILTSTONE
(LITHOFACIES B)


RED - BROWN WAVY/CONTORTED/
LENTICULAR INTERLAMINATED
MUDSTONE/SILTSTONE/SUBARKOSE
(LITHOFACIES D)


GREEN-GRAY FINE-MEDIUM-
GRAINED SUBARKOSE
(LITHOFACIES C,E)


PINKISH COARSE-
GRAINED LITHARENITE
(LITHOFACIES F)


NODULAR ANHYDRITE

FABRIC
SEDIMENTARY
STRUCTURES


INTRACLAST
COARSE SUBARKOSE

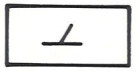
DOLOMITIC


SILTSTONE LENSE


CROSS-LAMINATION


PARALLEL LAMINATION


NO CORE


EROSIONAL CONTACT

GRADATIONAL CONTACT

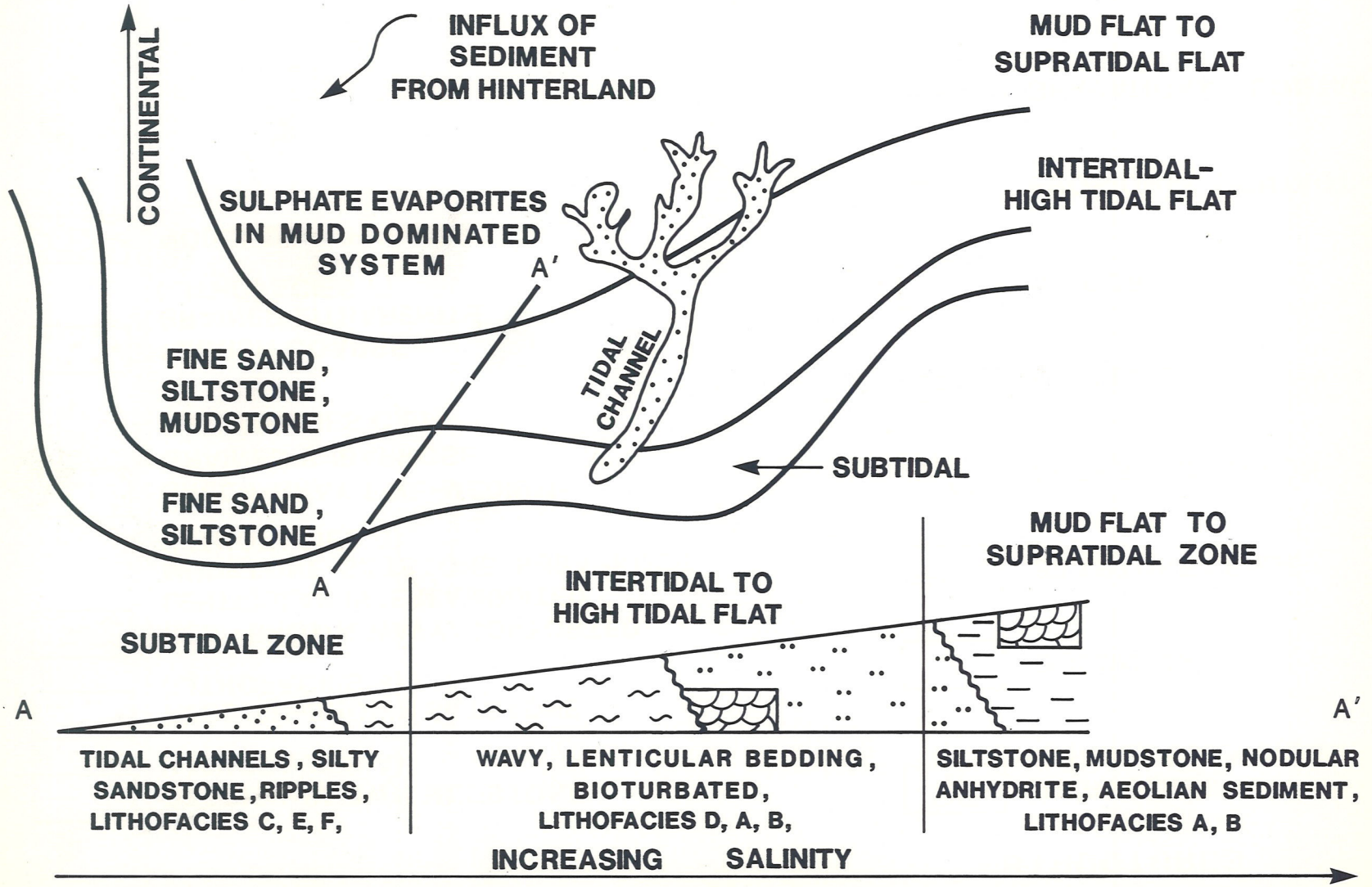

FIGURE 19 : SCHEMATIC DEPOSITIONAL MODEL FOR LOWER AMARANTH MEMBER

6. The presence of locally preserved mud cracks which indicate periodic wetting and exposure of sediment. This sedimentary structure is common to several depositional environments. However, when found in combination with the other sedimentary features of the Lower Amaranth Member supports a tidal flat (intertidal to mud flat) setting.

7. "Frosted" coarse-grained quartz (sand) and sand lenses suggest aeolian deposition. These "frosted" grains are another indicator of subaerial exposure of sediment.

8. Synsedimentary nodular anhydrite is formed in an environment with higher than normal marine salinity and an arid climate. Nodular anhydrite is commonly associated with sabkha to supratidal settings.

9. The dominance of subarkosic rocks and well preserved feldspar in association with a low-lying source area (Precambrian Shield, eastern Manitoba) suggests an arid climate which retarded the weathering process.

10. The presence of two distinct sand-bodies ("lower sandy unit") incorporated into a dominantly fining-upward sequence:

(a) The more prevalent sequence in the study area is composed of a basal, silty, glauconitic, fine-grained subarkose with locally preserved ripple-lamination and a local interfingering but overall blanket or sheet-type geometry. This sequence fines upward to a wavy-lenticular bedded facies (Lithofacies D) and/or siltstones and is interpreted as a tidal flat deposit. The basal subarkose was deposited in a shallow marine environment.

(b) The coarser grained sequence was deposited <u>locally</u> as a coarse-grained sublitharenite (lag deposit) fining upward to a parallel to cross-laminated, medium to fine-grained subarkose, a wavy to lenticular bedded facies (Lithofacies D) and/or siltstone. This sequence is interpreted as a tidal channel.

There are no modern analogs to ancient epeiric sea sedimentation and consequently, there is an ongoing controversy as to whether normal diurnal tides were operating in vast inland waterways such as the Williston Basin. Irwin (1965) and Shaw (1964) suggested that currents were largely wind generated. However, it is possible to see sedimentary structures and a depositional sequence in the Lower Amaranth Member similar to that present in modern tidal flat settings (Section 4.2).

4.2 Tidal Flat Sedimentation

Tidal flats occur along open coasts associated with generally quiescent conditions and relatively low relief, low wave energy, and appreciable tidal range. They are also found in protected high energy coastal settings. Tidal flats vary considerably in geographic extent, vertical thickness of accumulated sediment, and overall geometry (Weimar et al, 1981). In general, tidal flats are broad, featureless plains, where deposition of sediment results from lateral accretation of meandering tidal channels and creeks (Elliott, 1978, Weimar, 1981). Tidal action results in channel flooding and subsequent inundation of the adjacent area. During this process, fine-grained sediment is moved onshore, where it accumulates as intertidal flats (Blatt et al, 1980). The recession of tidal waters results in re-exposure of the tidal flat area. Wind processes may play a significant role in controlling sedimentation (Reineck and Singh, 1973; Weimar et al, 1981). Climatic parameters such as mean temperature and seasonal aridity strongly influence the initial mineralogical composition as well as early diagenetic processes and evaporation rate on the tidal flat.

Several workers have subdivided the tidal flat into zones based on tidal range. The discussion of Elliott (1978) was applied in this study. The supratidal zone is located above mean high tide. This mud-dominated zone is subjected to periodic wetting and drying conditions resulting in desiccation of sediment. In arid climates, the growth of

gypsum and other evaporites is common. However, in more temperate areas the high tidal flat is characterized by peat deposits and vegetation. The supratidal zone grades basinward into the seaward dipping intertidal zone.

The intertidal zone is located between high and low tide. The intertidal zone is often dissected by tidal channels and tidal creeks. Asymmetric/symmetric ripples and flaser, wavy, lenticular, and/or interlayered sandstone and siltstone are common. These sedimentary structures and bedding features are associated with rapidly fluctuating current and wave conditions. Bioturbation is prevalent in this area as well as the presence of shell horizons and algal laminae.

The subtidal zone is located below low tide range. The intertidal flat may pass into the subtidal area with no major change in sediment features. However, in sand dominated high-energy systems, such as the German coast of the North Sea (Reineck, 1975) and the Wash, western North Sea (Evans, 1975), the subtidal zone may be composed of a complex series of channels, bars, and shoals. These subtidal deposits may vary in composition from fine to coarse-grained sand. In an arid climate, salinity generally increases landward.

Models for modern and ancient tidal flats have generally been proposed based on work in sand dominated systems (Evans, 1965; Reineck and Singh, 1973; Klein, 1977) associated with high energy coastal settings

and temperate climates. The Lower Amaranth Member is a mud dominated system associated with a low energy epeiric sea characterized by low bottom slope, very shallow water conditions, restricted circulation, and vast areal extent (Shaw, 1964, Irwin, 1965). Consequently, sand dominated high-energy tidal flat models do not seem to apply.

One of the best modern analogs to the depositional setting in southwestern Manitoba is the mud-dominated, low-energy tidal flat on the Colorado Delta, northeastern Gulf of California (Thompson, 1968; 1975). Here, silty clay and fine-grained sand are supplied by the Colorado River to the north coast of the Gulf of California. A featureless mud plain has developed that grades into a broad, shallow low-dipping, subtidal plain. An arid climate prevails.

Sediments deposited in the subtidal to lower intertidal zone along the Gulf of California are composed of laminated silty clays with 1 mm thick laminae of coarse silt to fine sand interdispersed at regular 1-10 cm intervals. These sediments were deposited by suspension settling from tidal currents.

The intertidal zone along the Gulf of California is dominated by wavy, interlaminated, brownish-gray, silty-clay; silt; and clayey silt (1-8 mm thick laminae) (Thompson, 1968). Thompson (1968) also noted the presence of discrete small scale burrows and disrupted laminae. Above

high water, intense burrowing by feeder crabs has resulted in a lithologically mottled sediment of mixed shells, sand, silt, and clay. The deposits of the intertidal zone originate under the combined influence of small waves and tidal currents that sweep back and forth across the tidal flat.

Along the Gulf of California, the high tidal flat (supratidal zone) is a horizontal plain characterized by the deposition of clays and muds and the growth of evaporite minerals. Near the high water mark, clays settle as tides recede across the mud flat. Evaporite growth is due to hypersalinity and a hot, arid climate.

Thompson (1975) noted several variations in sediment from the subtidal to high tidal flat. These variations include:

1. textural changes from clayey silt to silty clay;

2. color changes from brownish-gray to reddish-brown sediments;

3. changes in lamination from lenticular to wavy to uniform;

4. an increase in gypsum and halite; and

5. an increase in deformed lamination due to shrinkage and evaporite formation.

4.3 Interpretation of Sedimentary Features

4.3.1 Significance of Interbedded Green and Red Bed Sequences

The reddish-brown color of Lithofacies A, B and D is attributed to the presence of hematite. Several origins for red sediments have been proposed in the literature. Krynine (1949), in his work in the deserts of southern Mexico, suggested a detrital origin. Red beds were formed by erosion of laterite soils and subsequent deposition of sediment. The association of red beds, in this desert basin, with evaporites and other indicators of seasonal dryness led Krynine (1949) to associate the presence of red beds with a prevailing arid climate.

Alternatively, more recent research has proposed a diagenetic origin for red bed sequences (Section 5.3.3). Walker (1967) suggested that red beds form in all climates given an available iron source and an oxygenated intersitial environment suitable for the alteration of iron silicates and the formation of ferric oxide. Interpreting a red bed sequence as an indication of an arid climate must be supported by paleontological evidence and/or the presence of indicators of seasonal dryness. In general, red bed sequences were deposited under oxygenated conditions. Oxygenated conditions are usually associated with continental and/or nearshore environments.

There is evidence that the red sediments of the Lower Amaranth Member were derived from both sources. McCabe (1956) and Stott (1954) described the exposure of the Devonian Ashern and Lyleton Formations (red bed sequences) at the basin margin as a result of post-Paleozoic erosion. They concluded that both the Precambrian Shield and these red bed units were the source of Amaranth sediment. There is also evidence of hematite grain coats around quartz grains (Plate 7A, 7B), often an indication of diagenetic hematite (Walker, 1967).

4.3.2 Dominance of Fine-Grained Sediments

The textural maturity of any rock is an important key to the physical processes operating in the depositional environment, as it reflects the effectiveness of the prevailing current in winnowing, sorting, and abrasion of detritus (Folk, 1972). The immature sediments of Lithofacies C and the mudstones and siltstones of Lithofacies A and B accumulated in a low-energy depositional environment associated with weak current action. For the most part, wave energy was never sufficient to winnow away silts and mud (Section 5.5).

4.3.3 Dominance of Subarkose Rocks

Arkose to subarkose rocks, such as those of the Lower Amaranth Member, are generally composed of sediments derived from granitic or metamorphic terrains. Feldspars are commonly altered to clay early

in the weathering process. Several conditions may influence the preservation of these minerals. Chemical weathering of rocks, in general, may be retarded by conditions of extreme aridity (Pettijohn et al, 1972). Folk (1972) has also suggested that high relief and rapid erosion are a favorable condition for the preservation of feldspar. When working with ancient sequences, the factor controlling preservation is very difficult to determine. However, the association of this subarkosic sequence with nodular anhydrite combined with the surrounding low source area (Stott, 1954; McCabe 1956) suggest that well-preserved feldspars in the Lower Amaranth Member indicates the influence of a prevailing arid climate.

4.3.4 "Floating" Quartz Grains

Well-rounded, medium to coarse "floating", quartz grains and lenses of medium to coarse-grained quartz are common to the Lower Amaranth Member. The presence of well-rounded coarse grains creates a distinct contrast (biomodality) to the overall fine-grained character of the rocks. Folk (1972) suggested that this mixing of sediment is often the product of two distinct processes operating in one depositional environment. Both Barchyn (Lower Amaranth, 1982) and Cummings (lower Watrous, 1953) have described a frosted texture to these "floating" quartz grains which may be the result of:

1. microcrystalline quartz overgrowths;
2. aeolian abrasion (Folk, 1972); or
3. chemical etching before or after deposition.

These grains were interpreted as aeolian in origin (Barchyn, 1982; Cummings, 1953). Similarly lenses of "frosted" grains were deposited by the same process. These aeolian features are common to many environments such as desert settings or near-shore mud flats and indicate that the sediments of the Lower Amaranth were subaerially exposed.

4.3.5 Nodular Anhydrite

Nodular anhydrite is fairly common in the siltstones and fine-grained subarkose of the Lower Amaranth Member. One of the more widely accepted models for the formation of nodular anhydrite is the displacive growth of gypsum and subsequent recrystallization (dehydration) to anhydrite (Dean et al, 1975).

Based on work in the recent sediments of the Persian Gulf, nodular anhydrite has been used as an indicator of subaerial exposure of sediments in a tidal flat or sabkha setting. The formation of nodular anhydrite is associated with evaporation of upward migrating $CaSO_4$ rich pore fluids (Schreiber et al, 1982). Alternatively, Dean et al (1975) noted that nodular anhydrite may also be found in deep water settings,

as the main requirements for formation are restrictive conditions and a calcium sulphate source.

The basin margin setting of southwestern Manitoba would favor a sabkha to tidal flat setting for the formation of nodular anhydrite as opposed to the deep water model. The presence of nodular anhydrite indicates hypersaline conditions and a prevailing arid climate.

4.3.6 Disruption and/or Absence of Sedimentary Features

The general absence of sedimentary structures in all lithofacies of the Lower Amaranth Member is worth noting for most sediments normally show some type of primary sedimentary structures (Pettijohn et al, 1972). This massive to mottled character is the result of the depositional process or the result of bioturbation and disruption of the original fabric (Pettijohn et al, 1972). Disruption and or obliteration of sedimentary structures may also be due to desiccation and/or the displacive growth of gypsum (Reif and Slatt, 1979). In many cases, the cause of turbation is difficult to determine. In the Lower Amaranth, there is indication of disruption of sedimentary structures due to desiccation, growth of nodular anhydrite and bioturbation. Barchyn (1982) also suggested that the generally disrupted nature of the sediment may be due to storms and flash floods in a prevailing arid climate associated with reworking of sediment.

4.3.7 Ripple Lamination

Ripple-lamination is preserved in 5-10% of the fine-grained subarkose examined in core and is also present in the subarkose of Lithofacies E. Preserved ripple-lamination indicates shallow water deposition and low current velocity (Blatt et al, 1980). In the Lower Amaranth Member, these sedimentary structures are occasionally outlined by heavy mineral concentration which may be attributed to wave swash.

4.3.8 Absence of Fossil Evidence

There is a marked absence of fossil remains in all lithofacies of the Lower Amaranth Member. Although bioturbation has been noted and several fecal pellets identified, it is very difficult to actually pinpoint distinct burrow structures. The marked absence and/or marked non-preservation of fossils can be attributed to several conditions:

1. a continental environment of deposition: Pettijohn et al (1972) noted that terrigeneous siltstones and sandstones are rarely rich in fossils but can contain good trace fossils;

2. the presence of saline conditions unsuitable for organic life;

3. solution or aragonitic or calcitic bioclasts during very early diagenesis leaving a non-recognizable trace.

4.4 Interpretation of Lithofacies

4.4.1 Lithofacies A - Massive to Interlaminated Mudstone to Silty Mudstone

Fine-grained sediments, such as the silts and muds associated with Lithofacies A, are normally transported in suspension. The deposition of mud is often controlled by suspension settling associated with weak currents and sedimentation in a low energy environment. The reddish-brown color of the mudstone indicates deposition in a well-oxygenated environment.

4.4.2 Lithofacies B - Massive to Interlaminated Siltstone to Sandy Siltstone

Although not a common feature in Lithofacies B, mud cracks suggest some periodic wetting and subaerial exposure of sediment. Mud cracks are common features of intertidal mud flats, as well as abandoned river channels, playa lakes, and salt marsh pans (Pettijohn et al, 1972).

In considering the fine-grained texture, the reddish-brown color, the presence of nodular anhydrite and the evidence suggesting desiccation and aeolian deposition the siltstones of Lithofacies B were deposited in a well-oxygenated, low-energy, hypersaline environment which was

periodically exposed to subaerial conditions. The siltstones were deposited on a supratidal flat or a continental sabkha setting.

4.4.3 Lithofacies C - Massive to Interlaminated, Silty, Very Fine-Grained, Lithic Subarkose

The glauconite noted in this lithofacies is a minor (1-2%) but persistent component. The origin of glauconite is somewhat uncertain. However, it tends to form under normal marine to weakly reducing conditions. Although it may be re-deposited in non-marine sands, glauconite is a relatively unstable mineral and will not persist over long distances of transport (Pettijohn et al, 1972). Glauconite may also form as a diagenetic product of biotite alteration or by iron enrichment and replacement of mud pellets and shells. Glauconite may precipitate in cavities or as grain coatings. The glauconite noted in the Lower Amaranth Member is well preserved. This type of glauconite is probably primary glauconite, a good indication of a marine-influenced depositional environment (Scholle, 1979).

Irregular, coarse-grained subarkosic intraclasts are common in this lithofacies giving the subarkose a pseudo-breccia appearance. Barchyn (1982) suggested that these clasts were the result of sediment reworking due to intermittent terrestrial storms and flash floods associated with an arid climate. These clasts could also represent collapse or caving of tidal creek banks.

In summary, the immature texture, and the presence of ripple-lamination suggest that Lithofacies C was deposited in a low-energy, shallow-water environment probably below wave base. Nodular anhydrite present in these rocks suggest high salinity. There is no fossil evidence to indicate whether these subarkose are marine or non-marine. However, the presence of well-preserved glauconite supports a marine-influenced environment. The marked absence of sedimentary structures suggests reworking of sediment and/or bioturbation. The presence of well-preserved feldspar combined with minor nodular anhydrite indicates a prevailing arid climate.

4.4.4 Lithofacies D - Interlaminated Mudstone, Siltstone, and Fine-Grained Subarkose

Wavy, parallel to subparallel and lenticular bedding described in this lithofacies is similar to that discussed by Reineck and Wunderlich (1968). Although, it is difficult to identify the internal ripple lamination. The origin of wavy bedding is related to alternating current or wave action where sand, silt, and mud are deposited dependent on the current intensity. The formation of wavy bedding is the result of infilling of the sand ripple trough by finer grained sediment (Reineck and Singh, 1973). Wavy bedding is formed in an environment where energy conditions are suitable for the deposition and preservation of both sand and mud (Reineck and Wunderlich, 1968). The presence of lenticular bedding results from the incomplete formation of sand ripples on a muddy substratum (Reineck and Wunderlich, 1968). Lenticular bedding

forms in a low energy, mud-dominated environment (Reineck and Singh, 1973). Wavy and lenticular bedding are present in intertidal/subtidal zones where the genesis is related to tidal rhythm (Reineck and Singh, 1973). This type of bedding has also been noted in marine deltas and lake bottom sediments associated with deltas.

4.4.5 Lithofacies E - Massive to Laminated, Medium-Grained, Lithic Subarkose

Parallel-lamination, cross-lamination, and ripple-lamination noted in this lithofacies are some of the most distinct structures present in the Lower Amaranth Member. The shape, arrangement, scale, and attitude of bedforms is governed by the characteristics of the parent bedform, the strength of the driving current and the size of the sediment load (Allen, 1982). Cross-bedding is the product of down-current, sand-dune migration (Pettijohn et al, 1972). Unidirectional sedimentary structures are present in aeolian and aqueous environments. The association of parallel-bedding, cross-bedding, overlain by ripple-lamination (Lithofacies Sequence I) is common in fluvial deposits (Allen, 1982). However, these sedimentary structures are outlined by concentrations of lithic grains which could also be due to the influence of wave swash (Plate 6A).

The medium-grained subarkose was deposited under moderate energy conditions. There are no diagnostic fossils or other evidence to support a marine or non-marine environment.

4.4.6 Lithofacies F - Massive, Coarse-Grained, Feldspathic Sublitharenite

Lithic arenites have typically been associated with molasse type deposits in foreland basins, fluvial deposits, and turbidites (Pettijohn et al, 1972). The well sorted texture of this lithofacies combined with the presence of mudstone rip-up clasts and a generally scoured erosional basal contact indicates deposition under moderate to high energy conditions.

A massive sedimentary unit is the result of the depositional process and/or the reworking or bioturbation of sediment. Pettijohn et al (1972) found it unlikely that burrowing organisms could move coarse-grained sandstone. Consequently, the massive nature of this litharenite is likely a function of very rapid sedimentation from suspension or deposition from a highly concentrated sediment dispersion.

In summary, this lithofacies was deposited under moderate to high energy conditions with no evidence to indicate a marine or non-marine environment. The relationship with underlying and overlying lithologies (as noted in the lithofacies descriptions) and the local development suggest that this unit represents a "channel-lag" deposit.

4.5 Interpretation of Lithofacies Sequence

4.5.1 Introductory Statement

No single lithofacies or sedimentary structure can be used to identify the depositional environment of an ancient sequence as many features of the rock are common to several sedimentary environments. The key to interpreting an ancient sequence lies in the relationship of these lithofacies; namely the depositional or lithofacies sequence, the presence of a coarsening upward or fining-upward sequence, the relative occurrence of these sequences in the area, and the geometrical relationship to other sequences observed in core.

The rocks of the Lower Amaranth Member are characterized by several repeated fining-upward sequences. Although many variations have been noted in core (Figure 12), the lithofacies sequences can be categorized into two main sequences:

1. a locally developed fining-upward sequence dominated by a coarse to medium-grained subarkose with parallel and cross-lamination represented by Lithofacies Sequence I; and

2. a dominant fining-upward sequence with a ripple-laminated, glauconitic, silty, fine-grained subarkose and a sheet-type geometry (Lithofacies II-VI).

Lithofacies I is interpreted as a tidal channel while Lithofacies II-VI are variations of a fining-upward sequences deposited on a broad low-energy tidal flat.

4.5.2 Interpretation of Lithofacies I (Coarser-grained Sequence)

Interpretation of Lithofacies Sequence I as a tidal channel is consistent with the following evidence:

1. the base of the sequence is a major erosional surface;

2. the presence of a basal coarse-grained sublitharenite with rip-up clasts (Lithofacies E) which is interpreted as a channel lag deposit;

3. an overall upward decrease in grain size;

4. sedimentary structures indicate a general decrease in current velocity;

5. sedimentary structures suggest unidirectional migration of sand: however the presence of lithic grains outlining sedimentary structures is commonly due to wave swash;

6. the local extent of this sequence;

7. the association geometrically (laterally adjacent) with the low-energy, tidal flat subarkose (Lithofacies Sequence II - VI).

4.5.3 Interpretation Lithofacies II - VI (Finer-grained Sequence)

Lithofacies Sequence II-VI are interpreted as tidal flat deposits where fine-grained glauconitic subarkose units represent laterally migrating tidal creeks over a broad tidal flat. Deposition of subarkose is associated with flooding of tidal creeks due to inundation of the tidal flat and subsequent settling of sediment following recession of waters. This interpretation is supported by the following evidence:

1. mildly erosive basal contacts of the fining-upward sequence;

2. cyclicity of the sequence;

3. the presence of glauconite;

4. a sequence which fines upward from a marine subarkose to a wavy-lenticular bedded facies; and

5. the interfingering but overall sheet-type geometry of the subarkose units common to many environments but supportive of a tidal flat setting as opposed to localized channel deposition.

4.6 Geological History of the Lower Amaranth Member

In summary, the Lower Amaranth Member was deposited on a broad featureless tidal flat similar to the setting along the north coast of the Gulf of California. The basal, reddish-brown siltstones of the Lower Amaranth were deposited in a supratidal mud flat to sabkha type setting along the restricted margin of the Williston Basin (Figure 20). Sediments were eroded from the Precambrian Shield to the east and from red-bed sequences (Lyleton and Ashern Formations) exposed at the basin margin and deposited on a broad mud flat. Sediment gradually began to infill paleotopographic lows on the post-Paleozoic unconformity surface. Nodular anhydrite was formed by the displacive growth of sediment.

A period of slightly coarser-grained sedimentation followed where the deposition of fine-grained subarkose was associated with inundation of the tidal flat, flooding of tidal creeks and the distribution of subarkosic sediment across the tidal flat area. The recession (regression) of water resulted in deposition of sediment by suspension settling. The silty, glauconitic subarkose of Lithofacies C was deposited in very shallow water probably below wave base. Any slight rise in

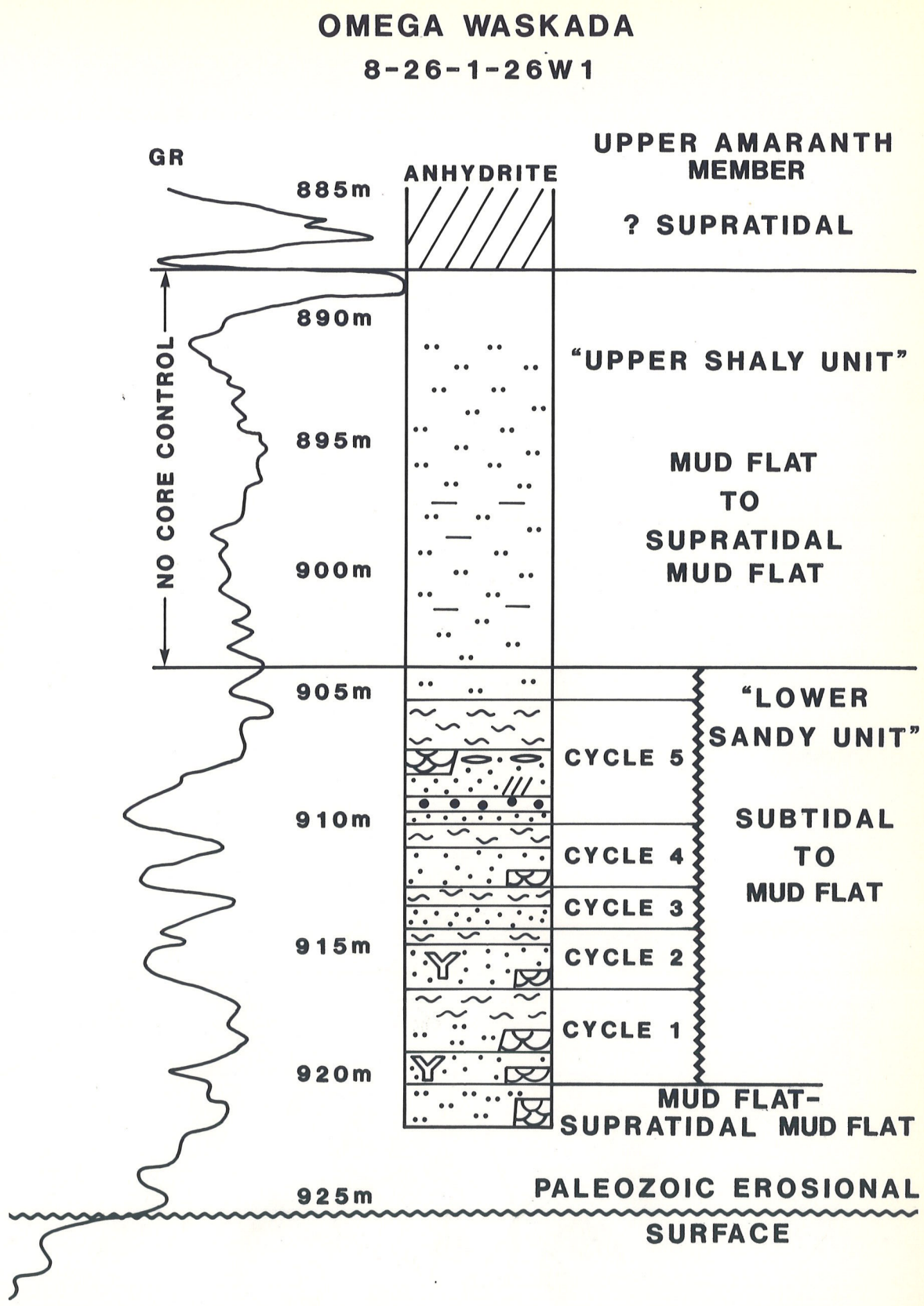

FIGURE 20 : TYPICAL AMARANTH DEPOSITIONAL SEQUENCE

sea level would have significantly affected the Amaranth sub-basin due to the relatively flat basin topography and low bottom slope. These silty subarkose have been extensively reworked and bioturbated. Barchyn (1982) suggested reworking due to terrestrial storms and flash floods associated with an arid climate.

Gradual recession of water from the tidal flat resulted in the deposition of the wavy-lenticular bedded subarkose, siltstone, and mudstone which is commonly associated with a zone of fluctuating current energy (Section 4.4.4). This type of bedding structure is present in modern intertidal flats such as the Colorado Delta originating under the influence of small waves and tidal currents which sweep back and forth across the tidal flat. The dominance of lenticular bedding in the Lower Amaranth probably indicates the presence of a muddy substratum associated with a low-energy, mud-dominated environment.

With further progradation of the tidal flat siltstones and mudstones were deposited. This depositional setting was, for the most part, subaerially exposed, where locally preserved mud cracks indicate wetting and drying of sediment. Aeolian processes were also active.

This deposition cycle was repeated several times in the geological history of the Lower Amaranth Member where each fining-upward sequence represents a slight transgressive-regressive pulse (LSU) (Figure 20). Coarse-grained sedimentation eventually terminated in later Lower

Amaranth time and the basin was dominated by muds and silt (USU). Seas became increasingly hypersaline resulting in the precipitation of the extensive Upper Amaranth evaporite. Overall, the Lower Amaranth represents the record of the beginning of a new era, a period of sedimentation following the post-Paleozoic erosional phase and the beginning of the clastic dominated Mesozoic Era.

CHAPTER 5: PETROGRAPHY, DIAGENESIS, AND RESERVOIR QUALITY OF THE LOWER AMARANTH MEMBER

5.1 Introductory Statement

An important feature of any ancient sedimentary sequence is the diagenetic history of the rocks following deposition and subsequent burial. The diagenetic history of the sedimentary sequence is often complex for several distinct diagenetic environments may have existed during the burial history. The precipitation of cement and the formation of authigenic clay minerals during diagenesis may significantly modify the reservoir quality of a sedimentary rock, controlling the capacity to entrap and/or produce hydrocarbon.

Two of the more significant diagenetic changes in the Lower Amaranth Member are the precipitation of anhydrite cement in pores and extensive dolomitization. Less common diagenetic alteration includes the formation of authigenic clay minerals, the corrosion and alteration of feldspars, and the formation of hematite pigment.

5.2 Petrography

5.2.1 Lithofacies A - Massive to Laminated Mudstone to Silty Mudstone

5.2.1.1 Detrital Mineralogy and Texture

Due to the fine-grained nature of this rock, the mineralogy is difficult to determine in thin section. The mudstone is composed primarily of quartz. Lithofacies A may contain 5-10% siltstone.

5.2.1.2 Authigenic Mineralogy and Texture

Lithofacies A is dolomitic. Dolomite is fine-grained and rhombic in texture.

5.2.2 Lithofacies B - Massive to Laminated Siltstone to Sandy Siltstone

5.2.2.1 Detrital Mineralogy and Texture

Lithofacies B is composed of 60-65% angular to subangular quartz with an 8-10% plagioclase and potassium feldspar component (Appendix B - B.2). Approximately 10% of Lithofacies B is composed of fine to medium-grained subangular to subrounded quartz. This quartz is randomly dispersed throughout the rock or present as lenses which are commonly associated with anhydrite cement (Plate 3A, 3C, 3D). Fine grained, disseminated hematite is present as well as illite clay (Plate 3C, 3D, Appendix B). Opaque grains (up to 5%) are scattered throughout the siltstone or concentrated in patches and/or along preserved laminae.

In thin section, synsedimentary anhydrite nodules show a distorted subrounded shape. Anhydrite appears to have grown by displacing the host sediment (Plate 8A, 8B). Nodules are composed of interlocking, elongate, lath-shaped crystals.

5.2.2.2 Authigenic Mineralogy and Texture

This siltstone lithofacies is dolomitic ranging from patchy dolomitization to complete recrystallization of the sediments. Minor "felted" anhydrite cement is also present (Plate 8C) as well as minor authigenic chlorite (Appendix B).

5.2.2.3 Porosity

This siltstone lithofacies shows good, fine-grained, intergranular porosity (Section 5.4). The porous, coarser-grained, sandstone lenses within this lithofacies are commonly cemented with anhydrite (Plate 3C, 3D). Dolomitization has resulted in the formation of micro-intercrystalline porosity.

5.2.3 Lithofacies C - Massive to Ripple Laminated, Silty, Very Fine-Grained, Lithic Subarkose

5.2.3.1 Detrital Mineralogy and Texture

This lithofacies is composed of approximately 60% quartz (Plate 4A). Quartz grains are of three distinct types: abundant fine-grained angular to subangular quartz showing straight extinction, minor, fine-

PLATE 8

Plate 8A

Photomicrograph of a sandy siltstone with nodular anhydrite showing displacive growth (a) (Lithofacies B).

16-12-26W1
906.5 metres

Plate 8B

Photomicrograph of the same sample as 8A (x-nichols). Note the lath-shaped anhydrite crystals.

16-1-2-26W1
906.5 metres

Plate 8C

Photomicrograph of siltstone with felted anhydrite cement. This photomicrograph is shown under x-nichols (Lithofacies B).

Plate 8D

Photomicrograph (x-nichols) of medium to coarse-grained subarkose showing anhydrite cement. (Lithofacies F).

11-30-1-25W1
911 metres

Plate 8E

Photomicrograph of medium-grained subarkose. Note the presence of dolomite rims (d) which were formed prior to anhydrite cementation (a) (Lithofacies E).

2-20-1-26W1
932 metres

Plate 8F

Photomicrograph of the same sample as Plate 8E under x-nichols. The arrow shows dolomite rims. Anhydrite (a).

2-20-1-26W1
932 metres

PLATE 8

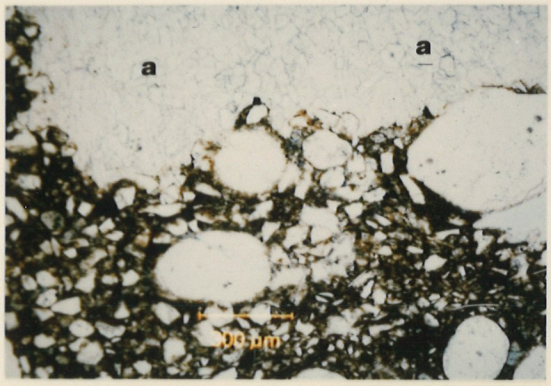

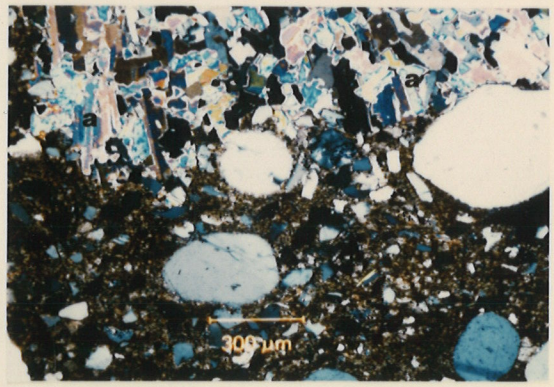

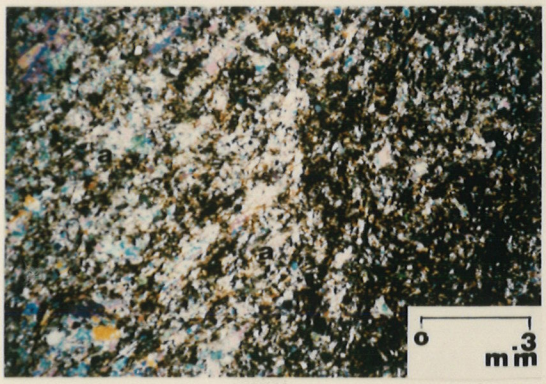

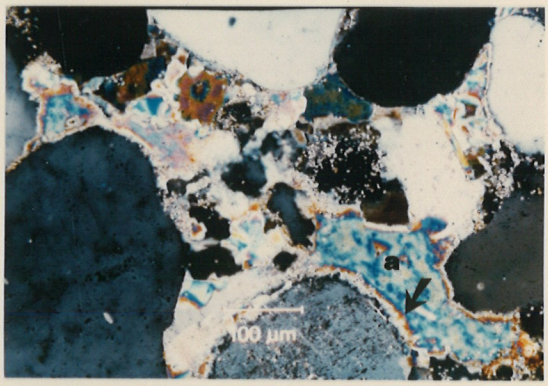

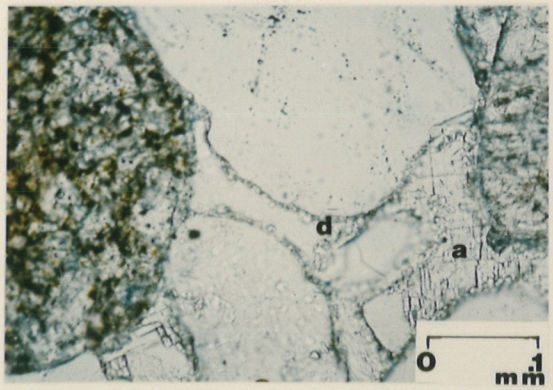

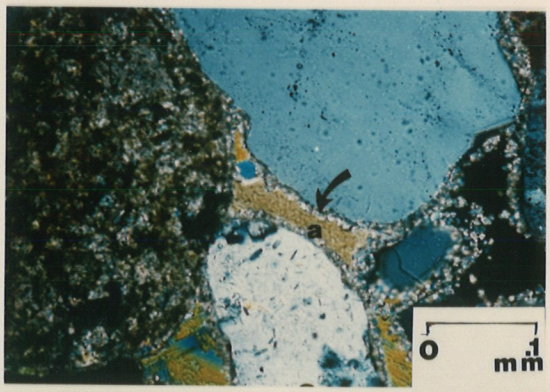

grained, sutured aggregates of quartz grains (Plate 4A, 4B), and randomly distributed well-rounded quartz grains give this fine-grained subarkose a somewhat bimodal character (Plate 4C). Approximately 10% of this rock is composed of potassium feldspar, with 2-3% plagioclase feldspar, and minor microcline (Plate 4A). McCabe (1956) noted both sodic plagioclase and orthoclase. XRD analyses indicate that the plagioclase and potassium feldspar contents are generally similar (Appendix B). All stages of feldspar corrosion is noted but for the most part feldspar minerals are very well preserved.

The composition of the fine-grained subarkose also includes approximately 8% opaque minerals. These minerals are scattered randomly throughout, or concentrated in lenses along bedding planes (Plate 4A). Other minor constituents include chert, aggregates of feldspar and quartz, garnet, glauconite, and hematite. Green, globular glauconite (1%) is present in 30-40% of the thin sections examined (Plate 4D). Where present, hematite is associated with the finer grained matrix component and found occasionally as grain coatings.

This subarkose is texturally immature with poor to moderate sorting. The rock framework is generally open with few grain to grain contacts and no evidence of extreme compaction. The percentage of clay matrix varies considerably; from 1-2% in the Omega Waskada 8-26-1-26 W1 and 6-25-1-26 W1 wells (Section 5.4) up to 15% in other areas (Plate 9A). The matrix is composed primarily of illite with a minor amount of very fine-grained subangular dolomite (Appendix B).

PLATE 9

Plate 9A

SEM photograph showing the overall texture of a fine-grained, silty subarkose (Lithofacies C).

1-13-1-26W1
917.9 metres

Plate 9B

SEM photograph of fine-grained, silty subarkose showing the dolomitized matrix (d) (Lithofacies C).

16-1-2-26W1
909.8 metres

Plate 9C

SEM photograph of the same sample as Plate 9B under higher magnification, showing the dolomitized matrix and micro-intercrystalline porosity (Lithofacies C).

16-1-2-26W1
909.8 metres

Plate 9D

SEM photograph of a fine-grained, silty subarkose showing dolomite (d) and porosity occluding anhydrite cement (a) (Lithofacies C).

16-1-2-26W1
976.5 metres

PLATE 9

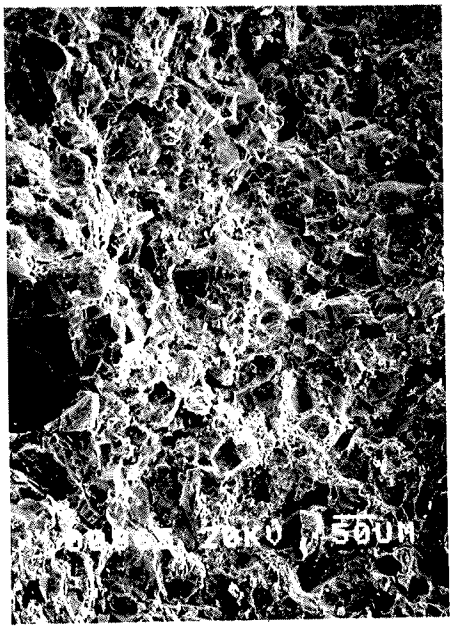

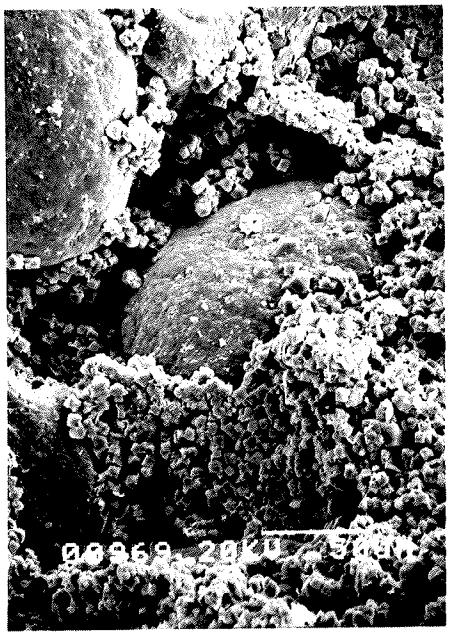

5.2.3.2 Authigenic Mineralogy and Texture

Examination of matrix dolomite under thin section and SEM shows a very fine-grained interlocking mesh of rhombic dolomite (Plate (9B-9D). Dolomitization and leaching have resulted in the formation of micro-intercrystalline porosity (Plate 9C). Fine-grained, dolomite rhombs are also present in the pore spaces of matrix-free, fine-grained subarkose (Section 5.4).

Minor (relative abundance - Appendix B) authigenic illite is present in the pore spaces of the fine-grained subarkose of the Waskada Field (Plate 10C). Illite clay has formed subsequent to the formation of pore-filling dolomite (Plate 10C). A minor component of authigenic, mixed-layer expandable chlorite; mixed-layer expandable chlorite/illite (Plate 10D); and chlorite is also present in the subarkose of the Lower Amaranth Member (Appendix B).

5.2.3.3 Porosity

Patchy, primary, intergranular porosity is present within the fine-grained subarkose. Porosity varies from 2-25% (Section 5.4). Secondary micro-intercrystalline porosity is present in the dolomitized matrix.

PLATE 10

Plate 10A

SEM photograph of fine-grained, silty subarkose showing anhydrite cement (a) and authigenic clay minerals forming subsequent to anyhydrite cementation.

9-24-2-29W1
980 metres

Plate 10B

SEM photograph of fine grained, silty subarkose showing clay grain coatings (cl) on quartz (Lithofacies C).

1-13-1-26W1
911 metres

Plate 10C

SEM photograph of very fine-grained, silty subarkose: a reservoir facies in the Waskada Field. This photograph shows illite clay (il) forming in pore spaces after the formation of dolomite (d). Note the presence of anhydrite cement (a).

6-25-1-26W1
916.5 metres

Plate 10D

SEM photograph of very fine-grained, silty subarkose: a reservoir facies in the southern Waskada Field. Note the presence of mixed layer chlorite-illite clay (mcl) forming in the pore space.

1-13-1-26W1
917.9 metres

PLATE 10

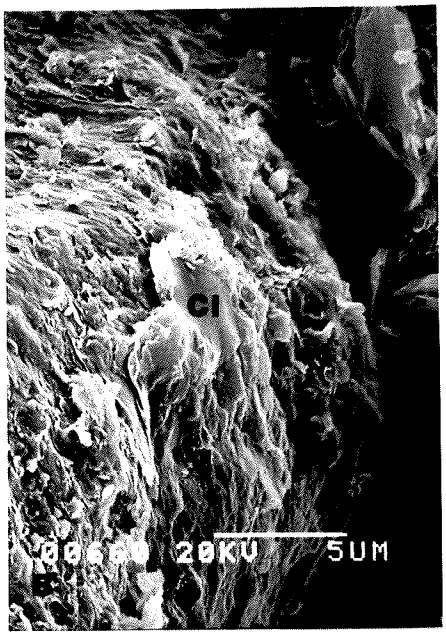

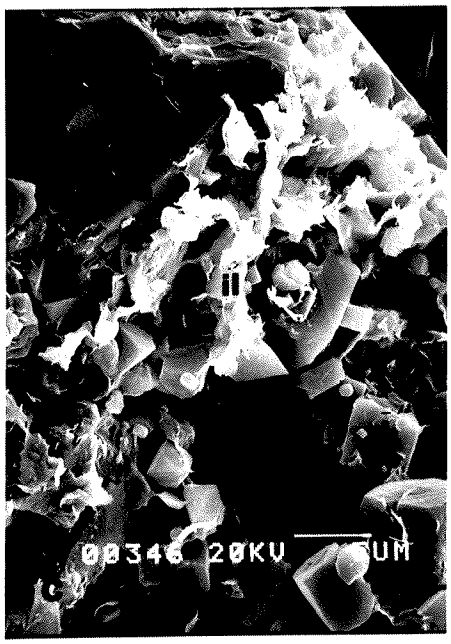

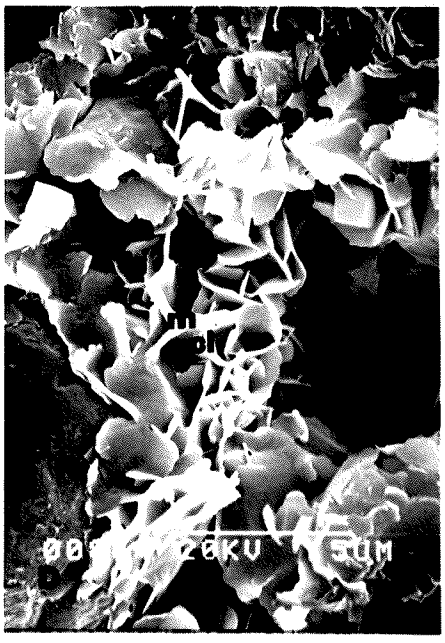

5.2.4 Lithofacies D - Interlaminated Mudstone, Siltstone, and Fine-grained Subarkose

This lithofacies is similar in mineralogical composition to lithofacies A, B, and C.

5.2.5 Lithofacies E - Parallel to Cross-Laminated, Medium-Grained, Lithic Subarkose

5.2.5.1 Detrital Mineralogy and Texture

Lithofacies E is composed of approximately 65% medium-grained, subrounded quartz grains and interlocking quartz aggregates. Approximately 5% fine-grained quartz is also present (Plates 11A). Lithofacies E contains 5-18% potassium and plagioclase feldspar, approximately 8% opaque minerals, and minor chert and chalcedony (Plate 7C, 11A).

This subarkose is texturally immature and sorting is moderate. The dolomitized clay matrix may vary from 1-10% (Plate 11B). However, matrix content is generally less significant. The more porous rocks of this lithofacies can be very friable and almost totally free of matrix and cementing material.

5.2.5.2 Authigenic Mineralogy and Texture

Authigenic hematite is present as grain coatings and along cleavage planes of quartz grains (Plate 7A, 7B). Plate 7A and 7B show the subsequent cementation of hematite coated grains by anhydrite. Close ex-

PLATE 11

Plate 11A

Photomicrograph of a medium-grained subarkose showing dolomite rims (d) around quartz grains (q) (Lithofacies E).

2-20-1-26W1
932 metres

Plate 11B

Photomicrograph (x-nichols) of a medium-grained subarkose showing chert grains and patches of anhydrite (a) cement. This photo also shows the dolomitized matrix (d) (arrow) (Lithofacies E).

16-1-2-26W1
909.8 metres

Plate 11C

Photomicrograph of fine to medium-grained subarkose showing a partially corroded feldspar grain. Blue color indicates porosity (Lithofacies E).

1-13-1-26W1
915.4 metres

Plate 11D

Photomicrograph of medium-grained subarkose showing a partially corroded feldspar grain infilled by anhydrite cement (a) (Lithofacies E).

2-20-1-26W1
929 metres

Plate 11E

Photomicrograph of sandy siltstone showing nodular anhydrite (a) (Lithofacies C).

1-13-1-26W1
921 metres

PLATE 11

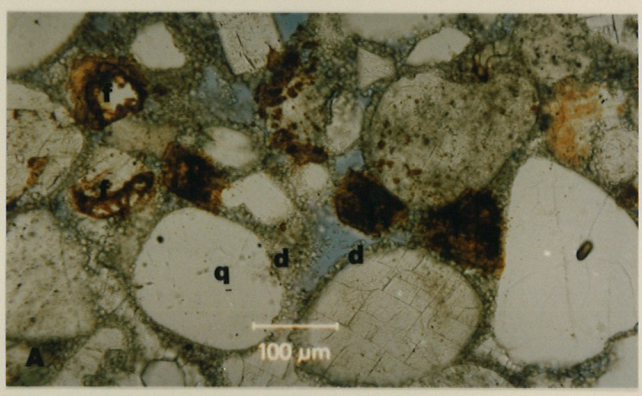

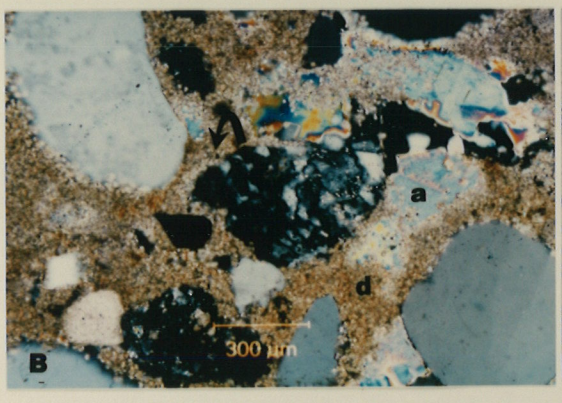

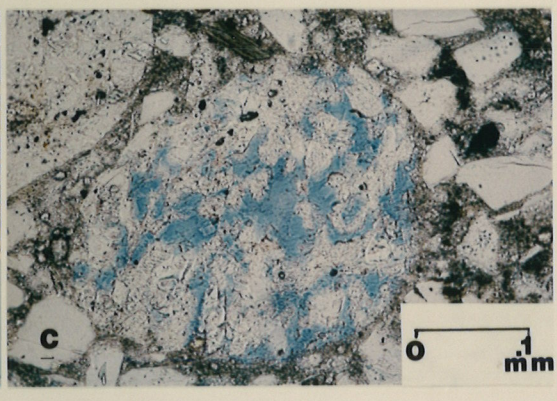

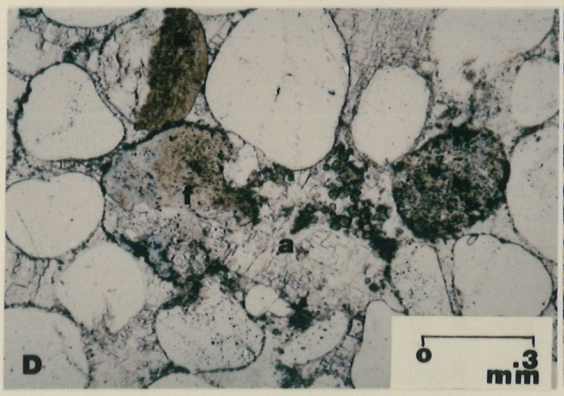

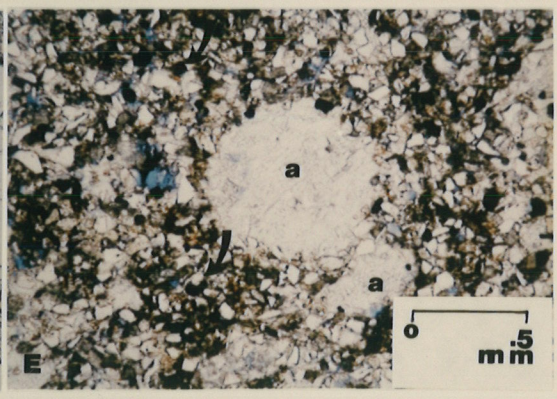

amination also reveals the presence of well-crystallized, rhombic dolomite as grain coating, within pore spaces, as well as dolomitization of matrix material (Plate 11A, 11B). An attempt was made to examine the clay mineralogy of Lithofacies E. However, in preliminary clay settling no significant clay fraction was apparent.

5.2.5.3 Porosity

These rocks show locally preserved poor to good primary intergranular porosity (Plate 11A). Although in general, any pre-existing porosity is occluded by poikilotopic anhydrite cement (Plate 11D). Leaching and partial to complete dissolution of feldspar grains have resulted in the formation of minor secondary intraparticle porosity (Plate 11C). In some cases, this intraparticle porosity is infilled by anhydrite cement (Plate 11D).

5.2.6 Lithofacies F - Massive, Coarse-grained, Feldspathic Sublitharenite

5.2.6.1 Detrital Mineralogy and Texture

Lithofacies F is composed of approximately 60-65% well-rounded quartz with minor aggregates of well-rounded sutured quartz grains. The remainder of the rock is composed of 5-18% potassium and plagioclase feldspar, 15% chert and rock aggregates of feldspar and quartz, and minor zebraic chalcedony.

The framework is open and with minor tangential grain to grain contacts. No evidence of extreme compaction was noted. This is a very clean rock with very minor (1%) clay matrix (Plate 7E).

5.2.6.2 Authigenic Mineralogy and Texture

Lithofacies G is well indurated by poikilotopic anhydrite cement (Plate 7E, 8D-8F). There is very minor development of quartz overgrowths.

5.2.6.3 Porosity

The corrosion of feldspar is associated with the formation of secondary porosity (1-2%). This secondary porosity is occasionally infilled with anhydrite cement. Otherwise this lithofacies is tight.

5.3 Diagenesis

5.3.1 Dolomitization

Dolomite is a major component in the rocks of the Lower Amaranth Member. It is present as dolomite rims, dolomite infilling pore spaces, and laterally extensive dolomitization of fine-grained sediment.

Several models have been suggested to explain the occurrence of dolomite. These models include seepage-reflux, the burial-compaction model, and mixed-water dolomitization which have been discussed in detail

by Morrow (1982) and Zenger and Dunham (1980). Their work also includes several variations on the three general models listed.

The seepage reflux model is well suited to explain the presence of dolomite in the Lower Amaranth Member. This interpretation is supported by the following:

1. the great lateral extent of dolomitization of fine-grained sediment;
2. the association of the Lower Amaranth with evaporites (nodular anhydrite and the overlying Upper Amaranth evaporite); and
3. deposition in a tidal flat (shallow-marine) environment.

A source of Mg^{2+} is one of the primary requirements for the formation of dolomite (Morrow, 1982; Zenger and Dunham, 1980). The dolomitization reaction occurs following gypsum (anhydrite) precipitation when the Mg^{2+}/Ca^{2+} ratio approaches 9.0 (Morrow, 1982). Isolated patches of dolomite often indicate a local source of Mg^{2+} ion-rich fluid whereas extensive dolomitization suggests a more prolific external source of Mg^{2+}. The widespread occurrence of dolomite in near-shore marine sediments is best explained by the seepage-reflux model due to the percolation of dense hypersaline brines through the sediment soon after deposition (Morrow, 1982).

5.3.2 Anhydritization

Anhydrite is present within the rocks of the Lower Amaranth Member as poikilotopic anhydrite cement and minor felted anhydrite cement which is associated with the fine-grained siltstones (Plate 8C). The majority of the anhydrite cement is present as large, lath-shaped crystals commonly known as "crystallographic" anhydrite (Plate 6E, 7A, 7B, 8D-8F). Anhydrite cement is preferentially associated with the coarser grained rocks of Lithofacies E and Lithofacies F.

Anhydrite cement was formed by the precipitation of anhydrite or gypsum from sulphate-rich formation waters which circulate preferentially through more porous and permeable sediments after lithification. These fluids may have been associated with the overlying Upper Amaranth evaporites and/or formation waters associated with the Lower Amaranth sequence.

5.3.3 Iron Oxides

Hematite grain coats and the presence of hematite pigment along cleavage planes suggests a diagenetic origin for a portion of the hematite present in the rocks of the Lower Amaranth Member (Plate 7A, 7B).

The conditions required for the formation of hematite have been discussed in Section 4.3.1 Authigenic hematite is the product of in-situ

alteration of ferromagnesium silicates to anhydrous ferric oxide and the subsequent aging to hematite (Walker, 1967).

5.3.4 Corrosion of Feldspar

Several varieties of feldspar are present in the Lower Amaranth Member. The two most significant constituents are angular to subangular plagioclase and potassium feldspar (Appendix B). Feldspars are present in various stages of preservation ranging from fresh grains to partial alteration (Plate 11C). However, for the most part, feldspars are fairly well preserved. There is no evidence of the formation of authigenic feldspar minerals.

The alteration of feldspar minerals is associated with the weathering process. Dissolution of feldspar is also common to the burial environment where secondary alteration is controlled by the pressure and temperature stability of the feldspar mineral (Thomas, 1985), and by the thermal history of the sedimentary sequence.

5.3.5 Authigenic Clay Minerals

Examination of the fine-grained subarkose (Lithofaces C) and the siltstones (Lithofacies B) of the Lower Amaranth Member indicate the presence of authigenic clay minerals (Appendix B). Authigenic clay min-

erals are most prevalent in the pore spaces of the matrix-free, fine-grained subarkose of the Waskada Field (Plate 10C, 10D).

Authigenic clay minerals can form at various times during the diagenetic history of a sedimentary sequence. Authigenic clay minerals form by several processes:

a) transformation (recrystallization) of a detrital clay;
b) alteration of a parent mineral or grain;
c) congruent dissolution of a parent mineral grain and re-precipitation from solution; and
d) direct precipitation in pore space from migrating silicate-bearing pore water (Pittman, 1972).

5.3.6 Diagenetic History of the Lower Amaranth Member

Based on the relationship of authigenic minerals to the host rock, a diagenetic sequence is proposed for the rocks of the Lower Amaranth (Figure 21). Diagenetic processes have been classified as syndepositional (pre-burial), early burial, and early to intermediate burial.

Syndepositional

Hematization
Formation of Nodular Anhydrite
Corrosion of Feldspar

Early Burial

Dolomitization
Compaction

Early-Intermediate Burial

Corrosion of Feldspar
Formation of Authigenic Clay Minerals
Precipitation of Anhydrite Cement

FIGURE 21: DIAGENETIC SEQUENCE - LOWER AMARANTH MEMBER

5.3.6.1 Syndepositional

The formation of nodular anhydrite, the alteration of ferromagnesium silicates to hematite, and the alteration of feldspar minerals are interpreted as syndepositional or pre-burial processes. Nodular anhydrite forms by the displacive growth of unlithified sediment (Plate 11E) (Section 4.3.5).

Hematite is known to form in the pre-burial environment (Walker, 1967). Petrographic examination of the Lower Amaranth Member (Plate 7A, 7B) showed the presence of hematite coated quartz grains which were subsequently cemented by anhydrite. Although this observation does not indicate a pre-burial genesis, it does indicate formation of hematite prior to the precipitation of anhydrite cement.

The leaching and breakdown of feldspar minerals is due to the weathering process common to subaerally exposed rocks and/or sediments (Section 4.3.3). The presence of pre-existing intraparticle porosity (leaching of feldspar) which has been occluded by anhydrite (Plate 11D) indicates that some feldspar corrosion occurred prior to the precipitation of anhydrite cement.

5.3.6.2 Early Burial

Dolomitization and sediment compaction in the Lower Amaranth Member are classified as early burial processes. Morrow (1982) differentiated between finely crystalline dolomite (<10-20 m) and a coarsely crystalline dolomite. The finer grained dolomite is commonly formed in a pre-burial to early burial diagenetic setting, whereas the coarsely grained dolomite is formed in a late replacement diagenetic environment (Morrow, 1982). An interlocking rhombic dolomite, characteristic of the Lower Amaranth Member, is the result of continual growth of original dolomite during subsequent burial (Morrow, 1982).

Dolomite rims in the Lower Amaranth Member were formed prior to anhydrite cementation (Plate 8E, 8F) as indicated by the presence of dolomite-rimmed quartz grains which have been subsequently cemented by anhydrite. Plate 10C illustrates the formation of pore-filling dolomite prior to the formation of authigenic illite. In this sample, illite clay has formed around the dolomite rhombs.

5.3.6.3 Early Intermediate Burial

The formation of authigenic clay minerals and the precipitation of poikilotopic and felted anhydrite cement are early to intermediate burial processes. As shown in scanning electron microscopy, authigenic clay minerals formed subsequent to the formation of pore-filling dolomite.

The presence of poikilotopic anhydrite cement within pore spaces which lithifies both hematite-coated quartz and dolomite-rimmed quartz, and within corroded feldspar grains suggest that the precipitation of anhydrite is one of the later diagenetic processes in the post-burial history of the Lower Amaranth. The coarsely crystalline nature of anhydrite cement also indicates that anhydrite precipitated at an early to intermediate burial stage.

5.4 Reservoir Quality of the Lower Amaranth Member

5.4.1 Reservoir Facies

The main reservoir rock in the Lower Amaranth Member is the fine-grained, silty subarkose of Lithofacies C. Porosity is dominantly modified, primary intergranular which varies from 2-25%. Micro-intercrystalline porosity is also present in the reservoir rock associated with dolomitization of the matrix and subsequent leaching.

5.4.2 Reservoir Distribution

In the study area, the Coulter and Waskada Fields contain the thickest development of fine-grained subarkose (Lithofacies C) (Figure 13-17) (Section 3.6). The Coulter Field is characterized by a very silty, fine-grained subarkose (Lithofacies C) with porosities from 2-10% and permeability <1 millidarcy. This rock is comprised of a 10% clay matrix component and interlaminated siltstone lenses. Consequently, porosity is patchy and unevenly distributed. Secondary micro-intercrystalline porosity is present in this siltier subarkose associated with dolomitization of the matrix. The cores from this field are commonly saturated with dead oil and show evidence of pin-point bleeding.

The best porosity and permeability is present in the central to south-central Waskada Field. Primary, intergranular porosity averages approximately 25% with permeabilities of 1-10 millidarcys occasionally reaching 100 millidarcies (Barchyn, 1982). These porosities and permeabilities are associated with a more friable, fine-grained subarkose (Lithofacies C), composed of 1-2% clay matrix with no anhydrite cement. In thin section, these rocks are well-sorted with even porosity distribution (Plate 12A).

Although it was beyond the scope of this study to map the extent of this porosity, from examining cores in the area, the most attractive reservoir rock is present in wells located in Sections 1, 9, 12, 13,

PLATE 12

Plate 12A

Photomicrograph of a fine-grained subarkose. This photo illustrates excellent primary intergranular porosity (Lithofacies C).

1-13-1-26W1
917 metres

Plate 12B

Photomicrograph of very fine-grained, silty subarkose to sandy siltstone showing patchy intergranular porosity (Lithofacies C).

16-1-2-26W1
901 metres

Plate 12C

Photomicrograph of very fine-grained subarkose showing patchy uneven intergranular porosity distribution (Lithofacies C).

16-1-26W1
909.8 metres

Plate 12D

Photomicrograph of very fine-grained subarkose showing good primary intergranular porosity with residual hydrocarbon (Lithofacies C).

8-26-1-26W1
913 metres

Plate 12E

Photomicrograph of the same sample as Plate 10D under higher magnification. Note the presence of residual hydrocarbon (Lithofacies C).

8-26-1-26W1
913 metres

PLATE 12

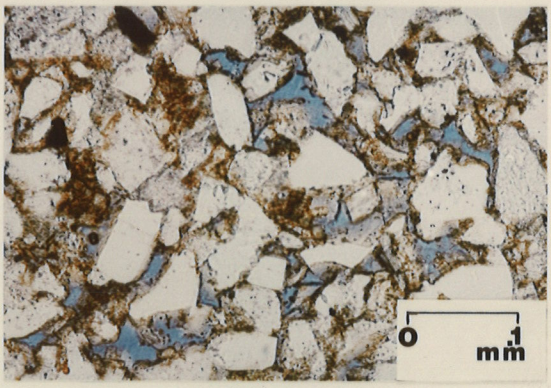

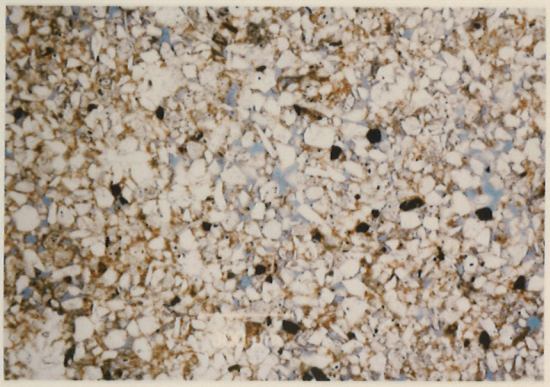

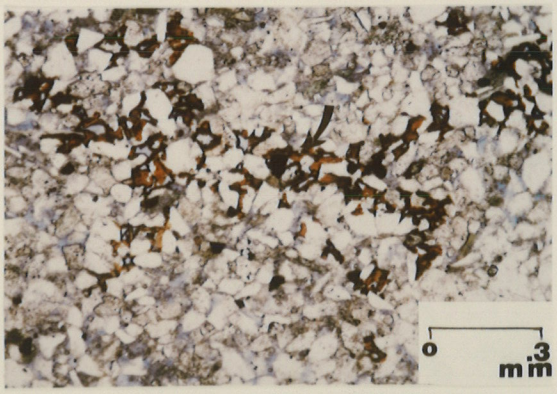

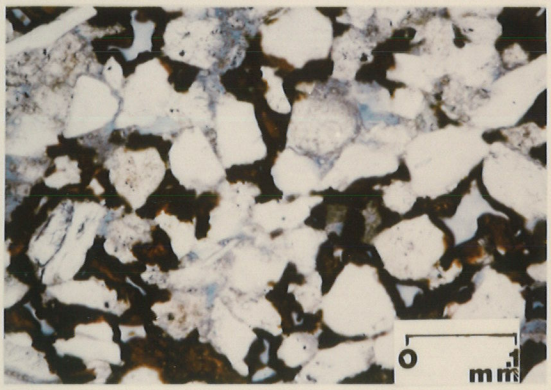

25, 26 Twp. 26, Rge. 1 W1 and extends easterly to Section 30, Twp. 25, Rge. 1, W1. Porosity and permeability decrease outward from the central Waskada Field where rocks become poorly sorted with an increase in the silty component (Plate 12B - 12E).

5.4.3 Controls on Porosity Development and Preservation

The three major controls on the development and preservation of porosity in the Lower Amaranth Member are the depositional environment, anhydritization, and dolomitization.

5.4.3.1 Depositional Setting

In the study area the best porosity and permeability is associated with the well-sorted, matrix-free, fine-grained subarkose of the central and south central Waskada Field. The textural variation in the fine-grained subarkose (Lithofacies C) is attributed to a localized higher energy regime during the deposition of sediment. This higher energy regime was probably associated with the "Waskada" dome structure in the central Waskada Field (Chapter 6) where sediments were well sorted, and winnowing of silts and clays occured due to current or wave action.

5.4.3.2 Anhydritization

Anhydrite cement is the second major control on porosity preservation in the Lower Amaranth Member. Any pre-existing porosity in the medium-grained subarkose (Lithofacies E) and the coarse-grained sublitharenite

(Lithofacies F) has been completely occluded by poikilotopic anhydrite cement. Porosity associated with medium-grained sand lenses in the fine-grained subarkose (Lithofacies C) is also occluded by anhydrite.

5.4.3.3 Dolomitization

A major control on porosity enhancement in the silty, fine-grained subarkose of the Lower Amaranth Member is dolomitization. Dolomitization and subsequent leaching has resulted in the formation of micro-intercrystalline porosity (Plate 13D).

Dolomite has also partially occluded porosity in the matrix-free, well-sorted, fine-grained subarkose in the central Waskada Field (Plate 13B, 13C). Migration of fine-grained, pore dolomite may result with the introduction of drilling and completion fluids to the reservoir. This may cause partial to complete blockage of the pore throats.

5.4.3.4 Authigenic Clay Minerals

Several varieties of authigenic clay minerals are present in the pore spaces of the fine-grained subarkose. Although these clays only partially alter existing porosity, expandable and mixed layer authigenic clay minerals (Appendix B) are sensitive to drilling and stimulation fluids. The introduction of these fluids into the reservoir can cause migration and swelling of clay minerals and blockage of pore throats resulting in a decrease in effective porosity and a subsequent decline

PLATE 13

Plate 13A

SEM photograph of silty, fine-grained subarkose showing the overall texture of a reservoir rock in the central Waskada Field.

6-26-1-26W1
917.1 metres

Plate 13B

SEM photograph of the same sample as Plate 11A under higher magnification. Note primary intergranular porosity partially occluded by dolomite (d).

6-26-1-26W1
917.1 metres

Plate 13C

SEM photograph of very fine-grained, silty subarkose: a reservoir facies in the Waskada Field. This photogrpah shows dolomite (d) partially occluding primary inter-granular porosity. Note the difference in grain size of this dolomite and the matrix dolomite to the left (d).

6-26-1-26W1
916.5 metres

Plate 13D

SEM photograph of very fine-grained, silty subarkose: showing micro-intercrystalline porosity in the dolomitized matrix (d).

16-1-2-26W1
909.8 metres

PLATE 13

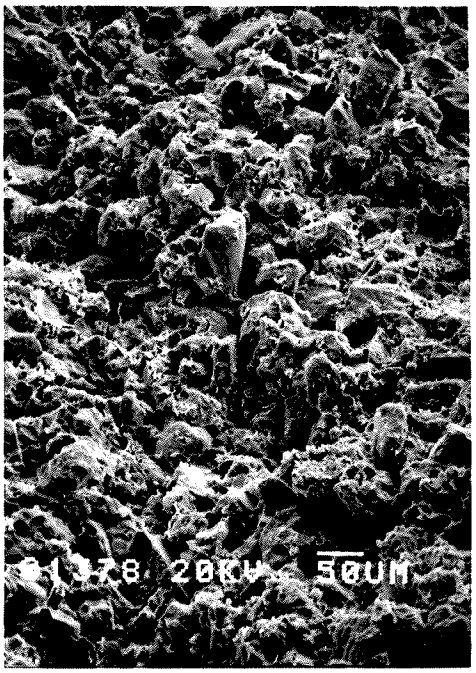

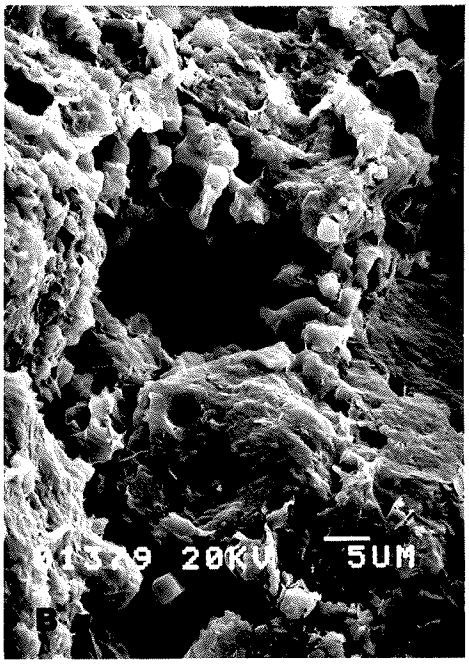

in the rate of oil production (Wilson and Pittman, 1977; Almon and Davis, 1978).

CHAPTER 6: SIGNIFICANCE TO OIL EXPLORATION

6.1 Exploration History - Southwestern Manitoba

Hydrocarbon exploration in southwestern Manitoba has been active since the early 1950's. Commercial oil production was established in the Pierson area in 1950 (Figure 2) from the Mission Canyon Formation, with several other small Mission Canyon pools delineated in the Waskada area (Rodgers, 1986).

The Waskada Lower Amaranth oil pool was discovered in 1980 when Omega Hydrocarbons recompleted a former Mission Canyon oil producer in the stratigraphically higher Lower Amaranth Member (Barchyn, 1982, 1984). This success marked the first commercial oil production from a non-Mississippian reservoir in the province (Barchyn, 1982). Since that time, several new Mission Canyon pools have also been discovered within the Waskada Field (Rodgers, 1986). Development in the Waskada area is currently in progress.

Following concurrently with the discovery at Waskada, a second area of Lower Amaranth oil potential was identified within the South Pierson Field by Cobra Oil and Gas Corporation. However, only limited development has occurred and the parameters of the pool are poorly defined (Barchyn, 1982). In 1983, Newscope Resources discovered a third

Lower Amaranth pool at Coulter, Manitoba (Figure 2). Although the field is currently under production, only minimal development ensued.

6.2 Hydrocarbon Entrapment in the Lower Amaranth Member

In the study area, Lower Amaranth oil accumulations are controlled by a combination of complex structure, stratigraphy and diagenesis.

6.2.1 The Significance of Structural Geology

McCabe (1959) described the presence of a Mission Canyon structural dome in the central portion of the present day Waskada Field. He attributed this structure to multi-stage dissolution of the underlying Devonian Prairie evaporite and the subsequent collapse of overlying strata. There is evidence, from deep well control, of at least one major solution event during early Mississippian time which is supported by an overthickened Bakken section extending through the entire central Waskada Field (McCabe, 1959). Late Mississippian and possibly Jurassic and Cretaceous salt solution has also been speculated in the Waskada area.

The "dome-type" feature at Waskada was subsequently exposed to erosion where porous carbonates of the MC-1 member were exposed to the surface and porous carbonates of the MC-3 member were preserved in paleotopographic lows (Figure 3) (Rogers, 1986, McCabe, 1959).

A similar structural style to the Waskada area is discussed by Halabura (in press) in the Pierson Field. Halabura (in press) and McCabe (1959) have described Mission Canyon anticlinal features which they attribute to multi-stage salt solution and collapse.

At Pierson these anticlinal structures were also breached by erosion exposing porous Mission Canyon Members to the subcrop. Porous units were preserved in paleotopographic lows (Halabura, in press).

6.2.2 The Significance of Diagenetic Alteration

Mississippian aged carbonates exposed at the unconformity surface are commonly characterized by an upper diagenetic zone or "dense-cap". This "dense-cap" is a dolomitized-anhydritized zone which is extremely variable in thickness. Formation of the "dense-cap" is the result of sulphate-rich formation waters associated with the Amaranth evaporite percolating downward into the porous carbonate (McCabe, 1959). The thickness of the Lower Amaranth Member and the porosity of the Mission Canyon Member exposed at the unconformity to some extent control the thickness of the "dense cap" (McCabe, 1959). Although for the most part, the thickness is extremely unpredictable.

In the Pierson area, the "dense-cap" forms an effective seal trapping hydrocarbon at the unconformity surface (Halabura, in press). However, in the central Waskada area, the "dense-cap" appears to be very thin

or absent (near Waskada dome). Bachryn (1982) suggested that due to the lack of an effective seal, oil has migrated upward from the Mission Canyon Formation into the porous Lower Amaranth Member. Consequently, oil production in the Pierson Field is dominantly from the Mission Canyon Formation, whereas the Waskada and Coulter Fields are characterized by Lower Amaranth oil accumulations.

6.3 Model for Lower Amaranth Oil Production (Newburg-South Westhope Fields, North Dakota)

Migration and accumulation of hydrocarbon in the Waskada Field, south western Manitoba is similar to the model discussed by Marafi (1970) for the Newburg-South Westhope Fields. The Newburg-South Westhope Fields are located in North Dakota approximately twenty kilometres south of the Waskada Field.

The Newburg-South Westhope Fields are examples of a stratigraphic-structural trap. These fields are situated along the eastern flank of a syncline associated with salt solution of the Devonian Prairie Formation and collapse of the overlying strata. Here, structurally-low, porous, Mississippian rocks of the Ratcliffe interval were preserved from erosion. Paleotopographic lows were infilled by thick deposits of the Saude Member of the Spearfish Formation (Section 2.3).

In North Dakota, the Saude Member is composed of a basal sand overlain by an impermeable, reddish siltstone and shale, which in turn is overlain by a "water wet" fine-grained sandstone, and finally by a second impermeable reddish siltstone and shale. The basal sand unit of the Saude Member in North Dakota pinches out against a structural high. Consequently, this sand is not present at Waskada (Barchyn, 1982; Braun, pers. comm.). The fine-grained "wet" sandstone of the Saude Member is equivalent to the hydrocarbon-bearing unit in Manitoba. This sandstone unit is the "lower sandy unit" of Barchyn (1982) (Figure 7).

Oil at Newburg-South Westhope is produced from the Ratcliffe interval of the Charles Formation and the overlying Saude Member of the Spearfish Formation (Figure 3). The two producing zones are separated by a major unconformity. Marafi (1970) suggested that oil migrated updip into the basal sand of the Saude Member from the underlying Ratcliffe. He considered the Ratcliffe interval and the Saude Member to be a common reservoir. The impermeable siltstones and shales of the Saude Member prevent updip hydrocarbon migration (Marafi, 1970). Consequently the Saude Member acts as both the reservoir and the seal.

Similarly the Waskada Field is an example of a stratigraphic-structural trap. Oil has migrated into structurally high porous carbonate of the Mission Canyon Formation. Owing to the absence of an effective seal, oil has continued to migrate into the overlying Lower Amaranth Member and laterally within the subarkose units (Figure 22). Hydrocarbon has

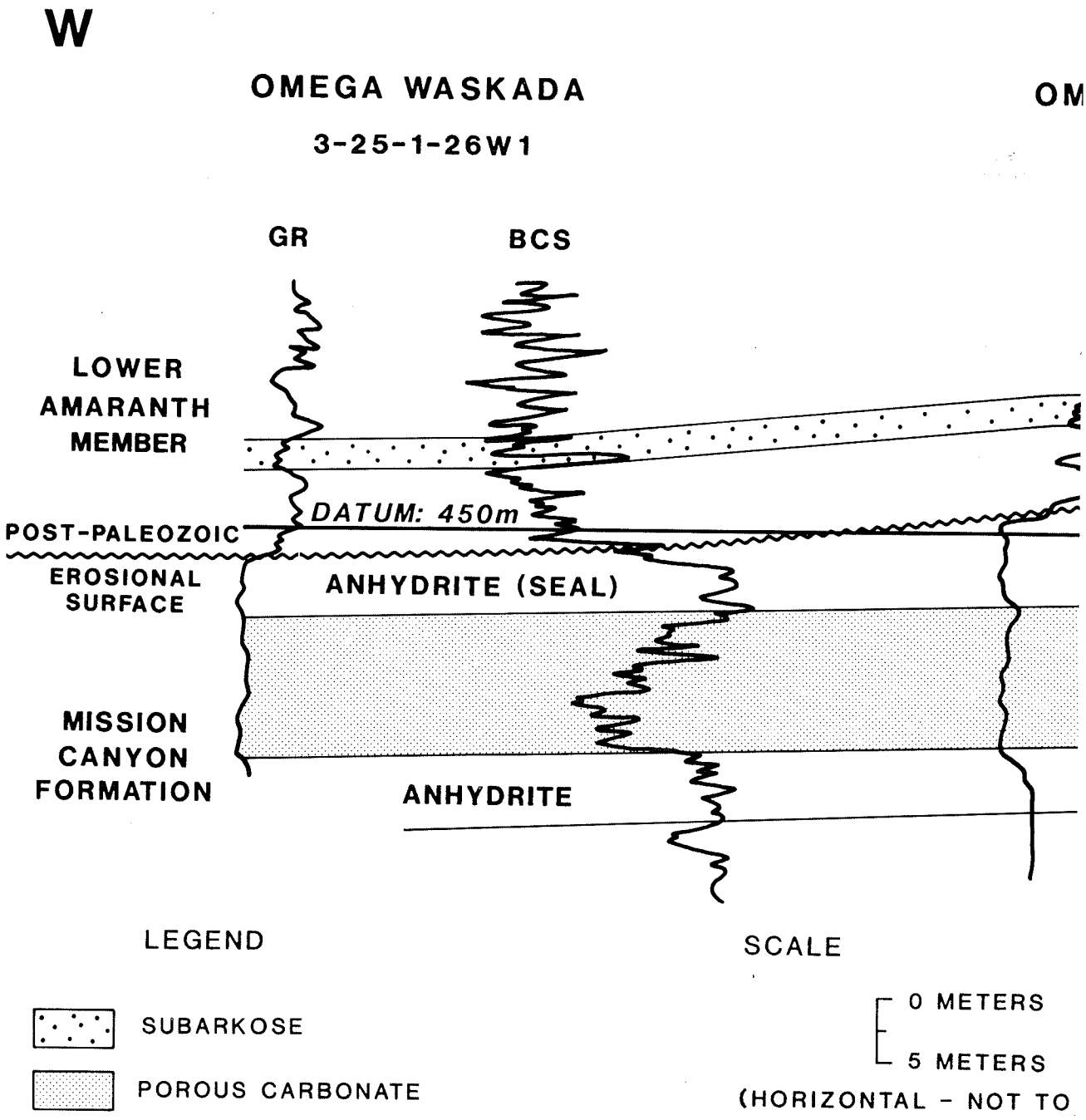

FIGURE 22 : SCHEMATIC STRUCTURAL (

E

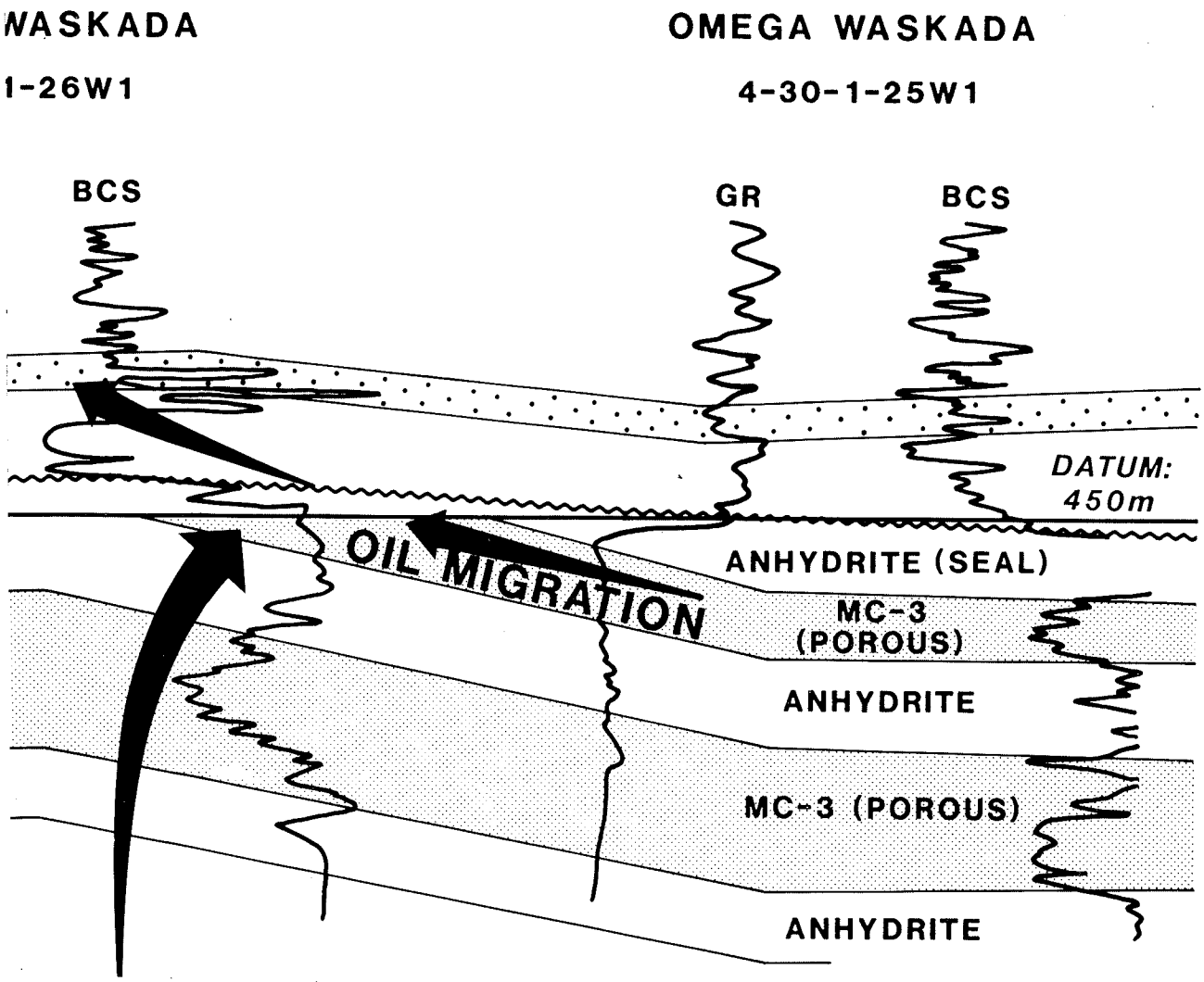

POROUS CARBONATE AT SUBCROP
ABSENCE OF TOP SEAL

SECTION, CENTRAL WASKADA FIELD

been trapped stratigraphically by the overlying impermeable siltstone and mudstone of the Lower Amaranth Member and laterally by the decrease in porosity and permeability within the sequence. (Barchyn, 1982; Halabura and Hansen, 1986).

6.4 Exploration For Lower Amaranth Oil Accumulations, Manitoba

The following points may be worth considering when exploring for hydrocarbon in the Lower Amaranth Member:

1. multi-stage salt solution and structural disturbance in the underlying Mississippian section;

2. the absence of a diagenetic "dense-cap" or other effective seal which allows the migration of hydrocarbon into the overlying Lower Amaranth; and

3. Mississippian highs are coincident with winnowing and better sorting of sediment of the Lower Amaranth Member.

The most promising areas to search for hydrocarbon in the Lower Amaranth Member is in the vicinity of salt solution and collapse features in the underlying Mississippian Mission Canyon Formation. These structures are best detected from seismic and isopachous maps of time stratigraphic units. Anomalous thickening of sediment within a given

horizon may indicate salt solution. In order to locate internal Mission Canyon anticlinal features, mapping of the individual members of the Mission Canyon Formation is also necessary. Structure on the unconformity surface may reflect differential erosion and does not necessarily indicate internal Mississippian structure due to salt solution.

6.5 Production History of the Waskada Field

Fifteen wells were chosen for production decline analysis from the Waskada Field based on continual production over a two year period (Petroleum Branch, Manitoba Department of Energy and Mines). Due to the lack of sufficient data at the time of study, several wells were chosen which had been "shut-in" for 2-3 month periods.

Initial production in the Lower Amaranth Member is at maximum 12 m^3/d to 2 m^3/d. The Lower Amaranth Member is characterized by a fairly rapid production decline rate of a 6-24 month period with production stabilizing at 1-3 m^3/d. This sequence is further characterized by high water cuts. Pressure maintenance by the use of waterflood and gas injection has been introduced to the field.

CHAPTER 7: SUMMARY AND CONCLUSIONS

1. The Lower Amaranth Member represents the first preserved sedimentation following a period of extensive post-Paleozoic erosion. The Lower Amaranth Member is separated from the underlying Mississippian sequence by a marked angular unconformity.

2. Age dating of the Lower Amaranth Member is controversial. The Lower Amaranth may be Triassic or middle Jurassic in age. Based on previous work in Manitoba, a middle Jurassic age has been accepted in this study.

3. Six lithofacies are recognized in the Lower Amaranth Member:

   A. Massive to Interlaminated Mudstone to Silty Mudstone;
   B. Massive to Interlaminated Siltstone to Sandy Siltstone;
   C. Massive to Interlaminated, Silty, Very Fine-Grained, Lithic Subarkose;
   D. Interlaminated Mudstone, Siltstone, and Fine-Grained Subarkose;
   E. Massive to Laminated, Medium-Grained, Lithic Subarkose; and
   F. Massive, Coarse-Grained, Feldspathic Sublitharenite.

   The Lower Amaranth Member can be divided into a basal "lower sandy unit" and an "upper shaly unit". In the "lower sandy unit", the

lithofacies were deposited as "stacked" or repeated fining-upward sequences which can be sub-divided into two main sequences:

(a) a coarse-sequence deposited locally as a coarse-grained sublitharenite (Lithofacies F) fining-upward to parallel to cross-bedded, medium-grained subarkose (Lithofacies E), a wavy-bedded facies (Lithofacies D), and a siltstone and/or mudstone (Lithofacies A, B); and

(b) a more prevalent sequence composed of a basal, silty, glauconitic, fine-grained subarkose, with locally preserved ripple lamination and a generally blanket-type geometry (Lithofacies C), which fines upward to a wavy-lenticular bedded facies (Lithofacies D) and a siltstone (Lithofacies B).

The "upper shaly unit" is composed of reddish-brown siltstone and mudstone with locally developed fine-grained subarkose.

4. The Lower Amaranth Member was deposited in a low-energy, hypersaline, tidal-flat environment with a prevailing arid climate. Sediments were deposited along the flank of the Williston Basin in the restricted Amaranth sub-basin. Deposition of sediment was associated with periodic inundation of the tidal flat and subsequent exposure of sediment.

5. The "cuesta" type topography of the Mississippian unconformity has influenced the thickness of the Lower Amaranth Member. Subparallel, elongate belts of thick Lower Amaranth are coincident with paleotopographic lows.

6. The main diagenetic events modifying sediments of the Lower Amaranth Member include dolomitization due to seepage refluxion, and precipitation of poikilotopic anhydrite cements.

7. The silty, fine-grained subarkose of Lithofacies C is the reservoir rock in the Lower Amaranth Member. Reservoir quality is controlled by the depositional environment, and by dolomitization and anhydrite cementation. Any pre-existing porosity in the coarser-grained rocks of Lithofacies E and F has been occluded by anhydrite cement.

   Porosity in Lithofacies C is primary intergranular and secondary micro-intercrystalline associated with the dolomitized matrix. Primary intergranular porosity is modified by fine-grained dolomite and authigenic clay minerals. The best porosity and permeability is developed in the central Waskada Field. For the most part, porosity is patchy with low permeability.

8. The Lower Amaranth Member is a target for the exploration of stratigraphically trapped hydrocarbons. The presence of hydro-

carbon is closely tied with structural disturbance in the underlying Mississippian sequence associated with dissolution of the Devonian Prairie evaporite and collapse of overlying strata. At Waskada, the absence of a "dense-cap" or other effective seal has allowed upward migration of hydrocarbon from the Mission Canyon Formation into the overlying Lower Amaranth sequence. Oil is trapped stratigraphically by a decrease in permeability-porosity and by the impermeable siltstone of the upper portion of the Lower Amaranth Member.

REFERENCES CITED

Allen, J.R.L. 1982. Sedimentary structures, their character and physical basis. Volume I and II. In: Developments in Sedimentology. New York: Elesevier. p. 593.

Almon, W.R. and Davies, D.K. 1978. Clay technology and well stimulation. Transactions of the Gulf Coast Association of Geological Societies - 28th Annual Meeting, p. 1-6.

Barchyn, D. 1982. Geology and hydrocarbon potential of the Lower Amaranth Formation, Waskada-Pierson area, southwestern Manitoba. Mineral Resources Division, Manitoba Department of Energy and Mines, Geological Report GR 82-6, p. 30.

Barchyn, D. 1984. The Waskada Lower Amaranth (Spearfish) oil pool, southwestern Manitoba: a model for Spearfish exploration in Saskatchewan. In: Lorsong, J. and Wilson, M. (eds): Oil and Gas in Saskatchewan. Saskatchewan Geological Society, Special Publication No. 7, p. 103-111.

Blatt, H., Middleton, G., and Murray, R. 1980. Origin of sedimentary rocks. New Jersey: Prentice-Hall Inc., p. 634.

Carlson, C.E. 1968. Triassic-Jurassic of Alberta, Saskatchewan, Manitoba, Montana, and North Dakota. American Association of Petroleum Geologists Bulletin, v. 52, no. 10, p. 1969-1983.

Choquette, P.W., and Pray, L.C. 1970. Geological nomenclature and classification of porosity in sedimentary carbonates. Bulletin of the American Association of Petroleum Geologists, v. 54, p. 207-244.

Christopher, J.E. 1984. Depositional patterns and oil field trends in the Lower Mesozoic of the northern Williston Basin, Canada. In: Lorsong, J. and Wilson, M.A. (eds): Oil and Gas in Saskatchewan. Saskatchewan Geological Society, Special Publication No. 7, p. 103-111.

Connolly, E. T. and Reed, P.A. 1983. Full spectrum formation evaluation, Canadian Well Logging Society, v. 12, p. 23-70.

Cummings, A.D., 1953. The Watrous strata in Saskatchewan. The first international Williston Basin symposium, North Dakota and Saskatchewan Geological Societies, p. 8.

Dean, W.E., Davies, G.R., Anderson, R.Y. 1975. Sedimentological significance of nodular and laminated anhydrite. Geology, v. 3, n. 7, p. 367-372.

De Mille, G., Shouldice, J.R., and Nelson, H.W. 1964. Collapse Structures related to evaporites of the Prairie Formation, Saskatchewan. Geological Society of America Bulletin, v. 75, p. 307-316.

Dow, W.C. 1967. The Spearfish Formation in the Williston Basin of western North Dakota. North Dakota Geological Survey, Bulletin 52, p. 27.

Elliott, T. 1978. Clastic shorelines. In: Reading, H.G. (ed). Sedimentary Environments and Facies, New York: Elsevier, p. 143-178.

Evans, G. 1965. Intertidal flat sediments and their environments of deposition in the Wash: Quarterly Journal Geological Society of London, v. 121, p. 209-245.

Evans, G. 1975. Intertidal flat deposits of the Wash, western margin of the North Sea. In: Ginsberg, R.N. (ed): Tidal Deposits - a Casebook of Recent Examples and Fossil Counterparts. New York: Springer-Verlag, p. 13-21.

Folk, R.L. 1972. Petrology of sedimentary rocks. Hemphill: Austin, Texas, p. 182.

Goddard, E.N., Trask, P.D., DeFord, R.K., Rove, O.N., Singewald, J.T., and Overbeck, R.M. 1948. Rock color chart. Geological Society of America: Boulder, Colorado.

Hadley, H.D., and Milner, R.L. 1953. Stratigraphy of the lower Cretaceous and Jurassic, northern Montana-southwestern Saskatchewan. In: Parker, J.M. (ed): Little Rocky Mountain-Montana, Southwestern Saskatchewan. Billings Geological Society Guidebook, Fourth Annual Field Conference, p. 85-86.

Halabura, S.P. (in press.). Petroleum Geology of the MC-3 Member, Mission Canyon Formation, Pierson Field. Manitoba. Minerals Resources Division, Manitoba Department of Energy and Mines.

Halabura, S.P., and Hansen, B.J. 1986. The subcrop-supracrop play concept: example from Manitoba Canada. American Association of Petroleum Geologists Bulletin, v. 69, p. 260.

Imlay, R.W. 1947. Marine Jurassic of the Black Hills area, South Dakota and Wyoming. Bulletin of the American Association of Petroleum Geologists, v. 31, p. 227-273.

Irwin, J.L. 1965. General theory of epeiric clear water sedimentation. American Assocation of Petroleum Geologists Bulletin, v. 49, p. 445-459.

Kirk, S.R. 1929. Cretaceous stratigraphy of the Manitoba escarpment. Canadian Geological Survey Report, Part B, p. 112-135.

Klein, G. DeV. 1977. Clastic Tidal Facies. Champaign, Illinois: Continuing Education Publication Company, p. 143.

Krynine, P.D. 1949. The origin of red beds. New York Academy of Science Transactions, ser. 2, v. 11, p. 60-68.

Maiklem, W.R., Debout, D.G., and Glaister, R.P. 1969. Classification of anhydrite: a practical approach. Bulletin of Canadian Petroleum Geology, v. 17, p. 194-233.

Marafi, H. 1970. Newburg-South Westhope Oil Fields, North Dakota. In: King, R.L. (ed.): Stratigraphic Oil and Gas fields - Classification, Exploration Methods, and Case Histories. American Association of Petroleum Geologists, Memoir 16, p. 633-640.

Martin, R. 1966. Paleogeomorphology and its application to exploration for oil and gas (with examples from Western Canada). Bulletin of the American Association of Petroleum Geologists, v. 50, p. 2277-2311.

McCabe, H.R. 1956. Lyleton and Amaranth red beds in southwestern Manitoba, Unpubl. M.Sc. Thesis, University of Manitoba, Winnipeg, p. 110.

McCabe, H.R. 1959. Mississippian stratigraphy of Manitoba. Mines Branch, Department of Mines and Natural Resources, Province of Manitoba, Report 58-1, p. 99.

Morrow, D.W. 1982. Diagenesis 2. Dolomite - Part 2. Dolomitization models and ancient dolostones. Geoscience Canada, v. 9, no. 2, p. 95-107.

Pettijohn, F.J., Potter, R.E., and Siever, R. 1972. Sand and sandstones. New York: Springer-Verlog, p. 618.

Pittman, E.D. 1972. Diagenesis of quartz in sandstones as revealed by scanning electron microscopy. Journal of Sedimentary Petrology, v. 42, p. 507-519.

Poulton, T.P. 1984. The Jurassic of the Canadian western interior from 49 N latitude to Beaufort Sea. In: Stott, D.F., and Glass, D.J. (eds.): The Mesozoic of Middle North America. Canadian Society of Petroleum Geologists, Memoir No. 9, p. 15-41.

Reif, E.M., and Slatt, R.M. 1979. Red bed members of the Lower Triassic Moenkipi Formation, Southern Nevada: sedimentology and paleogeography of a muddy tidal flat deposit. Journal of sedimentary petrology, v. 49, no. 3, p. 869-890.

Reineck, H.E. 1975. German North Sea tidal flats. In: Ginsburg, R.N. (ed.): Tidal Deposits - A Casebook of Recent Examples and Fossil Counterparts. New York: Springer- Verlog, p. 5-13.

Reineck, H.E., and Singh, I.B. 1973. Depositional Sedimentary Environments: New York: Springer-Verlog, p. 439.

Reineck, H.E., and Wunderlich, F. 1968. Classification and origin of flaser and lenticular bedding. Sedimentology, v. 11, p. 99-104.

Rodgers, M. 1986. Petroleum geology of the Mississippian Mission Canyon Formation, Waskada Field, southwestern Manitoba. Branch, Manitoba Energy and Mines, Petroleum Geology Report, PR 1-85.

Schmidt, G.T. 1953. Regional stratigraphic analysis of Middle and Upper marine Jurassic in northern Rocky - Great Plains. Bulletin of the American Association of Geologists, v. 37, no. 2, p. 355-393.

Scholle, P.S. 1979. A color illustrated guide to constituents, textures, cements and porosities of sandstones and associated rocks. American Association of Petroleum Geologists, Memoir 28, p. 201.

Shaw, A.B. 1964. Time in stratigraphy. New York: McGraw- Hill, p. 365.

Stott, D.F. 1954. The Jurassic stratigraphy of Manitoba. Unpubl. M.Sc. Thesis, University of Manitoba, Winnipeg, p. 131.

Stott, D.F. 1955. Jurassic stratigraphy of Manitoba. Manitoba Department of Mines and Mineral Resources, Province of Manitoba, Report 54-2, p. 78.

Thomas, J.B. 1985. Influence of porosity type and pore geometry on productive capability of sandstone reservoirs and clay-bearing sandstone reservoirs. In: Sandstone diagenesis: applications to exploration and exploitation. American Association of Petroleum Geologists Diagenesis School.

Thompson, R.W. 1968. Tidal flat sedimentation on the Colorado River Delta, Northwestern Gulf of California. Geological Society of America, Memoir 107, p. 133.

Thompson, R.W. 1975. Tidal-flat sediments of the Colorado River Delta, Northwestern Gulf of California. In: Ginsburg, R.N. (ed.): Tidal Deposits: A Casebook of Recent Examples and Fossil Counterparts. Springer-Verlag, p. 428.

Walker, T.R. 1967. Formation of red beds in modern and ancient deserts. Geological Society of America Bulletin, v. 78, p. 353-368.

Weimer, R.J., Howard, J.D. and Lindsay, D.R. 1981. Tidal flats and associated tidal channels. In: Scholle, P.S. and Spearing, D. (eds): Sandstone Depositional Environments. American Association of Petroleum Geologists, Memoir 31, p. 191-245.

Wickenden, R.T.D. 1945. Mesozoic stratigraphy of the eastern plains, Manitoba and Saskatchewan. Geological Survey of Canada, Memoir 239, p. 87.

Wilson, M.D., and Pittman, E.D. 1977. Authigenic clays in sandstones: recognition and influence on reservoir properties and paleoenvironment analysis. Journal of Sedimentary Petrography, v. 47, n. 1, p. 3-31.

Zenger, D.H., and Dunham, J.B. 1980. Concepts and Models of dolomitization - an introduction. In: Zenger, D.H., Dunham, J.B., and Ethington, R.L. (eds.): Concepts and models of dolomitization. Society of Economic Paleontologists and Mineralogists, Special Publication No. 28, p. 1-9.

Zieglar, D.L. 1955. Pre-Piper post-Minnekahta "red beds" in the Williston Basin. In: North Dakota Geological Society, 1955 Field Conference Guidebook, p. 49-55.

APPENDIX A

WELL DATA SUMMARY
LOWER AMARANTH MEMBER

Note: All depths in meters and measured from below kelly bushing.

N.D. - no thickness or data available.

X - indicates core examined.

WELL NO.	WELL NAME AND LOCATION	K.B. (m)	TOP OF LOWER AMARANTH	TOP OF MISSISSIPPIAN	ISOPACH LOWER AMARANTH	ISOPACH TOTAL SAND LOWER AMARANTH	CORE EXAMINED
1.	PEX et al Cramner 15-1-1-25 W1	474.3	-397.5	432.5	35.1	3	-
2.	Roxy-Andex E. Waskada 6-3-1-25 W1	471.8	-420.9	-456	35.1	3	-
3.	Andex et al Waskada 15-5-1-25 W1	470.6	-427.0	-459	32.0	2.8	-
4.	Chauvco Waskada 13-8-1-25 W1	471.8	-424.6	-457.5	32.9	ND	-
5.	Roxy-Andex et al S. Waskada 11-10-1-25 W1	472.4	-410.3	-444.4	34.0	3	-
6.	Roxy Andex et al Waskada 5-15-1-25 W1	470.6	-408.7	-444.1	35.4	3	-
7.	Dekalb et al Waskada 16-15-1-25 W1	474.6	-399.9	-433.7	33.8	2.1	X
8.	Sasko et al E. Waskada 2-16-1-25 W1	473.0	-413.6	-447.8	34.1	2	X
9.	PEX et al Waskada 8-17-1-25 W1	473.4	-411.5	-445.9	34.4	3.1	-
10.	Chevron Waskada 3-18-1-25 W1	471.8	-424.6	-458.1	33.5	3.5	X

WELL NO.	WELL NAME AND LOCATION	K.B. (m)	TOP OF LOWER AMARANTH	TOP OF MISSISSIPPIAN	ISOPACH LOWER AMARANTH	ISOPACH TOTAL SAND LOWER AMARANTH	CORE EXAMINED
11.	KLM et al Waskada 12-18-1-25 W1M	470.6	-417.0	-451.1	34.1	3.5	-
12.	Tundra et al Waskada 6-19-1-25 W1	472.1	-417.6	-452.6	35.1	3.2	-
13.	Omega Waskada 7-20-1-25 W1	473.7	-412.7	-444.7	32.0	3.5	-
14.	Voyager Eastland Waskada 13-21-1-25 W1	474.6	-409.7	-445.6	36.0	4	-
15.	Sasko et al Waskada 4-22-1-25 W1	475.5	-403.9	-435.9	32.0	3	X
16.	Dekalb et al Waskada 14-23-1-25 W1	473.7	-392.9	-428.6	35.7	3.3	-
17.	Roxy-Andex et al E. Waskada 8-26-1-25 W1	475.2	-389.2	-423.1	33.8	4	-
18.	Peregrine ALS-WHR Waskada 10-27-1-25 W1	476.0	-393.2	-426.1	32.9	1.8	-
19.	PEX et al Waskada 10-28-1-25 W1	476.7	-400.2	-433.4	33.2	3.5	X
20.	Omega Waskada 4-30-1-25 W1	472.9	-417.3	-450.2	32.9	ND	-

WELL NO.	WELL NAME AND LOCATION	K.B. (m)	TOP OF LOWER AMARANTH	TOP OF MISSISSIPPIAN	ISOPACH LOWER AMARANTH	ISOPACH TOTAL SAND LOWER AMARANTH	CORE EXAMINED
21.	Omega Waskada 9-30-1-25 W1	472.7	-410.0	-444.1	34.1	4.5	-
22.	Omega Waskada 11-30-1-25 W1	472.4	-411.8	-445.0	33.2	3.3	X
23.	Omega Waskada 2-31-1-25 W1	473.1	-409.7	-445.6	36.0	3.5	-
24.	Omega Waskada 14-31-1-25 W1	474.0	-409.4	-445.9	36.6	2	X
25.	Andex PCV et al Waskada A3-32-1-25 W1	474.0	-404.2	-440.7	36.6	2	-
26.	PCI et al Waskada 8-32-1-25 W1	475.5	-398.4	-434.3	36.0	3	-
27.	Omega Waskada 14-32-1-25 W1	474.3	-400.5	-434.7	34.1	3	X
28.	PEX et al Waskada 6-33-1-25 W1	477.9	-394.7	-426.7	32.0	3	-
29.	PCI et al Waskada 11-33-1-25 W1	477.9	-393.8	-428.9	35.0	3.5	-
30.	Dekalb et al Waskada 4-35-1-25 W1	477.1	-389.2	-425.2	36.0	1.2	-
31.	Chevron Waskada 9-1-1-26 W1	466.7	-427.6	-458.7	31.1	3.2	X

WELL NO.	WELL NAME AND LOCATION	K.B. (m)	TOP OF LOWER AMARANTH	TOP OF MISSISSIPPIAN	ISOPACH LOWER AMARANTH	ISOPACH TOTAL SAND LOWER AMARANTH	CORE EXAMINED
32.	Chevron Waskada 10-1-1-26 W1	468.8	-427.9	-463.6	35.6	2.1	-
33.	Ward Williston Cr 2-2-1-26 W1	465.1	-441.4	-477.3	32.3	ND	-
34.	Dome Provo Waskada 1-10-1-26 W1	463.3	-448.1	-486.5	38.4	ND	-
35.	Omega Waskada 16-11-1-26 W1	466.3	-439.5	-463.3	24.1	4.2	-
36.	Chevron Waskada 1-12-1-26 W1	468.2	-428.6	-459.6	31.1	48.8	-
37.	Chevron Waskda 3-12-1-26 W1	467.6	-428.9	-463.3	34.4	3.5	-
38.	Chevron Waskada 7-12-1-26 W1	-	-	-	-	-	X
39.	Omega Waskada 1-13-1-26 W1	470.3	-423.4	-456.9	33.5	3.5	X
40.	Omega Waskada 15-13-1-26 W1	470.0	-422.2	-456.3	34.1	3	-
41.	Omega Waskada 15-14-1-26 W1	469.4	-431.0	-467.9	36.9	3.8	-

WELL NO.	WELL NAME AND LOCATION	K.B. (m)	TOP OF LOWER AMARANTH	TOP OF MISSISSIPPIAN	ISOPACH LOWER AMARANTH	ISOPACH TOTAL SAND LOWER AMARANTH	CORE EXAMINED
42.	Omega Waskada 16-14-1-26 W1	-	-	-	-	-	X
43.	Tri-West S. Waskada 7-16-1-26 W1	460.3	-448.1	-481.3	33.2	4.2	-
44.	Anglo et al Souris Valley 16-18-1-26 W1	435.6	-456.6	-492.3	35.7	N.D.	-
45.	North American Arthur 2-20-1-26 W1	454.8	-447.5	-485.0	37.5	3	X
46.	North American Arthur 6-21-1-26 W1	461.5	-442.0	-447.6	35.7	N.D.	-
47.	Omega et al Waskada 5-24-1-26 W1	469.1	-420.3	-456.6	36.3	N.D.	-
48.	Omega Waskada 9-24-1-26 W1	472.7	-420.0	-454.5	34.4	3.3	X
49.	Omega Waskada 11-24-1-26 W1	469.7	-417.9	-452.0	34.1	5.5	X
50.	Omega Waskada 3-25-1-26 W1	470.9	-418.2	-453.2	35.1	3.5	-
51.	Omega Waskada 6-25-1-26 W1	471.2	-420.6	-456.6	36.0	5.5	X

WELL NO.	WELL NAME AND LOCATION	K.B. (m)	TOP OF LOWER AMARANTH	TOP OF MISSISSIPPIAN	ISOPACH LOWER AMARANTH	ISOPACH TOTAL SAND LOWER AMARANTH	CORE EXAMINED
52.	Omega Waskada A8-25-1-26 W1	472.4	-415.4	-451.4	36.0	3	-
53.	Omega Waskada 9-25-1-26 W1	471.2	-411.2	-445.0	33.9	5	-
54.	Omega Waskada 14-25-1-26 W1	471.2	-415.4	-442.6	27.1	3.2	X
55.	Omega Waskada 6-26-1-26 W1	470.0	-420.3	-455.4	35.1	4	X
56.	Omega Waskada 8-26-1-26 W1	469.7	-419.4	-454.5	35.1	4.5	X
57.	Roxy-Clarion Waskada 9-26-1-26 W1	468.8	-419.4	-456.0	36.6	3.5	-
58.	Omega Waskada 4-27-1-26 W1	464.2	-427.0	-461.5	34.4	4	-
59.	1-32-1-26 W1	459.3	-435.0	-470.9	36.0	N.D.	-
60.	Omega Dalny 3-34-1-26 W1	464.5	-423.4	-457.5	34.1	3.3	X
61.	Omega Waskada 2-36-1-26 W1	470.9	-413.9	-445.9	32.0	4	-
62.	Omega Waskada 9-36-1-26 W1	473.4	-407.5	-442.3	34.9	3.1	-

WELL NO.	WELL NAME AND LOCATION	K.B. (m)	TOP OF LOWER AMARANTH	TOP OF MISSISSIPPIAN	ISOPACH LOWER AMARANTH	ISOPACH TOTAL SAND LOWER AMARANTH	CORE EXAMINED
63.	TJB Coulter 4-1-1-27 W1	454.8	-474.6	-514.5	39.9	N.D.	-
64.	Texaco Coulter Vale 3-2-1-27 W1	452.9	-481.1	-521.8	40.8	4.5	-
65.	Ward Coultervale 1-3-1-27 W1	452.0	-495.6	-541.6	46.0	4.5	-
66.	Antler River Coultervale 5-9-1-27 W1	457.8	-491.3	-530.0	38.7	4.5	X
67.	Pascar Coultervale Hunt No. 1 10-9-1-27 W1	456.9	-489.5	-522.7	33.2	N.D.	-
68.	Rio-Prado Souris Downey 12-9-1-27 W1	460.2	-488.9	-524.9	36.0	N.D.	-
69.	Antler River Coulter A13-10-1-27 W1	456.9	-486.5	-523.3	36.9	N.D.	-
70.	Souris Valley Pascar No. 1 13-10-1-27 W1	455.7	-487.4	-524.6	37.2	4	-
71.	Voyager Blackpool Coulter 5-16-1-27 W1	457.8	-486.5	-521.8	35.4	6	X

WELL NO.	WELL NAME AND LOCATION	K.B. (m)	TOP OF LOWER AMARANTH	TOP OF MISSISSIPPIAN	ISOPACH LOWER AMARANTH	ISOPACH TOTAL SAND LOWER AMARANTH	CORE EXAMINED
72.	Newscope Coulter 13-16-1-27 W1	456.6	-488.3	-523.6	35.4	3.5	-
73.	Great Northern Souris Valley Coulter 16-16-1-27 W1	456.3	-481.0	-518.2	37.2	N.D.	-
74.	Newscope et al Coulter 5-17-1-27 W1	458.7	-493.2	-531.0	37.8	4	-
75.	Newscope Coulter 7-18-1-27 W1	460.0	-492.3	-526.4	34.1	4	X
76.	Souris Valley R. Moore No. 1 5-20-1-27 W1	456.7	-483.4	-518.2	34.7	N.D.	-
77.	Newscope Coulter 9-20-1-27 W1	453.2	-481.9	-518.2	36.3	4.5	-
78.	Newscope et al Coulter 11-20-1-27 W1	457.5	-482.2	-517.9	35.7	4.5	X
79.	Pascar Westover No. 1 1-21-1-27 W1	457.8	-479.8	-517.6	37.8	4.5	-
80.	Newscope et al Coulter 5-21-1-27 W1	456.6	-483.1	-519.1	36.0	4	-
81.	Newscope et al Coulter 7-21-1-27 W1	455.7	-477.0	-512.7	35.7	3.5	-

WELL NO.	WELL NAME AND LOCATION	K.B. (m)	TOP OF LOWER AMARANTH	TOP OF MISSISSIPPIAN	ISOPACH LOWER AMARANTH	ISOPACH TOTAL SAND LOWER AMARANTH	CORE EXAMINED
82.	Great Lakes Northern Carbon & Chemical Co. #1 Westover 8-21-1-27 W1	455.7	-478.2	-514.8	36.6	N.D.	-
83.	Newscope et al Coulter 11-21-1-27 W1	454.2	-478.6	-515.1	36.6	N.D.	-
84.	Voyager Blackrock Coulter 5-22-1-27 W1	453.8	-479.5	-516.3	36.9	6	-
85.	Newscope et al Coulter A12-22-1-27 W1	455.1	-475.8	-512.7	36.9	4.5	X
86.	Great Northern Carbon No #1 Bell 12-22-1-27 W1	452.6	-477.6	-513.6	36.0	N.D.	-
87.	Great Lakes Carbon Co. #2 Westover 2-27-1-27 W1	456.6	-477.9	-512.7	34.7	2	-
88.	Kodiak Dunning #1 16-28-1-27 W1	456.5	-471.2	-506.6	35.4	1	-
89.	Newscope et al Coulter 3-29-1-27 W1	456.9	-479.5	-514.8	35.4	1.5	X
90.	Newscope et al Coulter 1-30-1-27 W1	457.2	-482.5	-518.2	35.7	2	-

WELL NO.	WELL NAME AND LOCATION	K.B. (m)	TOP OF LOWER AMARANTH	TOP OF MISSISSIPPIAN	ISOPACH LOWER AMARANTH	ISOPACH TOTAL SAND LOWER AMARANTH	CORE EXAMINED
91.	Antler River Coulter 9-30-1-27 W1	457.5	-479.2	-515.1	36.0	1.5	-
92.	Champlain Lyleton 1-3-1-28 W1	458.1	-533.7	-574.6	42.4	5.7	-
93.	Kissinger Almx Lbty Lyleton 3-4-1-28 W1	462.4	-534.3	-547.6	40.2	5	-
94.	Cleary Souris Valley Moore 11-13-1-28 W1	451.4	-497.4	-532.5	35.1	N.D.	-
95.	Souris Valley Gordon White No. 1 5-14-1-28 W1	454.3	-515.1	-553.2	38.1	N.D.	-
96.	Frankana et al Lyleton 14-15-1-28 W1	460.6	-512.1	-552.3	40.2	5.4	-
97.	Rideau Pipestone Lyleton 16-15-1-28 W1	459.6	-513.9	-552.0	38.1	5	X
98.	CPOG Lyleton 1-16-1-28 W1	460.9	-515.7	-555.9	40.2	4.8	-
99.	Rio-Prado Souris Fenton 5-17-1-28 W1	462.7	-536.8	-568.8	32.1	5	-
100.	Rideau Pipestone Lyleton 12-17-1-28 W1	463.9	-529.7	-567.8	38.1	5.8	X

WELL NO.	WELL NAME AND LOCATION	K.B. (m)	TOP OF LOWER AMARANTH	TOP OF MISSISSIPPIAN	ISOPACH LOWER AMARANTH	ISOPACH TOTAL SAND LOWER AMARANTH	CORE EXAMINED
101.	Rideau Pipestone Lyleton 12-23-1-28 W1	458.1	-502.6	-539.5	36.9	N.D.	-
102.	Rideau Lyleton 13-26-1-28 W1	459.3	-496.8	-533.4	36.6	3.5	-
103.	Ameran et al Lyleton 15-26-1-28 W1	458.7	-494.1	-531.0	36.9	5	X
104.	Rideau Pipestone Lyleton 9-27-1-28 W1	459.3	-499.9	-537.4	37.5	2.3	-
105.	Rideau Lyleton 14-27-1-28 W1	460.6	-504.8	-542.2	37.5	3.9	X
106.	Triwest Summit Lyleton 15-29-1-28 W1	462.2	-513.7	-551.1	37.4	4.2	-
107.	Calstan Lyleton 3-33-1-28 W1	464.5	-506.0	-543.2	37.2	4.2	-
108.	Calstan Lyleton 7-33-1-28 W1	464.5	-502.6	-540.1	37.5	3.3	-
109.	Rideau Lyleton 5-34-1-28 W1	461.2	-500.2	-536.5	36.3	4	X
110.	Ameran et al Lyleton 15-35-1-28 W1	458.1	-489.2	-525.8	36.6	3.8	X

WELL NO.	WELL NAME AND LOCATION	K.B. (m)	TOP OF LOWER AMARANTH	TOP OF MISSISSIPPIAN	ISOPACH LOWER AMARANTH	ISOPACH TOTAL SAND LOWER AMARANTH	CORE EXAMINED
111.	Poplar Admiral 15-5-1-29 W1	479.5	-555.3	-593.5	38.1	N.D.	-
112.	8-15-1-29 W1	468.8	-545.9	-587.0	41.2	N.D.	-
113.	Imperial Copley 11-18-1-29 W1	479.8	-569.4	-606.6	37.2	9.1	-
114.	Well Cleary Souris Valley White 5-34-1-29 W1	484.6	-521.2	-559.6	38.4	7.6	-
115.	Omega Waskada 8-5-2-25 W1	477.3	-394.4	-427.6	33.2	2	-
116.	Roxy Andex et al Waskada 7-7-2-25 W1	474.0	-398.7	-431.9	33.2	3	X
117.	Omega Waskada 7-8-2-25 W1	477.0	-392.9	-426.7	33.8	N.D.	-
118.	Omega Waskada 14-9-2-25 W1	477.9	-384.4	-417.0	32.6	3.5	-
119.	Chauvco et al Waskada 15-10-2-25 W1	479.5	-378.0	-412.1	34.1	3.1	-
120.	Voyager et al Cramner 10-12-2-25 W1	485.9	-355.4	-393.8	38.4	2.5	x

WELL NO.	WELL NAME AND LOCATION	K.B. (m)	TOP OF LOWER AMARANTH	TOP OF MISSISSIPPIAN	ISOPACH LOWER AMARANTH	ISOPACH TOTAL SAND LOWER AMARANTH	CORE EXAMINED
121.	Roxy Andex et al N. Cramner 4-13-2-25 W1	479.5	-364.2	-400.0	35.7	2.8	-
122.	Sasko et al Waskada 6-18-2-25 W1	474.6	-391.7	-424.6	32.9	2.5	-
123.	Newscope et al N. Cramner 13-22-2-25 W1	479.8	-370.6	-400.0	29.4	5	X
124.	Newscope et al N. Cramner 1-28-2-25 W1	477.6	-368.2	-399.3	31.1	1.8	-
125.	Murphy et al Waskada 8-32-2-25 W1	478.2	-370.0	-399.6	29.6	N.D.	X
126.	Omega Andex Waskada 4-1-2-26 W1	469.4	-422.8	-459.3	36.6	2	-
127.	Omega Andex Waskada 8-1-26-26 W1	472.1	-412.1	-449.6	37.5	2	-
128.	Omega Sasko Waskada 10-1-2-26 W1	471.2	-417.6	-451.1	33.5	2.5	-
129.	Roxy Andex 16-1-2-26 W1	474.0	-406.3	-442.9	36.0	4.5	X

WELL NO.	WELL NAME AND LOCATION	K.B. (m)	TOP OF LOWER AMARANTH	TOP OF MISSISSIPPIAN	ISOPACH LOWER AMARANTH	ISOPACH TOTAL SAND LOWER AMARANTH	CORE EXAMINED
130.	Omega Waskada 2-2-2-26 W1	467.9	-420.9	-460.6	39.6	5	-
131.	Omega Waskada 6-2-2-26 W1	468.5	-417.3	-455.4	38.1	3.5	-
132.	Omega Waskada 2-3-2-26 W1	467.0	-420.9	-457.2	36.3	3.0	-
133.	Omega Waskada 9-3-2-26 W1	467.0	-419.7	-456.9	37.2	2.8	-
134.	Omega et al Waskada 1-4-2-26 W1	464.2	-428.6	-465.4	36.9	3.1	
135.	Omega Waskada 9-4-2-26 W1	463.9	-423.4	-458.4	35.1	2.5	-
136.	Omega Waskada 10-4-2-26 W1	463.6	-428.2	-465.1	36.9	3.5	-
137.	Roxy et al Dalny 1-9-2-26 W1	462.4	-427.3	-459.3	32.0	3	-
138.	Omega Waskada 3-10-2-26 W1	466.0	-423.7	-459.3	35.7	4.5	-
139.	Calstan Imperial Dalny 8-10-2-26 W1	467.3	-418.5	-455.1	36.6	2.5	-
140.	Omega Waskada Prov. 2-11-2-26 W1	465.4	-423.4	-458.4	35.1	3	-

WELL NO.	WELL NAME AND LOCATION	K.B. (m)	TOP OF LOWER AMARANTH	TOP OF MISSISSIPPIAN	ISOPACH LOWER AMARANTH	ISOPACH TOTAL SAND LOWER AMARANTH	CORE EXAMINED
141.	Omega Waskada 6-11-2-26 W1	-	-	-	-	-	X
142.	Omega Waskada 10-11-2-26 W1	469.7	-413.6	-450.5	36.9	3.6	-
143.	Omega Waskada 16-11-2-26 W1	-	-	-	-	-	X
144.	Sasko et al Waskada 4-12-2-26 W1	470.3	-409.3	-445.0	35.7	3.5	-
145.	Roxy-Andex et al Waskada 4-13-2-26 W1	468.5	-403.5	-437.7	34.7	3.1	X
146.	Omega Waskada 3-14-2-26 W1	470.3	-413.0	-447.5	34.4	3	X
147.	Grizzley et al Waskada 15-14-2-26 W1	467.9	-409.4	-446.5	37.2	3.4	-
148.	Midwest Imp. Dalny 6-16-2-26 W1	463.0	-427.6	-461.8	34.1	3.6	-
149.	Roxy-Andex et al Waskada 11-25-2-26 W1	474.6	-386.8	-429.2	42.4	N.D.	-
150.	L.L.&E. Melita 2-30-2-26 W1	438.0	-424.6	-459.0	34.4	4.5	-
151.	5-32-2-26 W1	454.2	-424.6	-457.8	33.2	N.D.	-

WELL NO.	WELL NAME AND LOCATION	K.B. (m)	TOP OF LOWER AMARANTH	TOP OF MISSISSIPPIAN	ISOPACH LOWER AMARANTH	ISOPACH TOTAL SAND LOWER AMARANTH	CORE EXAMINED
152.	Chauvco et al Dalny 13-32-2-26 W1	451.1	-420.6	-456.6	37.2	2	X
153.	LL&E et al Dalny 10-36-2-26 W1	460.5	-388.6	-421.0	32.3	5	-
154.	Antler River Coulter 5-5-2-27 W1	456.6	-472.7	-506.3	33.5	2.5	X
155.	Antler River Coulter 8-6-2-27 W1	457.8	-473.4	-508.4	35.1	N.D.	X
156.	Voyager Blackrock Coulter 9-10-2-27 W1	457.0	-458.4	-495.0	36.6	N.D.	-
157.	Anglo Gould 3-14-2-27 W1	455.4	-449.6	483.5	33.8	2.4	-
158.	1-19-2-27 W1	442.3	-463.6	-496.5	32.9	1.9	-
159.	Chevron et al Dalny 15-24-2-27 W1	453.2	-429.5	-465.4	36.0	3	-
160.	K.R. Canso N. Coulter 15-27-2-27 W1	452.3	-440.4	-470.6	30.2	1.5	
161.	Imperial South Elva 13-30-2-27 W1	456.9	-457.5	-492.6	35.1	1.5	-
162.	14-3-2-28 W1	-	-	-	-	-	X

WELL NO.	WELL NAME AND LOCATION	K.B. (m)	TOP OF LOWER AMARANTH	TOP OF MISSISSIPPIAN	ISOPACH LOWER AMARANTH	ISOPACH TOTAL SAND LOWER AMARANTH	CORE EXAMINED
163.	Cobra Shell Lyleton 14-5-2-28 W1	466.3	-500.8	-540.4	39.6	4.5	-
164.	Banf et al Lyleton 15-5-2-28 W1	463.6	-500.1	-540.4	40.2	N.D.	-
165.	Cobra et al Lyleton 1-9-2-28 W1	466.0	-491.3	-530.4	39.0	4	X
166.	Rio-Prado Souris Hill No. 1 16-9-2-28 W1	461.5	-490.7	-529.1	38.4	N.D.	-
167.	Chandler Coulter 1-11-2-28 W1	456.3	-481.3	-518.5	37.2	1.5	-
168.	Kissinger et al Pierson 14-20-2-28 W1	455.1	-485.9	-522.4	36.6	3.2	-
169.	Anglo et al Souris Valley Shannon 1-22-2-28 W1	458.9	-478.5	-515.4	36.9	N.D.	-
170	Cobra et al E. Pierson 12-27-2-28 W1	463.9	-473.4	-508.7	35.4	3	X
171.	Chandler E. Pierson 15-27-2-28 W1	461.8	-472.1	-509.3	37.2	2	-
172.	GNOL et al E. Pierson 10-28-2-28 W1	465.3	-475.8	-510.0	34.1	2.1	-

WELL NO.	WELL NAME AND LOCATION	K.B. (m)	TOP OF LOWER AMARANTH	TOP OF MISSISSIPPIAN	ISOPACH LOWER AMARANTH	ISOPACH TOTAL SAND LOWER AMARANTH	CORE EXAMINED
173.	Copperhead Pierson 4-29-2-28 W1	464.2	-484.6	-521.5	36.9	2	-
174.	Dome Proud Calstan Eva Prov. 16-29-2-28 W1	467.6	-479.8	-515.4	35.7	3.6	-
175.	Cobra et al S. Pierson 2-30-2-28 W1	467.3	-490.4	-526.4	36.0	4	-
176.	Lyleton et al S. Pierson 5-30-2-28 W1	467.0	-488.9	-523.3	34.4	3	-
177.	Lyleton S. Pierson 11-30-2-28 W1	467.0	-486.8	-522.7	36.0	N.D.	X
178.	Cobra et al Pierson 12-30-2-28 W1	467.6	-487.1	-523.6	36.6	N.D.	-
179.	Murphy Pierson 11-8-2-29 W1	480.4	-524.3	-561.7	37.5	7.5	-
180.	Murphy et al S. Pierson 16-11-29-29 W1	468.8	-510.8	-551.1	40.2	4.5	X
181.	Cobra et al S. Pierson 9-24-2-29 W1	465.7	-495.0	-531.9	36.9	1.9	X
182.	Lyleton et al S. Pierson 14-24-2-29 W1	469.4	-493.8	-531.3	37.5	N.D.	X

WELL NO.	WELL NAME AND LOCATION	K.B. (m)	TOP OF LOWER AMARANTH	TOP OF MISSISSIPPIAN	ISOPACH LOWER AMARANTH	ISOPACH TOTAL SAND LOWER AMARANTH	CORE EXAMINED
183.	Lyleton et al S. Pierson 7-25-2-29 W1	468.8	-488.0	-526.1	38.1	3.8	X
184.	Lyleton et al S. Pierson 8-25-2-29 W1	467.0	-487.7	-524.0	36.3	4.5	-
185.	Lyleton et al Pierson 9-25-2-29 W1	466.0	-487.4	-524.3	36.9	3.8	-
186.	Lyleton et al Pierson 16-25-2-29 W1	467.0	-486.5	-523.3	36.9	4.2	-
187.	Cobra et al S. Pierson 12-26-2-29 W1	471.2	-495.6	-530.6	35.1	3	X
188.	Transworld S. Pierson 6-28-29 W1	479.2	-502.0	-537.7	35.7	3.8	X
189.	2-29-2-29 W1	481.0	-513.9	-544.4	30.5	4.5	-
190.	Chandler West Pierson 13-32-2-29 W1	480.9	-503.2	-540.1	36.9	4.5	-
191.	Chandler E. Pierson 15-32-2-29 W1	481.9	-496.8	-534.9	38.1	N.D.	-
192.	Chandler E. Pierson 5-36-2-29 W1	468.8	-484.6	-521.8	37.2	3.5	-
193.	Souris Valley McKee 1-15-3-25 W1	473.7	-346.3	-379.8	33.5	N.D.	-

WELL NO.	WELL NAME AND LOCATION	K.B. (m)	TOP OF LOWER AMARANTH	TOP OF MISSISSIPPIAN	ISOPACH LOWER AMARANTH	ISOPACH TOTAL SAND LOWER AMARANTH	CORE EXAMINED
194.	LL&E Waskada 15-20-3-25 W1	468.6	-355.1	-388.0	32.9	2.9	-
195.	Barron Kidd Sambrook 15-25-3-25 W1	475.2	-328.9	-358.2	29.3	3.5	-
196.	Clarion et al South Napinka 4-32-3-25 W1	463.3	-339.5	-371.6	32.0	2.3	-
197.	Sasko S. Melita 12-12-3-27 W1	457.2	-420.6	-449.6	29.0	1	X
198.	Cleary Souris Valley Innes 4-17-3-27 W1	465.1	-436.5	-471.5	35.1	N.D.	-
199.	Ocelot 4-1-3-28 W1	462.4	-464.5	-501.4	36.9	N.D.	-
200.	Tundra et al Pierson 11-7-3-28 W1	472.7	-472.4	-504.1	31.7	4.5	-
201.	Tundra et al Pierson 13-8-3-28 W1	471.5	-469.7	-506.3	36.6	3	-
202.	Tacoma E. Pierson 12-10-3-28 W1	468.5	-464.2	-500.8	36.6	2.4	-
203.	Rio Prado Souris Gibson 2-14-3-28 W1	466.0	-456.0	-491.0	35.0	N.D.	X

WELL NO.	WELL NAME AND LOCATION	K.B. (m)	TOP OF LOWER AMARANTH	TOP OF MISSISSIPPIAN	ISOPACH LOWER AMARANTH	ISOPACH TOTAL SAND LOWER AMARANTH	CORE EXAMINED
204.	Imperial Edward 4-16-3-28 W1	470.6	-465.1	-502.0	36.9	3.1	-
205.	Tacoma N. Pierson 10-16-3-28 W1	470.3	-549.9	-495.3	35.4	3.3	-
206.	Tundra et al Pierson 16-18-3-28 W1	472.4	-467.9	-505.4	37.5	3	X
207.	A&B et al Pierson 11-19-3-28 W1	472.7	-467.9	-504.4	36.0	2.1	X
208.	A4-21-3-28 W1	471.5	-461.1	-497.7	36.6	3	-
209.	K.R. Canso E. Pierson 2-22-3-28 W1	471.2	-454.8	-493.2	38.4	2	-
210.	Quest Pierson A4-22-3-28 W1	469.1	-457.5	-495.6	38.1	1.5	X
211.	Tacoma N. Pierson 4-22-3-28 W1	469.9	-457.2	-493.2	36.0	1.1	-
212.	Roblin 2-27-3-28 W1	467.3	-453.8	-484.9	31.1	N.D.	-
213.	Texaco McCall Graham Creek 4-29-3-28 W1	473.7	-464.8	-495.9	31.4	N.D.	-

WELL NO.	WELL NAME AND LOCATION	K.B. (m)	TOP OF LOWER AMARANTH	TOP OF MISSISSIPPIAN	ISOPACH LOWER AMARANTH	ISOPACH TOTAL SAND LOWER AMARANTH	CORE EXAMINED
214.	4-30-3-28 W1	475.5	-465.7	-499.9	32.9	1.8	-
215.	Imperial Pierson 12-2-3-29 W1	477.0	-490.4	-526.4	36.0	N.D.	X
216.	Chandler Pierson 6-3-3-29 W1	479.8	-497.4	-533.4	36.0	1.5	-
217.	Anglo et al Souris Valley Wicks 1-8-3-29 W1	484.0	-502.3	-537.1	34.7	0	X
218.	Chandler W. Pierson 13-8-3-29 W1	488.9	-490.1	-526.1	36.0	1.5	-
219.	9-10-3-29 W1	478.0	-488.3	-518.8	30.5	1.4	-
220.	Copperhead 2-11-3-29 W1	476.1	-487.0	-522.4	35.4	N.D.	-
221.	Calstan Standard Pierson 5-11-3-29 W1	477.6	-489.8	-520.6	30.8	N.D.	-
222.	Calstan Pierson Prov. 10-11-3-29 W1	475.2	-484.0	-517.2	33.2	1.9	X
223.	Tundra Pierson 4-12-3-29 W1	474.9	-482.8	-518.8	36.0	N.D.	-

WELL NO.	WELL NAME AND LOCATION	K.B. (m)	TOP OF LOWER AMARANTH	TOP OF MISSISSIPPIAN	ISOPACH LOWER AMARANTH	ISOPACH TOTAL SAND LOWER AMARANTH	CORE EXAMINED
224.	Imperial Pierson 5-12-3-29 W1	474.0	-481.6	-519.7	36.9	N.D.	-
225.	Columbia et al Pierson 10-12-3-29 W1	474.9	-476.1	-513.0	36.9	3.5	X
226.	Tundra Pierson A12-12-3-29 W1	472.4	-477.3	-518.5	41.2	N.D.	-
227.	Copperhead MMR Pierson 2-13-3-29 W1	473.7	-477.0	-513.9	36.9	3.5	-
228.	Imperial Pierson 5-15-3-29 W1	480.9	-489.5	-525.5	36.0	2.7	-
229.	Berry Pierson 7-16-3-29 W1	482.2	-490.1	-521.2	31.1	2.7	-
230.	CDR Imperial N. Pierson 8-21-3-29 W1	482.2	-486.2	-515.7	30.0	2	-
231.	Tacoma Pierson 10-23-3-29 W1	478.5	-471.2	-507.8	36.6	3.3	-
232.	Tacoma N. Pierson 10-24-3-29 W1	475.5	-470.6	-502.9	32.3	3.3	-
233.	Imperial Pierson 8-26-3-29 W1	477.6	-466.0	-502.6	36.6	3.6	-

WELL NO.	WELL NAME AND LOCATION	K.B. (m)	TOP OF LOWER AMARANTH	TOP OF MISSISSIPPIAN	ISOPACH LOWER AMARANTH	ISOPACH TOTAL SAND LOWER AMARANTH	CORE EXAMINED
234.	Tacoma N. Pierson 4-27-3-29 W1	484.0	-482.2	-517.0	34.7	2.4	-
235.	CDR Calstan N. Pierson 12-29-3-29 W1	493.2	-485.2	-523.6	38.4	2.1	-
236.	Can Prospect Cayunga 13-31-3-29 W1	498.3	-480.1	-515.4	35.4	N.D.	-

APPENDIX B

X-RAY DIFFRACTION ANALYSIS

LOWER AMARANTH MEMBER

X-RAY DIFFRACTION ANALYSIS

LOWER AMARANTH MEMBER

B.1 General Procedures

X-ray analyses were performed on the bulk and <4 m fraction of the fine-grained, silty subarkose (Lithofacies C) and the sandy siltstones (Lithofacies B) of the Lower Amaranth Member. Analyses were performed on a Phillips 1730 using Cu< radiation. Operating conditions included a power setting of 40 kV, 25mA, with a scanning speed of 0.1 2 /step, and a time constant of one second.

No attempt was made to quantify the analyses results and only relative concentrations have been reported (Table I, II). Identification of minerals was based on the shape, position, and peak intensity. Relative concentrations were determined from the peak area. The main peak of each phase has been labelled on the diffractometer patterns included with this appendix (Figures 23-28).

B.2 Bulk Mineralogy

Fourteen XRD-bulk mineralogy analyses were performed. Each sample was hand ground to a fine powder, packed in an aluminium holder, and tamped until smooth. In general, analysis results show a high and consistent concentration of quartz, dolomite, and potassium and plagioclase feld-

spar in all samples excluding sample #14 (Table I). Low concentrations of illite (muscovite) and chlorite are also present (Table I). The anhydrite concentration of these rocks varies considerably. In several samples, minor amounts of calcite, anaclime, and probably tridymite and stillbite were noted.

A typical diffractometer pattern for the suite of samples examined is best illustrated in the Omega Dalny 6-11-2-26 W1 well (Figure 23). This sample contains concentrations of plagioclase and potassium feldspar common to most of the rocks analyzed. This sample also contains a very high concentration of anhydrite. In contrast, the sample taken from the Chevron Waskada (3-18-1-25 W1) well (Figure 24) shows a low anhydrite content. The sample analyzed from the Chevron Waskada 9-1-1-26 W1 well (Figure 25) shows a low concentration of plagioclase feldspar.

B.3 Clay Mineralogy

Eleven samples were selected for clay mineral analysis. These samples were sonified for three five-minute periods and suspended overnight in distilled water. On re-examination, the water was clear. This was assumed to indicate a fairly low concentration of $<2\mu$ m material. Consequently, clay analysis was only performed on the $<4\mu$ m fraction.

The samples were agitated and suspended in distilled water for 1.56 hours. The upper 10 centimetres of liquid was siphoned and centrifuged for a few seconds, in order to collect any suspended material. This concentration was pipetted onto a glass slide. In order to identify clay minerals, the samples were exposed to ethylene glycol vapor overnight and heated to 550°C for one hour.

Clay minerals present in these samples include low concentrations of a highly crystalline illite (muscovite), chlorite, expandable chlorite/-mixed-layer chlorite, and mixed layer chlorite/illite (Table II). A typical clay mineral suite for the sandy siltstones of the Lower Amaranth Member is best illustrated by the Lyleton et al Pierson 11-30-2-28 W12 well (Figure 26) and the A and B et al Pierson 11-189-3-28 W1 well (Figure 27). The diffractometer patterns obtained from the analysis of the Chevron Waskada 9-1-1-26 W1 well (Figure 28) shows the typical clay mineralogy of a reservoir rock from the southern Waskada field.

Legend

Concentration - Table I and II

VH - very high	ML - medium low
H - high	L - low
MH - medium high	VL - very low
M - medium	T - trace

TABLE I: XRD: BULK MINERALOGY

RELATIVE ABUNDANCE

SAMPLE LOCATION	DESCRIP-TION	ILLITE	CHLORITE	QUARTZ	ANHY-DRITE	K-FELD-SPAR	PLAG. FELD-SPAR	CALCITE	DOLO-MITE	TRIDY-MITE/ STILL-BITE	ANA-CLIME
2-16-1-25W1 915 m	reddish-brown sandy sltst.	ML	L	H	VH	MH	MH	-	H	T	L
6-11-2-26W1 910 m	silty v.f.gr. sst.(?subark.)	L	T	H	VH	MH	MH	-	H	T	-
11-30-2-28W1 955 m	reddish-brown sandy sltst.	ML	L	H	ML	M	MH	VL	H	L	T
14-24-2-29W1 986 m	silty v.f.gr. sst.(?subark.)	ML	L	H	H	MH	MH	-	H	VL	-
1-9-2-28W1 922.6 m	reddish-brown sandy sltst.	VL	T	H	VL	MH	MH	-	H	L	-
9-1-1-26W1 918 m	interlaminated sltst./subark.	L	VL	H	MH	MH	ML	-	MH	VL	-
5-34-1-28W1 982 m	silty v.f.gr. sst(?subark.)	ML	L	H	MH	M	MH	VL	H	L	T
11-14-3-28W1 967 m	reddish-brown sandy sltst.	ML	L	H	VH	MH	MH	-	MH	MH	T
5-9-1-27W1 975 m	silty v.f.gr. sst.(?subark.)	ML	VL	H	H	M	MH	T	MH	VL	-

TABLE I - Continued

SAMPLE LOCATION	DESCRIPTION	ILLITE	CHLORITE	QUARTZ	ANHYDRITE	K-FELDSPAR	PLAG. FELDSPAR	CALCITE	DOLOMITE	TRIDYMITE/ STILLBITE	ANACLIME
16-14-1-25W1 917.1 m	silty v.f.gr. sst.(?subark.)	ML	L	H	VH	MH	MH	VL	MH	VL	-
8-6-2-27W1 963.5 m	f.-med. gr. sst.(?subark.)	L	L	MH	VH	MH	H	-	H	VL	-
16-14-1-26W1 923.8 m	reddish-brown sandy sltst.	L	VL	H	M	MH	H	VL	MH	VL	VL
3-18-1-25W1 909 m	reddish-brown sandy sltst.	L	VL	H	VL	M	M	T	MH	VL	-
6-11-2-26W1 905.8 m	reddish-brown sandy sltst.	VL	VL	H	VL	-	M	VL	MH	L	-

TABLE II: XRD ANALYSIS: < 4μm CLAY FRACTION
RELATIVE ABUNDANCES

SAMPLE LOCATION	DESCRIPTION	ILLITE	CHLORITE	EXPANDABLE CHLORITE/ CHLORITE MIXED LAYER	CHLORITE/ ILLITE MIXED LAYER	GYPSUM?
2-16-1-25W1 915 m	reddish-brown sandy sltst.	H	M	-	-	VH
6-11-2-26W1 910 m	silty v.f.gr. sst.(subark.?)	H	M	-	-	-
11-30-2-28W1 955 m	reddish-brown sandy sltst.	VH	H	-	-	-
14-24-2-29W1 986 m	silty v.g.fr. sst.(?subark.)	H	M	-	-	M
1-9-2-28W1 918 m	reddish-brown sandy sltst.	M	T	-	-	-
9-1-1-26W1 918 m	interlaminated sltst./subark.	VH	M	H	M	-
5-34-1-28W1 982 m	silty v.f.gr. sst.(?subark.)	H	M	-	-	-
11-19-3-28W1 967 m	reddish brown sandy sltst.	M	M	-	-	-
5-9-1-27W1 975 m	silty v.f.gr. sst.(?subark.)	L	L	-	-	VH

TABLE II: XRD ANALYSIS: 4μm CLAY FRACTION
RELATIVE ABUNDANCES

SAMPLE LOCATION	DESCRIPTION	ILLITE	CHLORITE	EXPANDABLE CHLORITE/ CHLORITE MIXED LAYER	CHLORITE/ ILLITE MIXED LAYER	GYPSUM?
8-26-1-26W1 913 m	silty f. gr. subarkose	L	L	L	-	L
6-25-1-26W1 916.5 m	silty f. gr. subarkose	M	L	-	-	-

Mineralogy - Bulk Mineralogy - Clay Fraction

Anhydrite - anhy
Calcite - calc
Chlorite - chlor
Dolomite - dol
Expandable mixed-layer chlorite/chlorite - mx-chlor
Illite - ill
Mixed layer chlorite/illite - mx-chlor-ill
Plagioclase feldspar - plag fld
Potassium feldspar - k fld
Pyrite - pyr
Quartz - qtz
Tridymite/Stillbite - tr-st

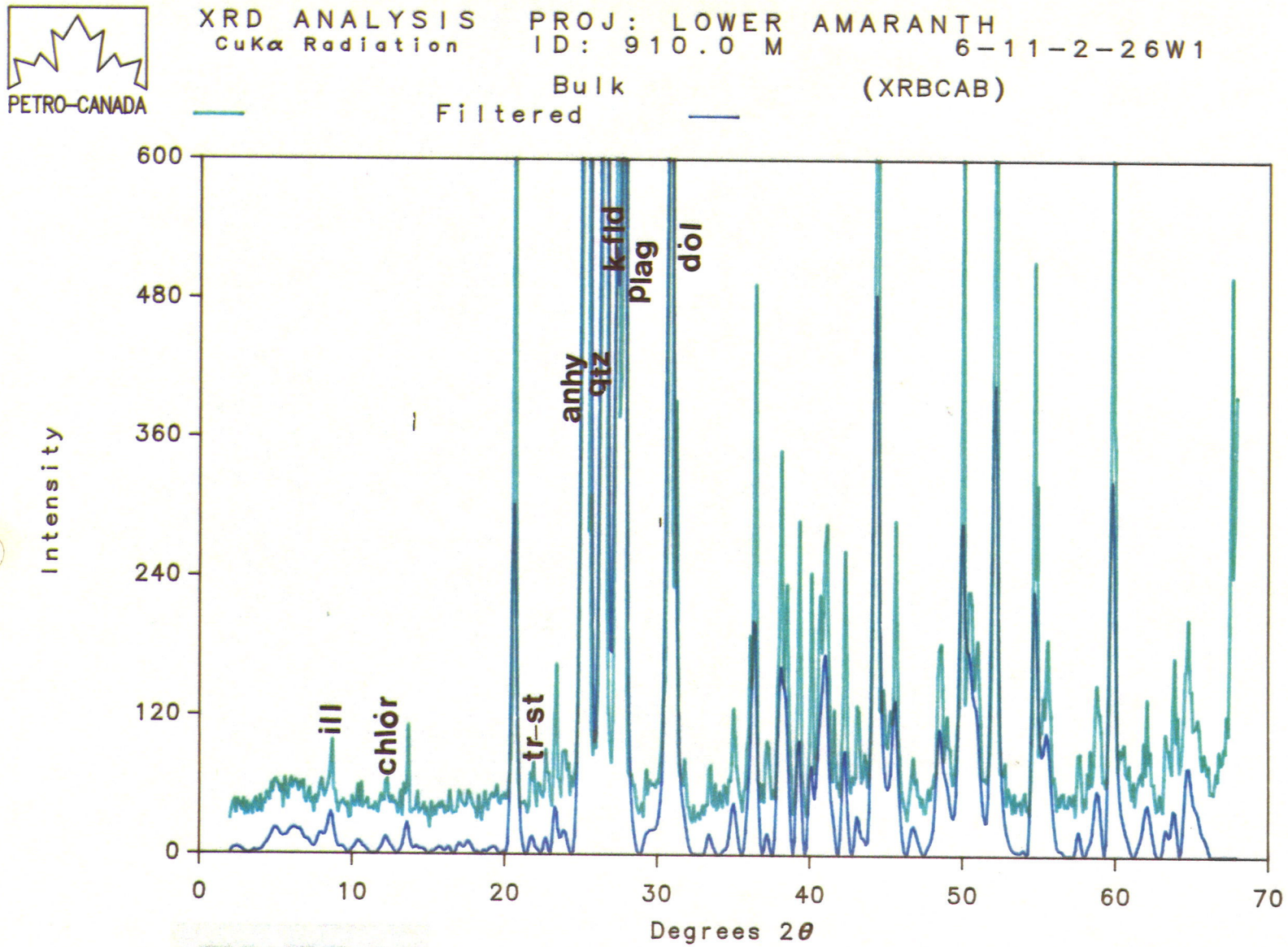
PETRO-CANADA
XRD ANALYSIS
CuKα Radiation
PROJ: LOWER AMARANTH
ID: 910.0 M
6-11-2-26W1
Bulk
(XRBCAB)
Filtered
Intensity
600
480
360
240
120
0
0
10
20
30
40
50
60
70
Degrees 2θ
ill
chlor
tr-st
anhy
qtz
k-fld
plag
dol

FIGURE 23

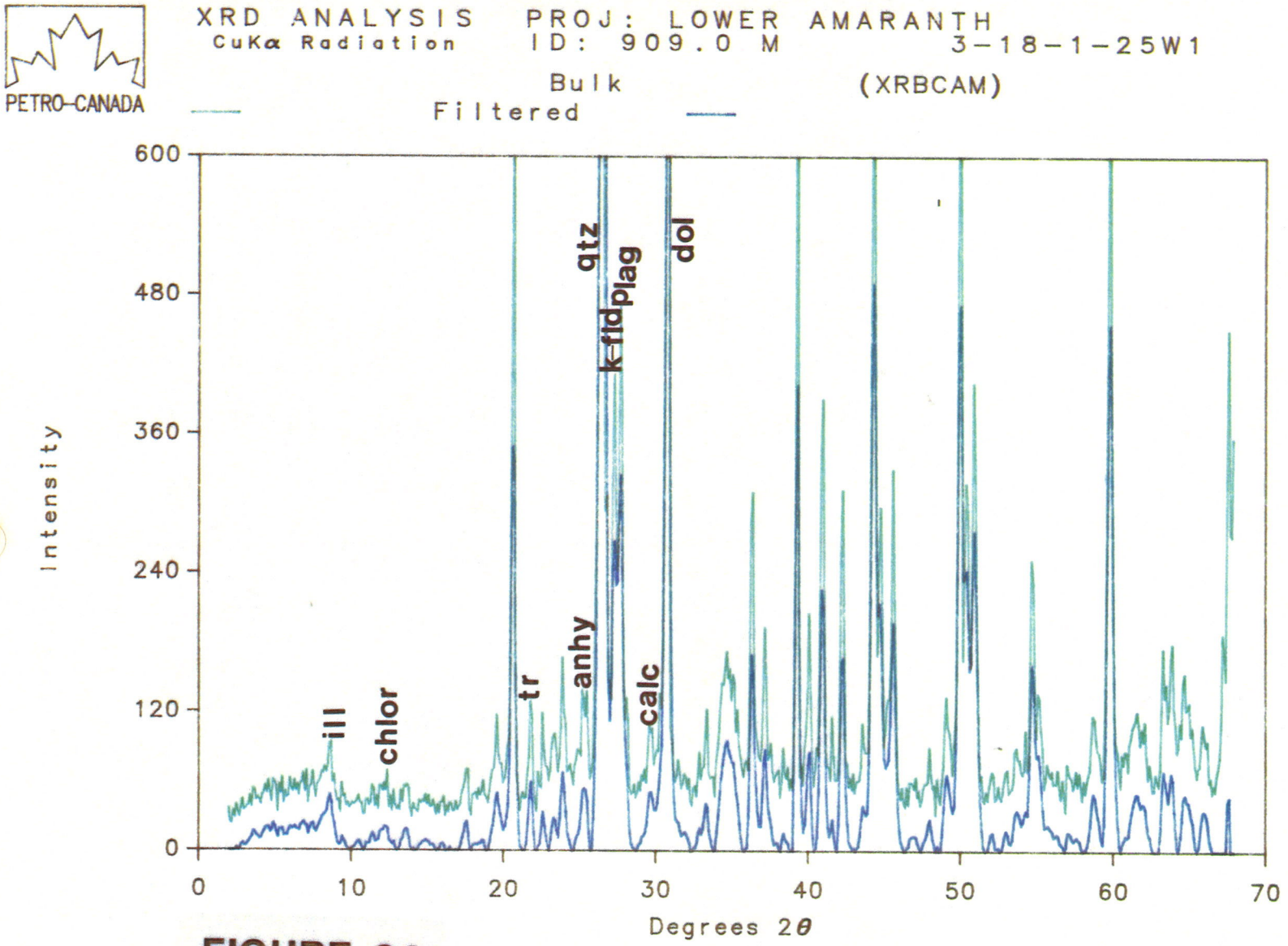
PETRO-CANADA
XRD ANALYSIS
CuKα Radiation
PROJ: LOWER AMARANTH
ID: 909.0 M
3-18-1-25W1
Bulk
(XRBCAM)
Filtered
Intensity
600
480
360
240
120
0
ill
chlor
tr
anhy
qtz
k-fld
plag
calc
dol
0
10
20
30
40
50
60
70
Degrees 2θ

FIGURE 24

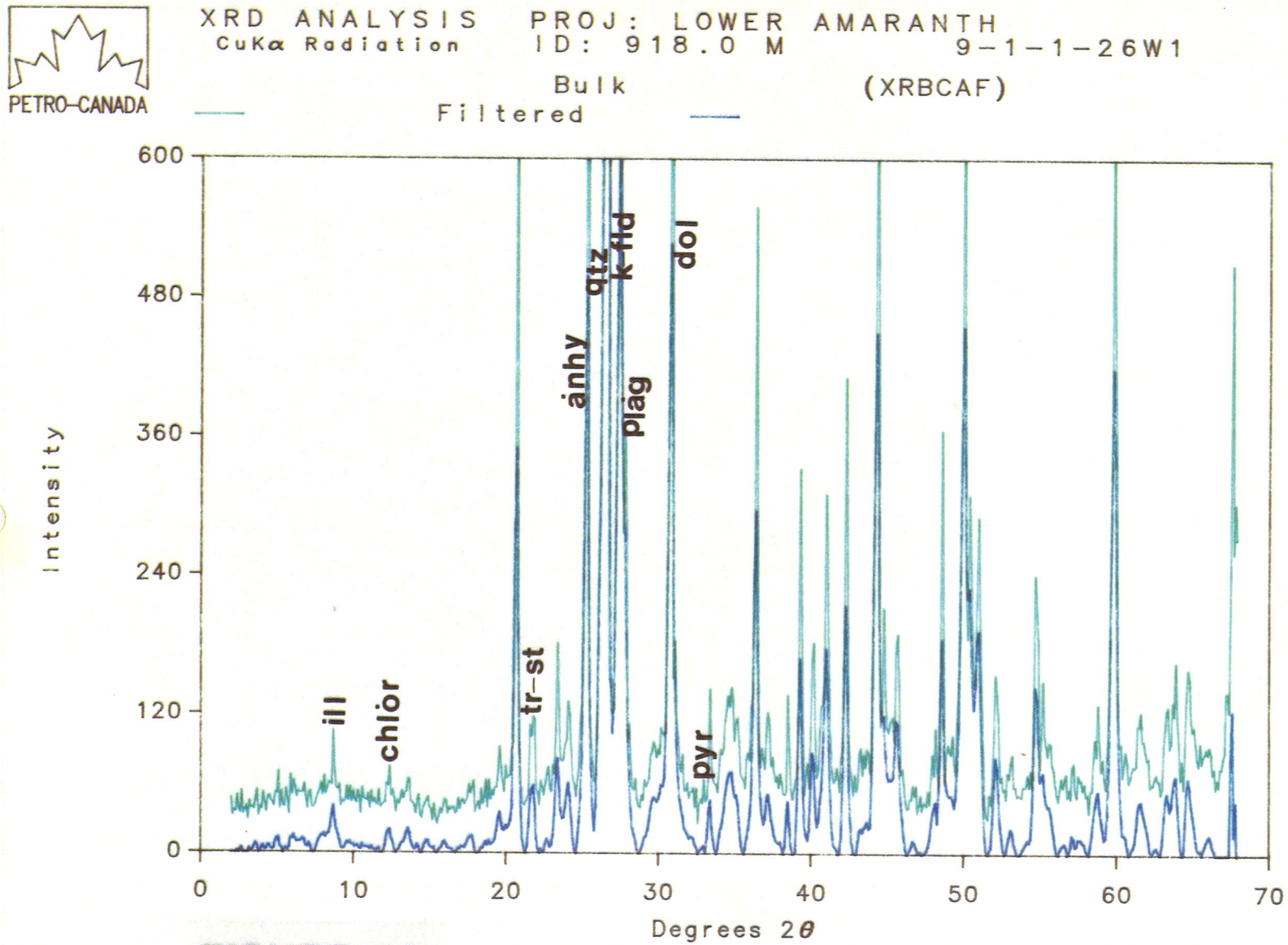
PETRO-CANADA
XRD ANALYSIS PROJ: LOWER AMARANTH
CuKα Radiation ID: 918.0 M 9-1-1-26W1
Bulk (XRBCAF)
Filtered
Intensity
600
480
360
240
120
0
0
10
20
30
40
50
60
70
Degrees 2θ
ill
chlor
tr-st
anhy
qtz
k-fld
plag
dol
pyr

FIGURE 25

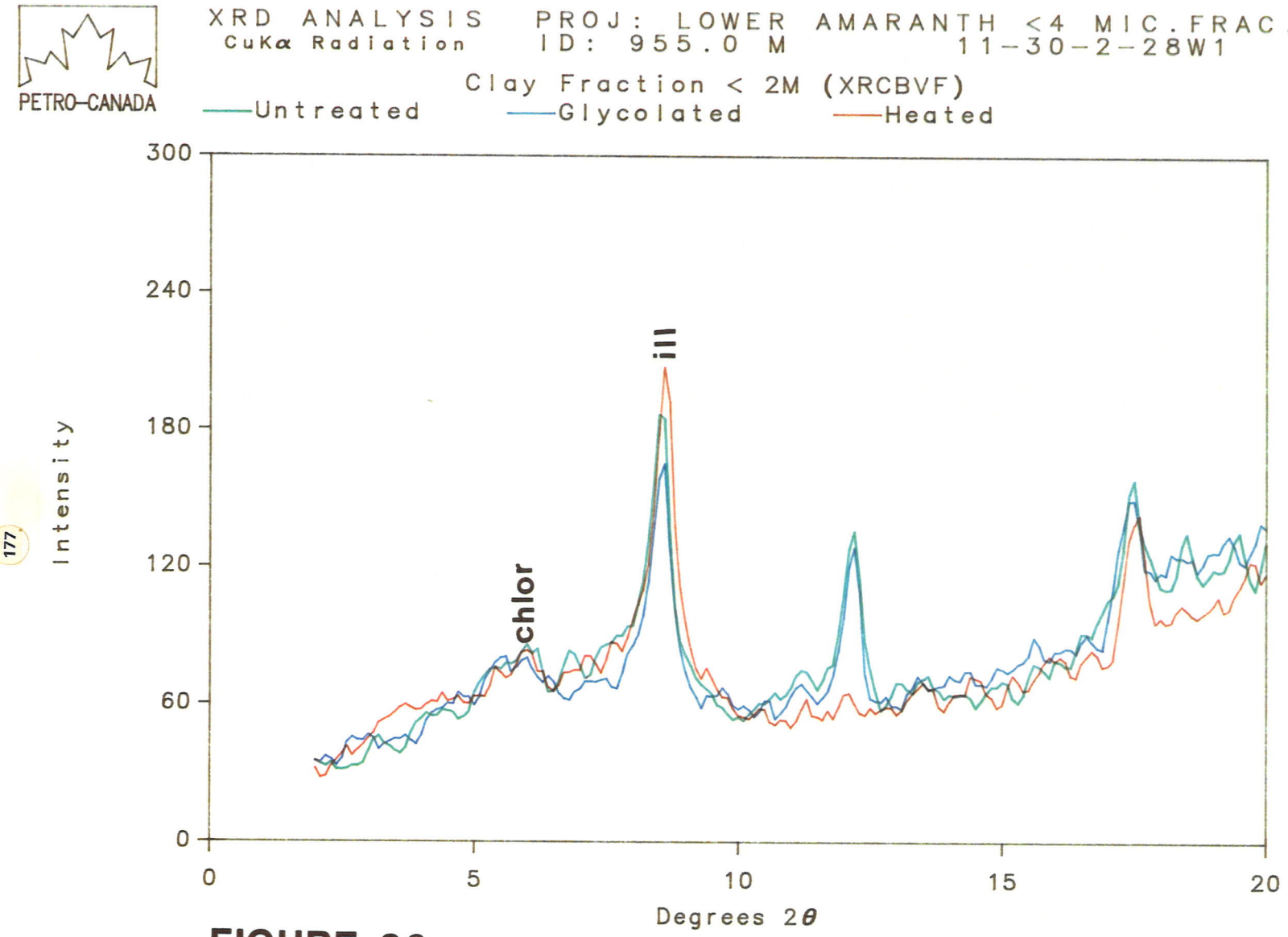
PETRO-CANADA
XRD ANALYSIS
CuKα Radiation
PROJ: LOWER AMARANTH <4 MIC.FRAC.
ID: 955.0 M
11-30-2-28W1
Clay Fraction < 2M (XRCBVF)
Untreated
Glycolated
Heated
Intensity
300
240
180
120
60
0
chlor
ill
0
5
10
15
20
Degrees 2θ

FIGURE 26

PETRO-CANADA

XRD ANALYSIS PROJ: LOWER AMARANTH <4 MIC.FRAC.
CuKα Radiation ID: 967.0 M 11-19-3-28W1

Clay Fraction < 2M (XRCBYK)

—Untreated —Glycolated —Heated

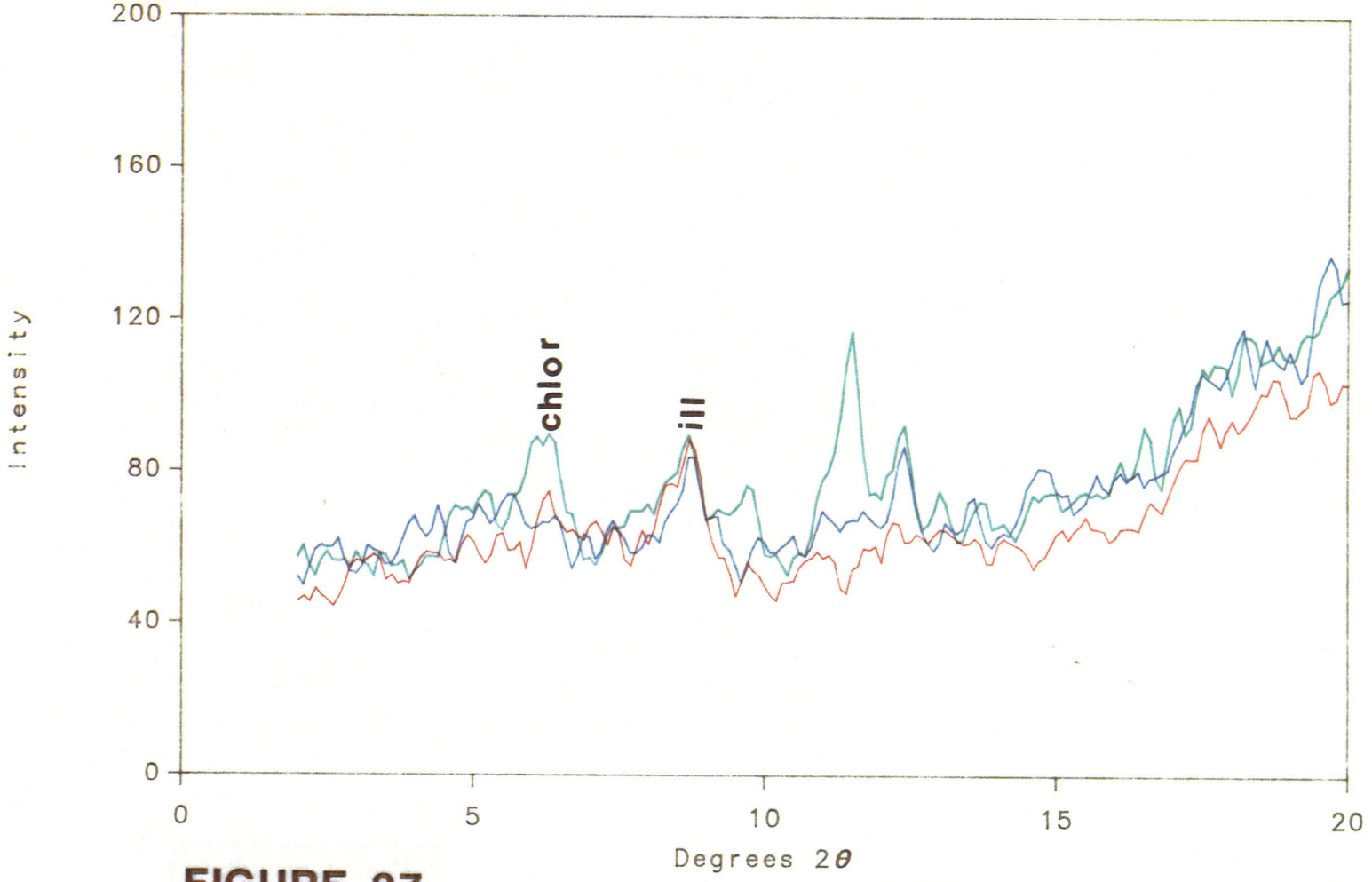

FIGURE 27

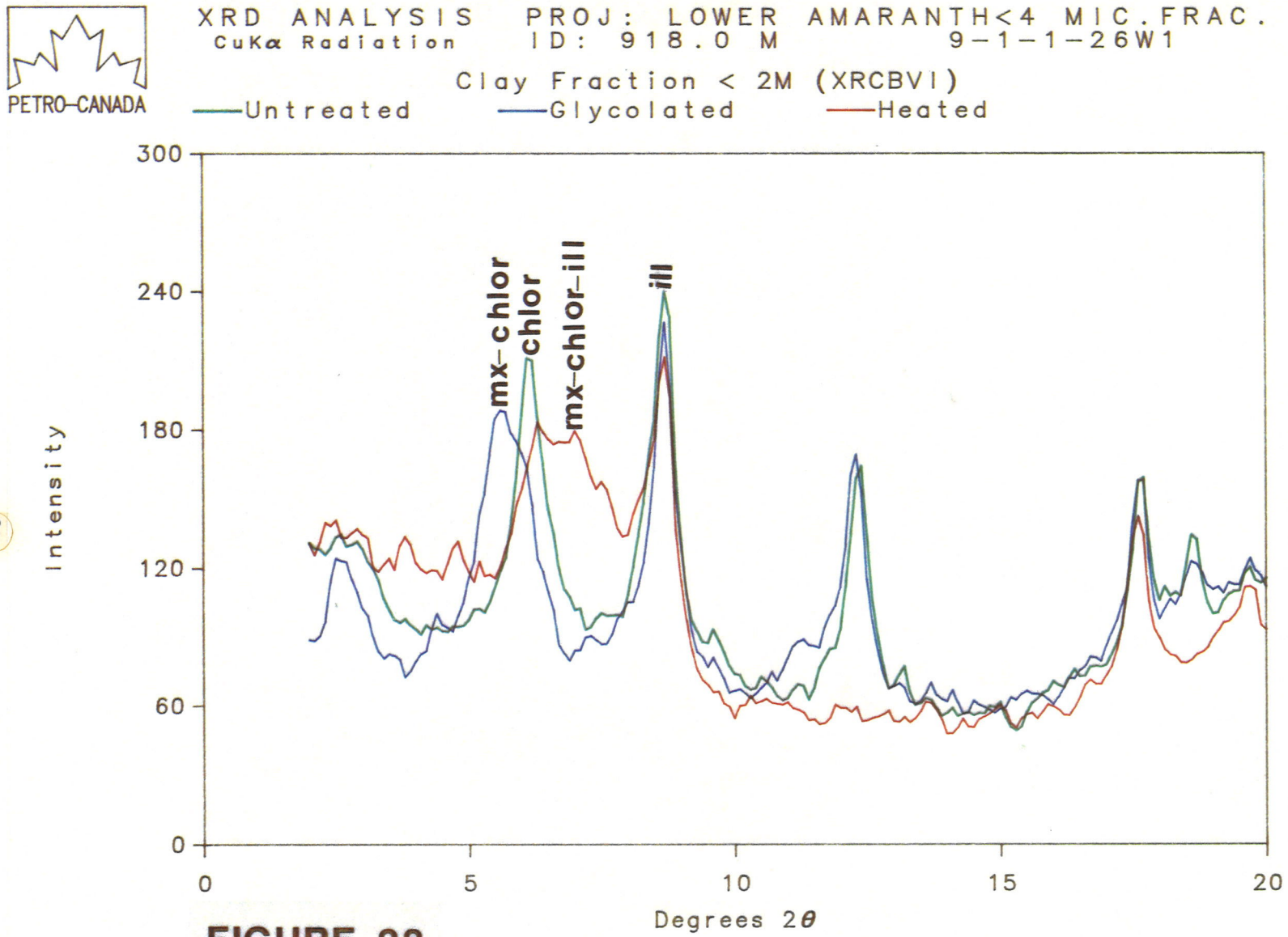
PETRO-CANADA
XRD ANALYSIS PROJ: LOWER AMARANTH<4 MIC.FRAC.
CuKα Radiation ID: 918.0 M 9-1-1-26W1
Clay Fraction < 2M (XRCBVI)
Untreated
Glycolated
Heated
mx-chlor
chlor
mx-chlor-ill
ill
Intensity
300
240
180
120
60
0
0
5
10
15
20
Degrees 2θ

FIGURE 28

R.28 R.27 R.26 R.25W1

T.3

T.2

-430 -440 -450 -460 -470 -480 -490 -500 -510 -520 -530 -540

-360 -370 -380 -390 -400 -410 -420 -430

MC-3 MEMBER (HALABURA, IN PRESS)

CHARLES FORMATION

MC-3 MEMBER (M.D.M.R.)

MC-1 MEMBER (M.D.M.R.)

WASKADA FIELD

SOUTH PIERSON FIELD

Elva

Waskada

Lyleton

Cameron

Goulter

CANADIAN PACIFIC

INTER CITY OIL

SOURIS RIVER

R.29 R.28 R.27 R.26

T.3

T.2

PIERSON FIELD

SOUTH PIERSON FIELD

CHARLES FORMATION

MC-3 MEMBER (HALABURA, IN PRESS)

-430 -440 -450 -460 -470 -480 -490 -500 -510 -520 -530 -540 -550

Pierson Elva Lyleton Souris Cameron Goulter

CANADIAN PACIFIC

SASKATCHEWAN MANITOBA

INTER CITY OIL

445 256 251 3 83

T.2

T.1

SASKATCHEWAN
MANITOBA

SOUTH PIERSON FIELD

COULTER FIELD

CHARLES FORMATION

CHARLES FORMATION (HALABURA, IN PART)

Lyleton

Coulter

SOURIS RIVER

CANADA
UNITED STATES

R.29 R.28 R.27 R.26

WELL STATUS INFORMATION

- Location
- Standing
- Producer
- Abandoned producer
- Dry and abandoned
- Water injection well
- Water injection well (former producer)
- Abandoned water injection well
- Abandoned water injection well (former producer)
- Salt water disposal
- Salt water disposal (former producer)
- Abandoned salt water disposal
- Abandoned salt water disposal (former producer)
- Dual completion
- Abandoned dual completion
- Water supply well
- Abandoned water supply well
- Abandoned structure test hole
- Surface location - directional well
- Gas injection well

Scale: 1:100,000

1 0 5km

T.2

T.1

R.28 R.27 R.26 R.25W1

CHARLES FORMATION

CHARLES FORMATION (HALABURA, IN PRESS)

MC-3 MEMBER (M.D.M.R.)

MC-1 MEMBER (M.D.M.R.)

MC-1 MEMBER (M.D.M.R.)

WASKADA FIELD

COULTER FIELD

TH PIERSON FIELD

Waskada

Coulter

Cameron

Lyleton

CANADIAN PACIFIC

CANADA
UNITED STATES

MANITOBA
NORTH DAKOTA

ATION

producer)

producer)

- Dual completion
- Abandoned dual completion
- Water supply well
- Abandoned water supply well
- Abandoned structure test hole
- Surface location - directional well
- Gas injection well

Scale: 1:100,000

1 0 5km

STRUCTURAL CONTOUR MAP
POST-PALEOZOIC EROSIONAL SURFACE
SOUTHWESTERN MANITOBA

CONTOUR INTERVAL: 5 METERS

MISSISSSIPPIAN SUBCROP EDGES —

(from: Halabura, in press; Manitoba Department Minerals Resources)

FIGURE:4

B. HANSEN **JUNE, 1986**

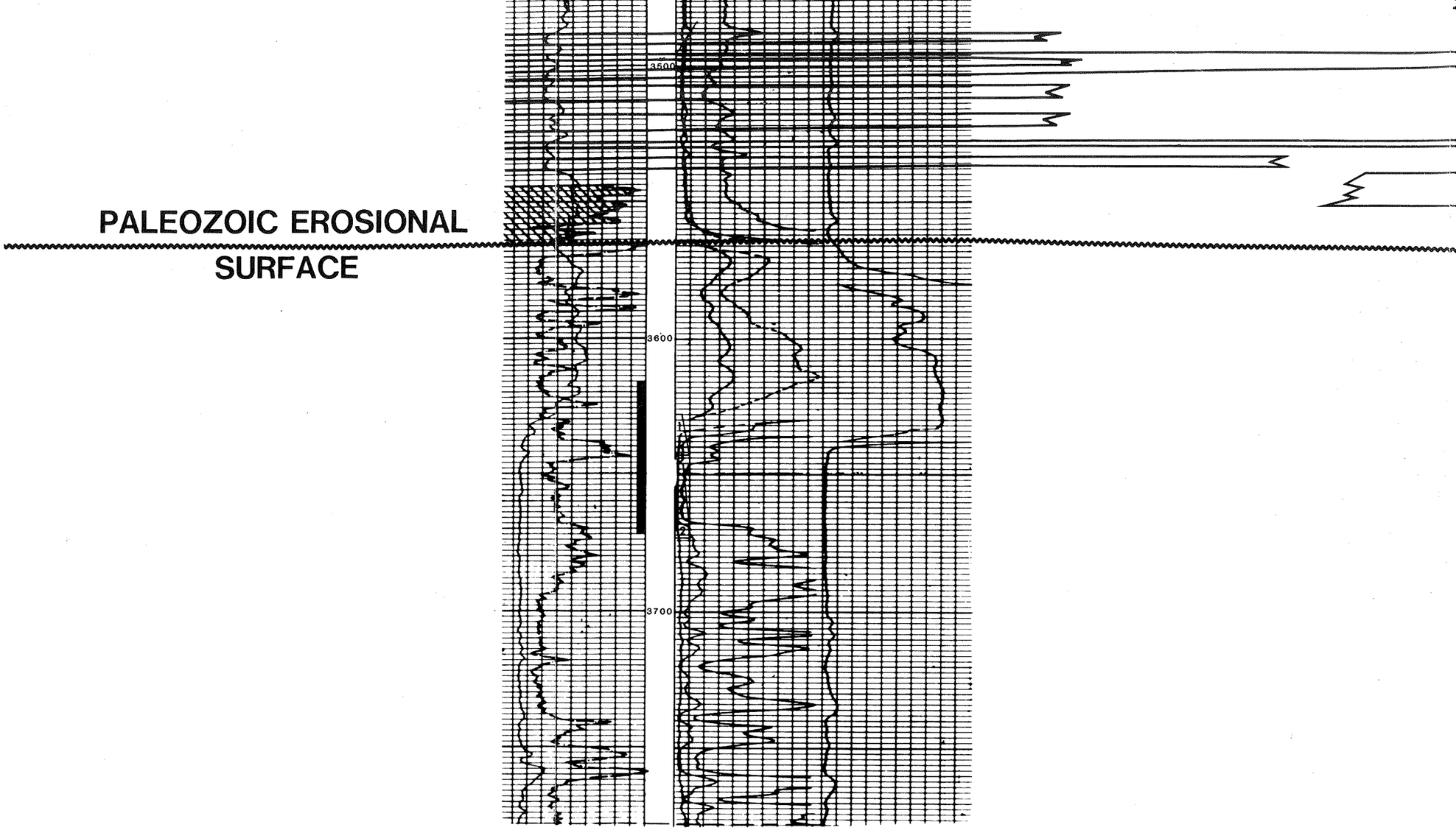

DST #1. 3628-3643 ft. : MISRUN
#2. 3646-3673 ft. : 3370 ft. S. WTR.

NO PERFS REPORTED

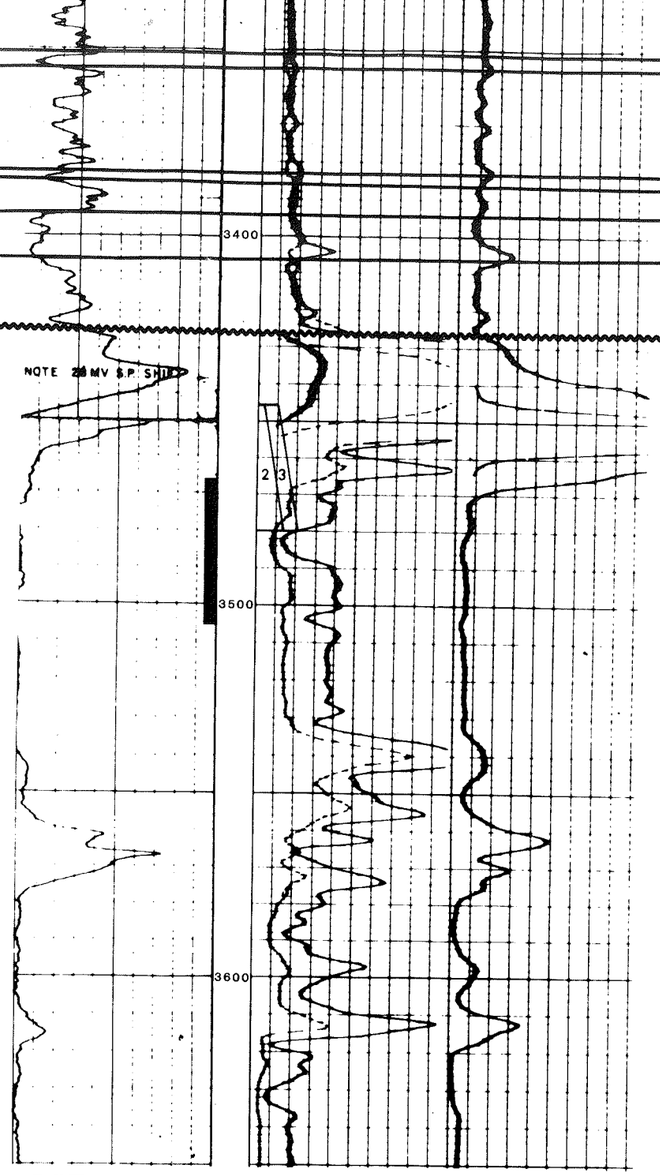

DST #1. 3800-3831 ft.: 1236 ft. S. WTR.
#2. 3445-3480 ft. : 92 ft. MUD
#3. 3445-3480 ft. : 90 ft. WTR. CUT MUD
NO PERFS REPORTED

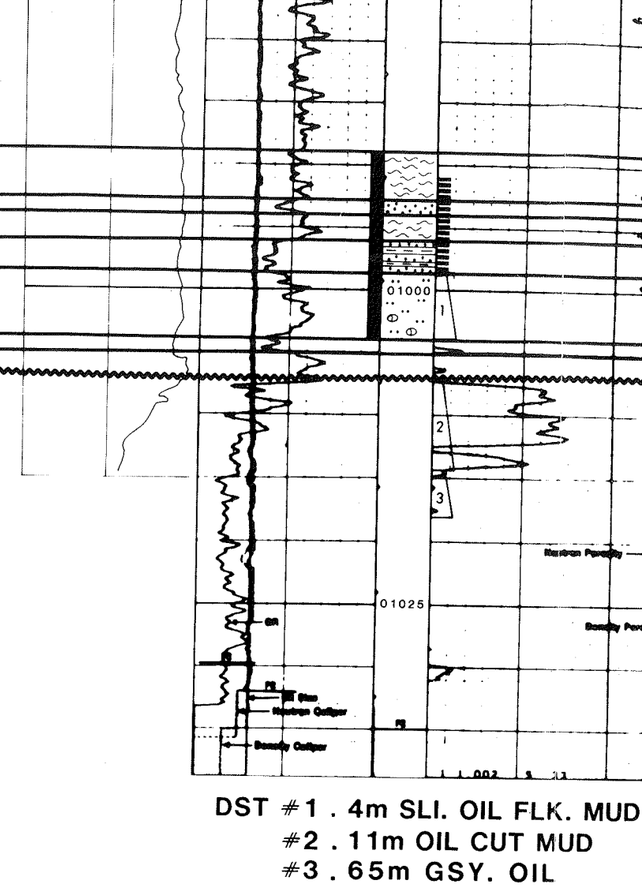

DST #1 . 4m SLI. OIL FLK. MUD
#2 . 11m OIL CUT MUD
#3 . 65m GSY. OIL

DST #1 . 4m SLI. OIL FLK. MUD
#2 . 11m OIL CUT MUD
#3 . 65m GSY. OIL

DST #1 . 975-992.6m : 18 m
OIL CUT MUD
NO PERFS REPORTED

NO CORES CUT
NO DST
NO PERFS REPORTED

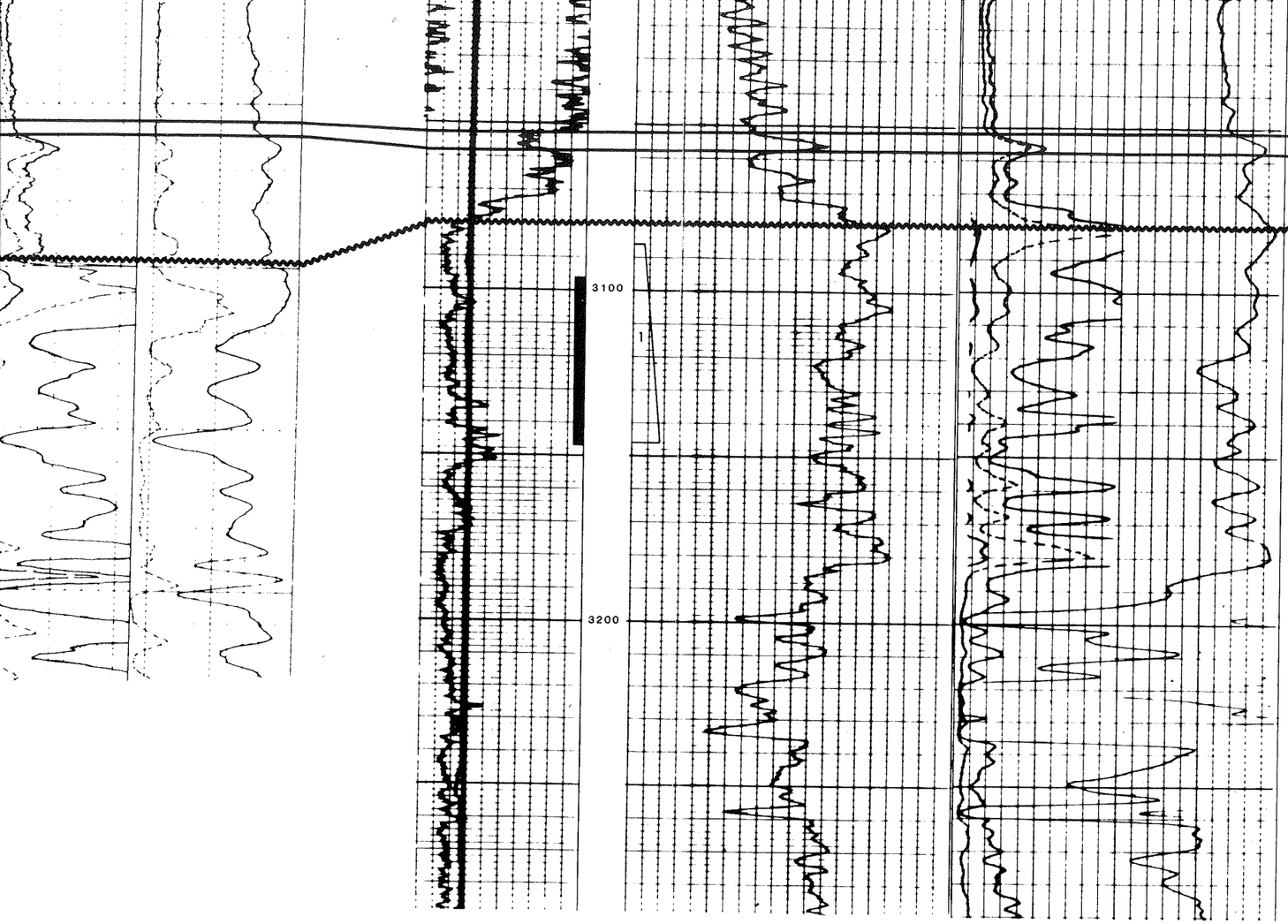

DST #1. 3086-3146 ft.: 60 ft. MUD, 220 ft. WTR. CUT MUD
NO PERFS REPORTED

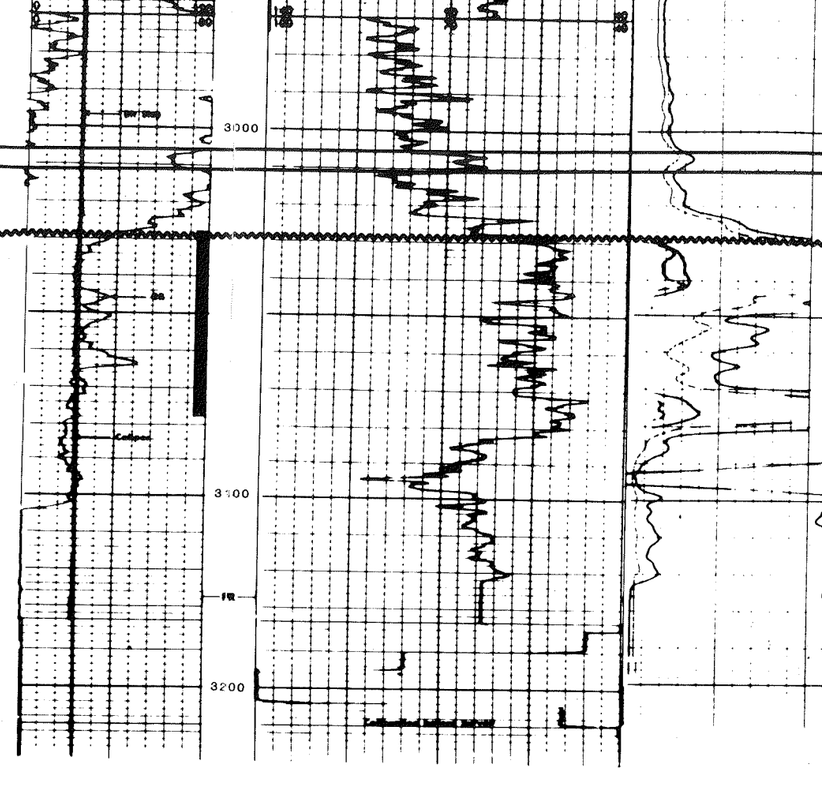

NO DST
NO PERFS REPORTED

A

SW

IMPERIAL COPLEY
11-18-1-29W1

1956

KB: 479.8m

TD: 1152.1m

DATUM: TOP LOWER AMARANTH

PALEOZOIC EROSIONAL SURFACE

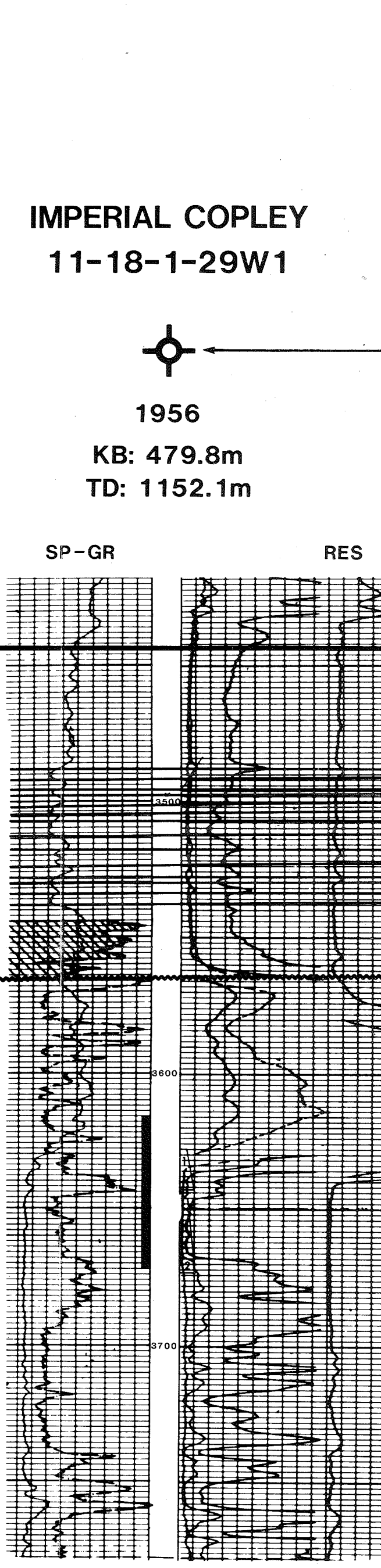

DST #1. 3628-3643 ft. : MISRUN

#2. 3646-3673 ft. : 3370 ft. S

NO PERFS REPORTED

L COPLEY

1-29W1

WELL CLEARY SOURI

5-34-1-29W

4.0mi
6.4 Km

)56

79.8m

152.1m

1955

KB: 489.4m

TD: 1205.0m

RES

SP

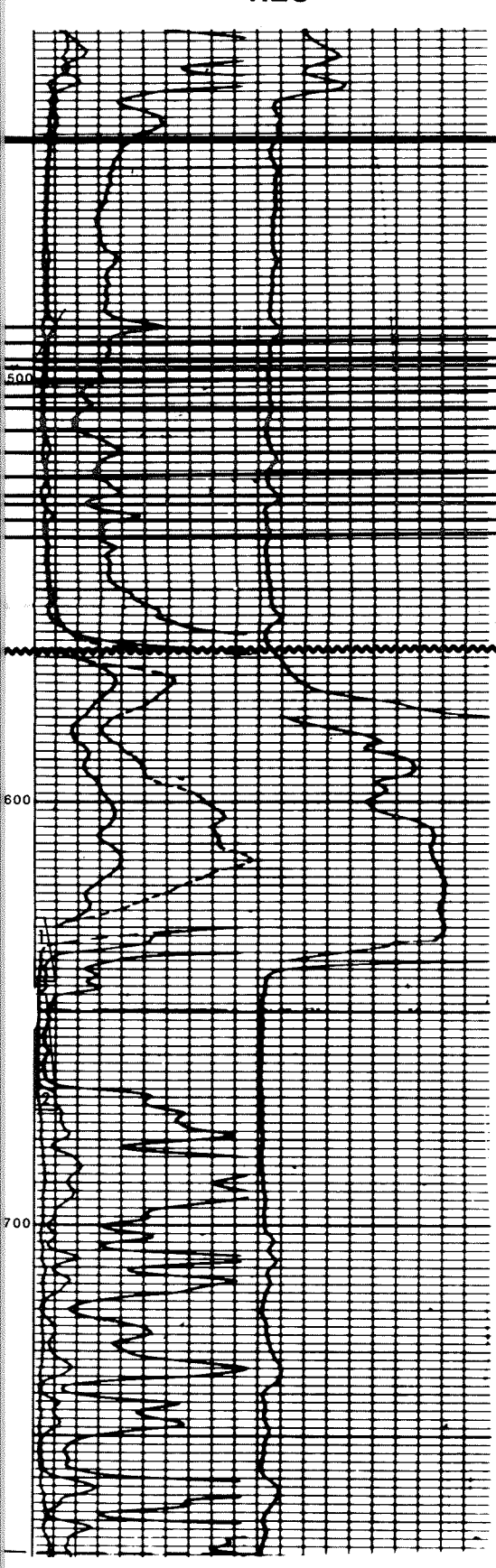

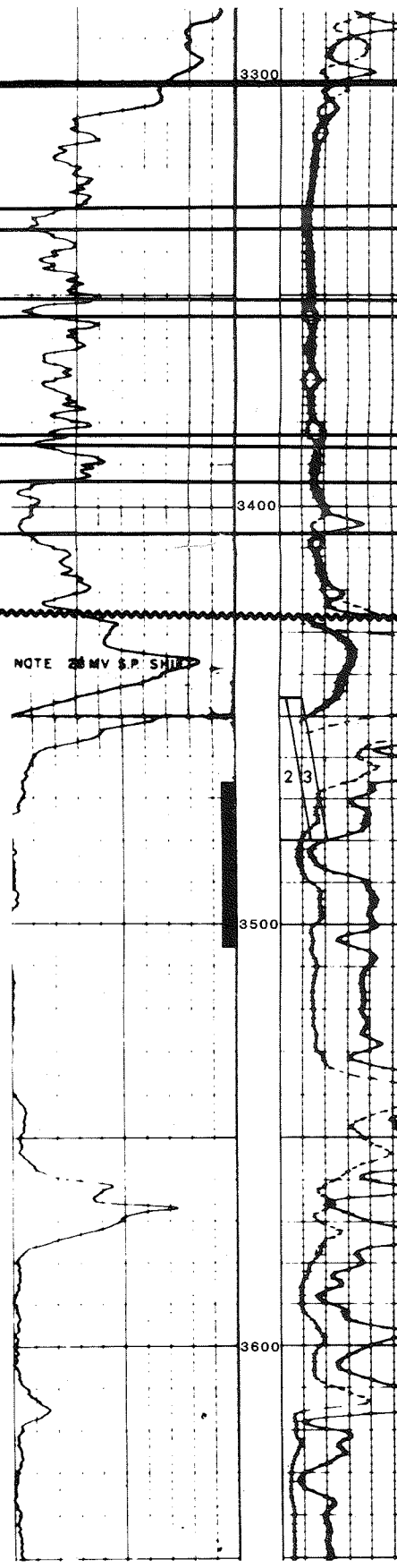

3-3643 ft. : MISRUN

6-3673 ft. : 3370 ft. S. WTR.

PORTED

DST #1. 3800-3831 ft.

#2. 3445-3480 ft

#3. 3445-3480 ft

NO PERFS REPORTED

WELL CLEARY SOURIS VALLEY
5-34-1-29W1

4.0mi
6.4 Km

1955

KB: 489.4m

TD: 1205.0m

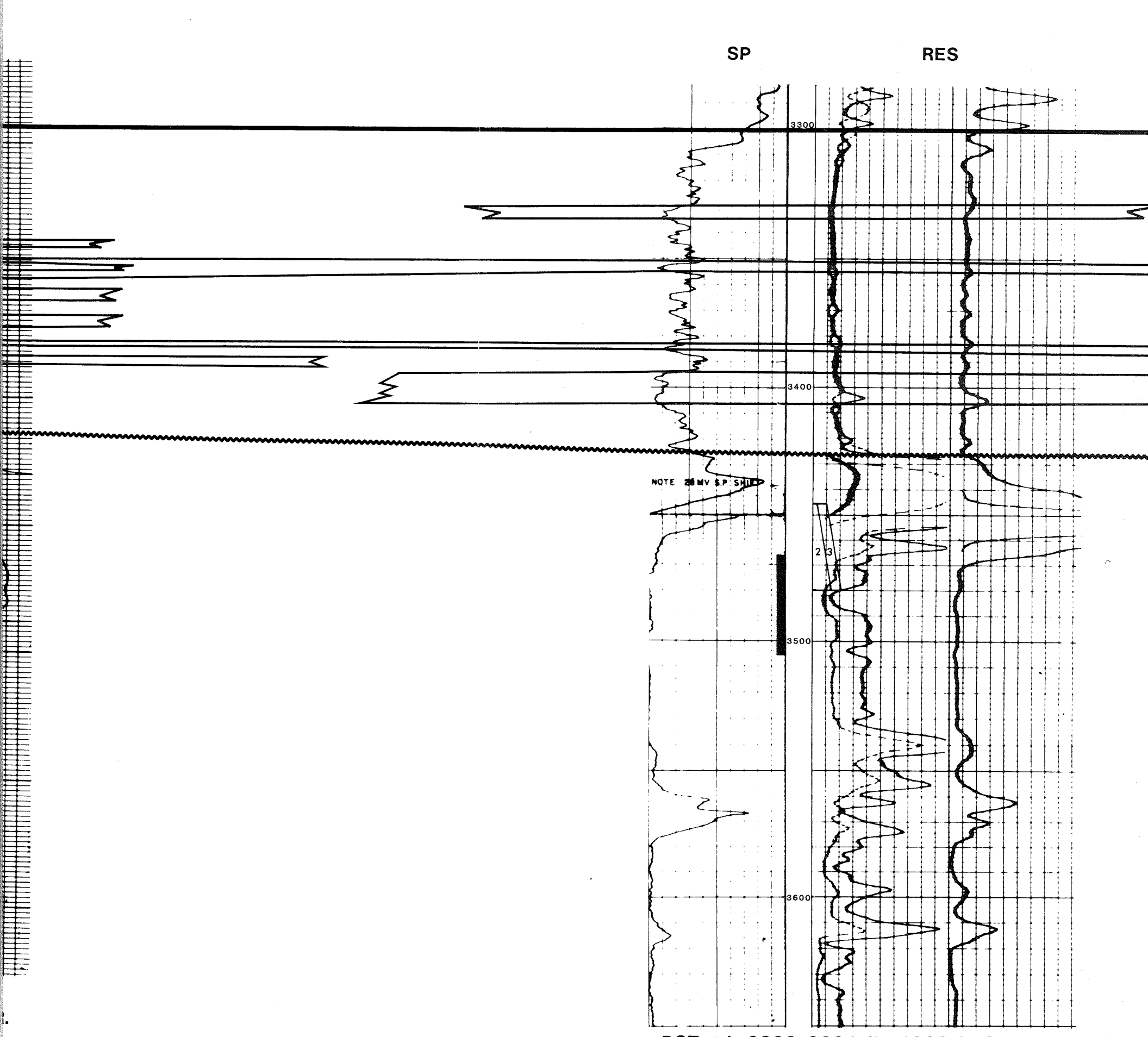

DST #1. 3800-3831 ft.: 1236 ft. S. WTR.
#2. 3445-3480 ft. : 92 ft. MUD
#3. 3445-3480 ft. : 90 ft. WTR. CUT MUD

NO PERFS REPORTED

)URIS VALLEY
29W1

COBRA-
14

4.6mi
7.4Km

4m
.0m

K
TI

RES

SP

GR

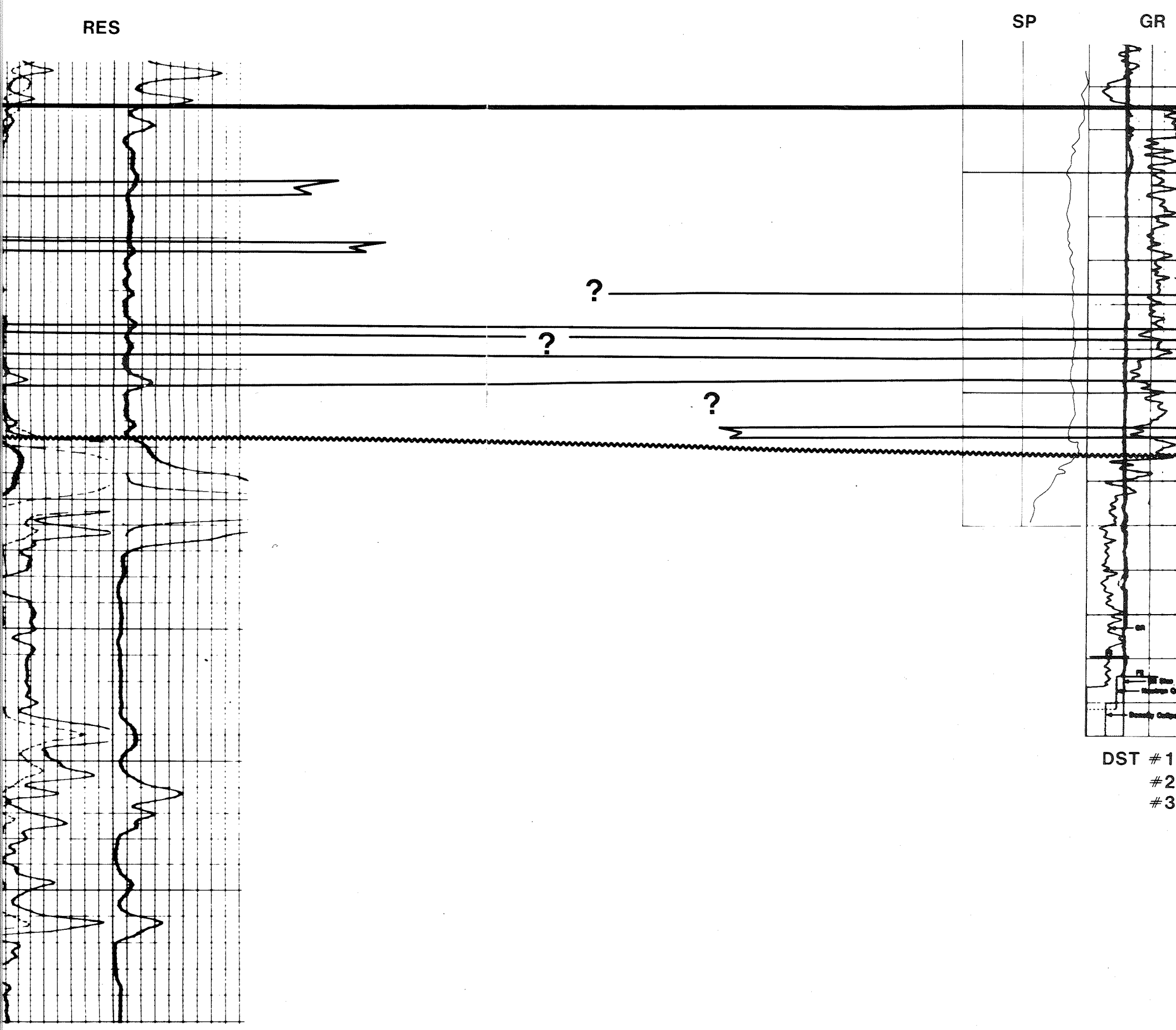

DST #1
#2
#3

31 ft.: 1236 ft. S. WTR.
80 ft. : 92 ft. MUD
80 ft. : 90 ft. WTR. CUT MUD
ED

COBRA-SHELL LYLETON
14-5-2-28W1

1980

KB: 466.4m

TD: 1033.0m

1.5mi
2.4Km

COBRA ET AL LYLETON
1-9-2-28W1

KB: 466.0m

TD: 1026.0m

2.0mi
3.2Km

SP GR COMP. NEUTRON GR COMP. NEUTRON

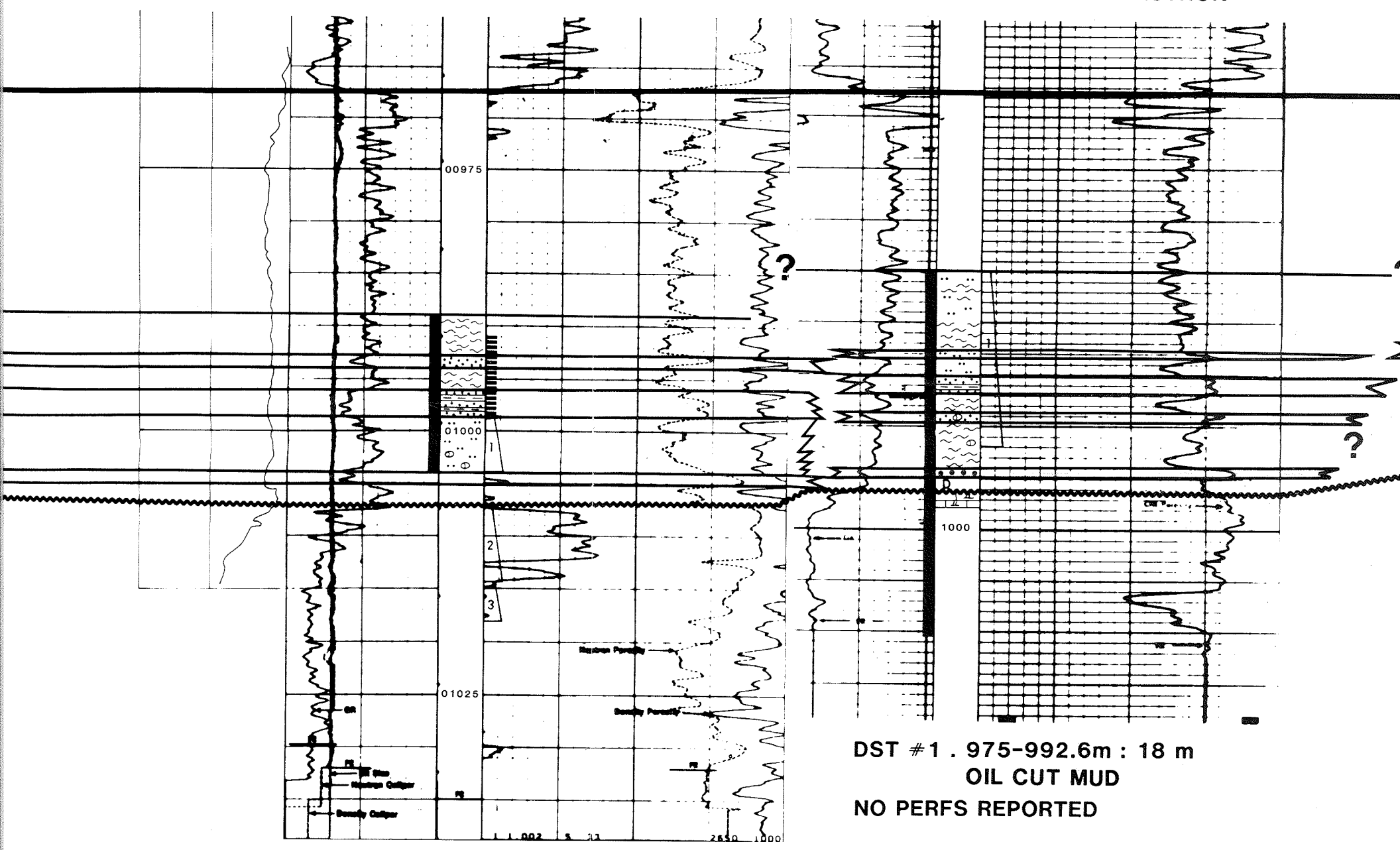

DST #1 . 4m SLI. OIL FLK. MUD
#2 . 11m OIL CUT MUD
#3 . 65m GSY. OIL

DST #1 . 975-992.6m : 18 m
OIL CUT MUD

NO PERFS REPORTED

R COULTER
2-28W1

2.9mi
4.7Km

MIDWEST IMPERIAL COULTER
1-19-2-27W1

56.6m
297.2m

KB: 442.3m
TD: 1036.3m

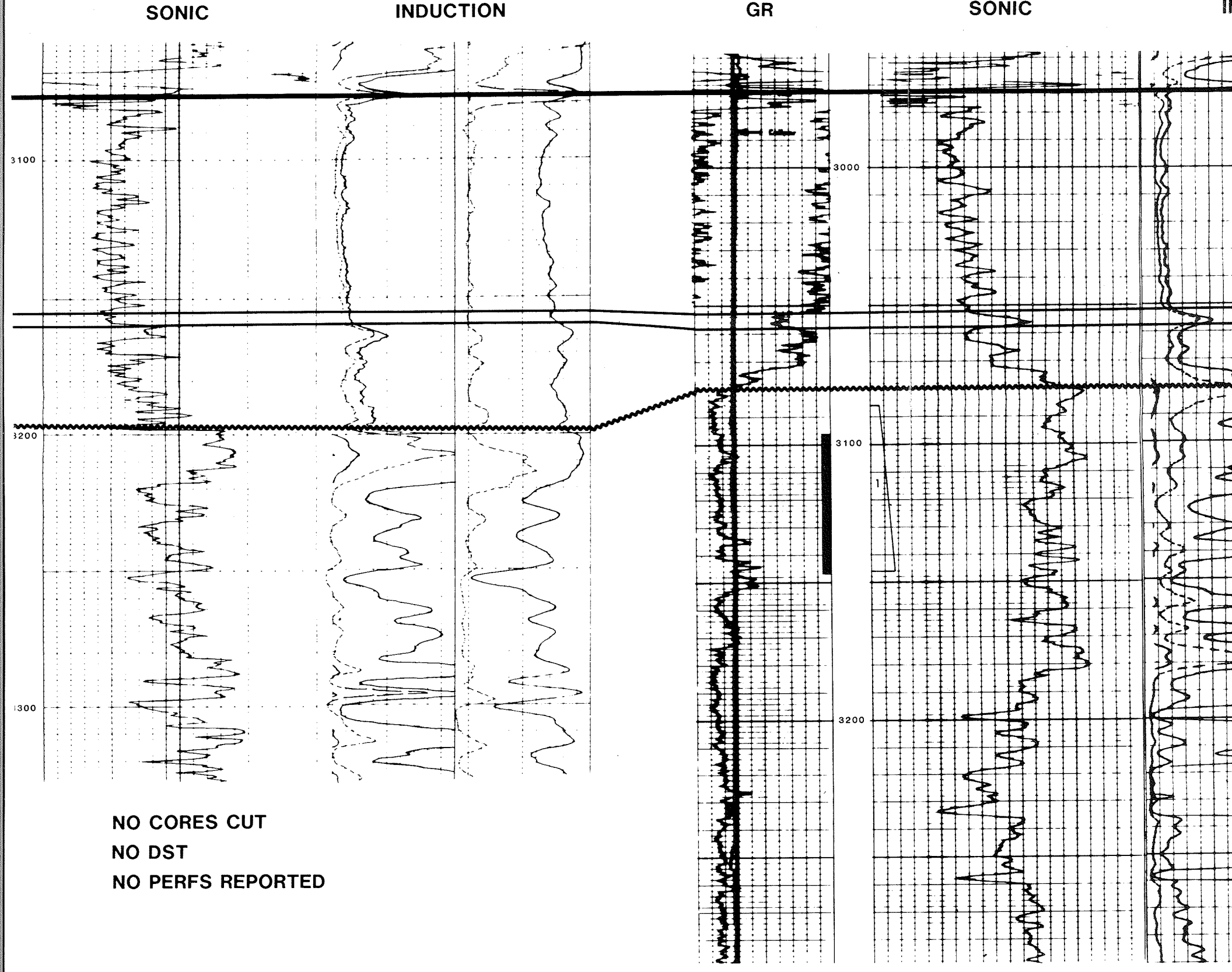

NO CORES CUT
NO DST
NO PERFS REPORTED

DST #1. 3086-3146 ft.: 60 ft. MUD, 220 ft. WT
NO PERFS REPORTED

TER

K.R. CANSO N. COULTER
15-27-2-27W1

3.3mi
5.3Km

KB: 452.6m
TD: 953.4m

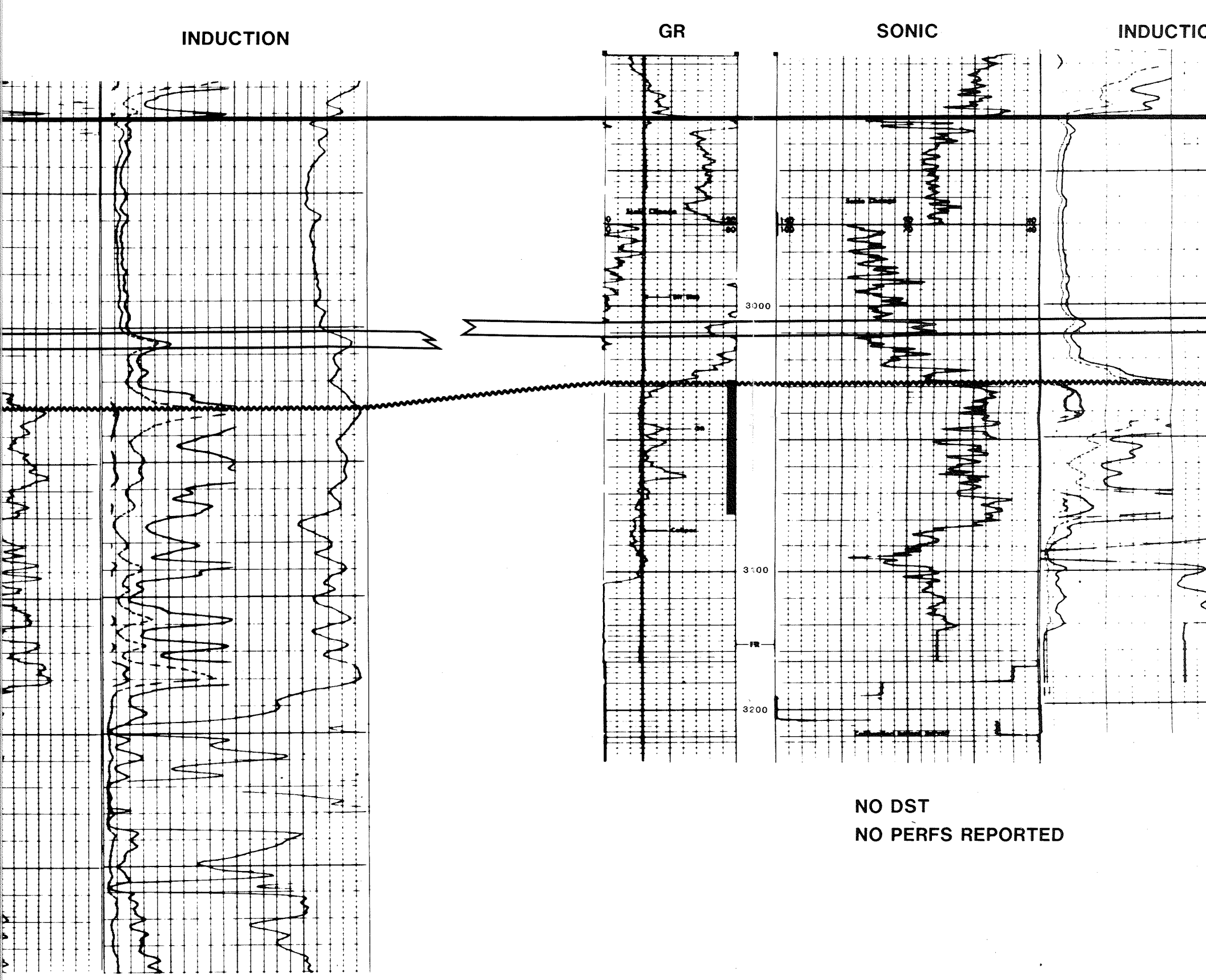

NO DST
NO PERFS REPORTED

ft. MUD, 220 ft. WTR. CUT MUD

CHAUVCO ET AL N. DALNY
13-32-2-26W1

3.7mi
6Km

1982

KB: 451.3m

TD: 943.0m

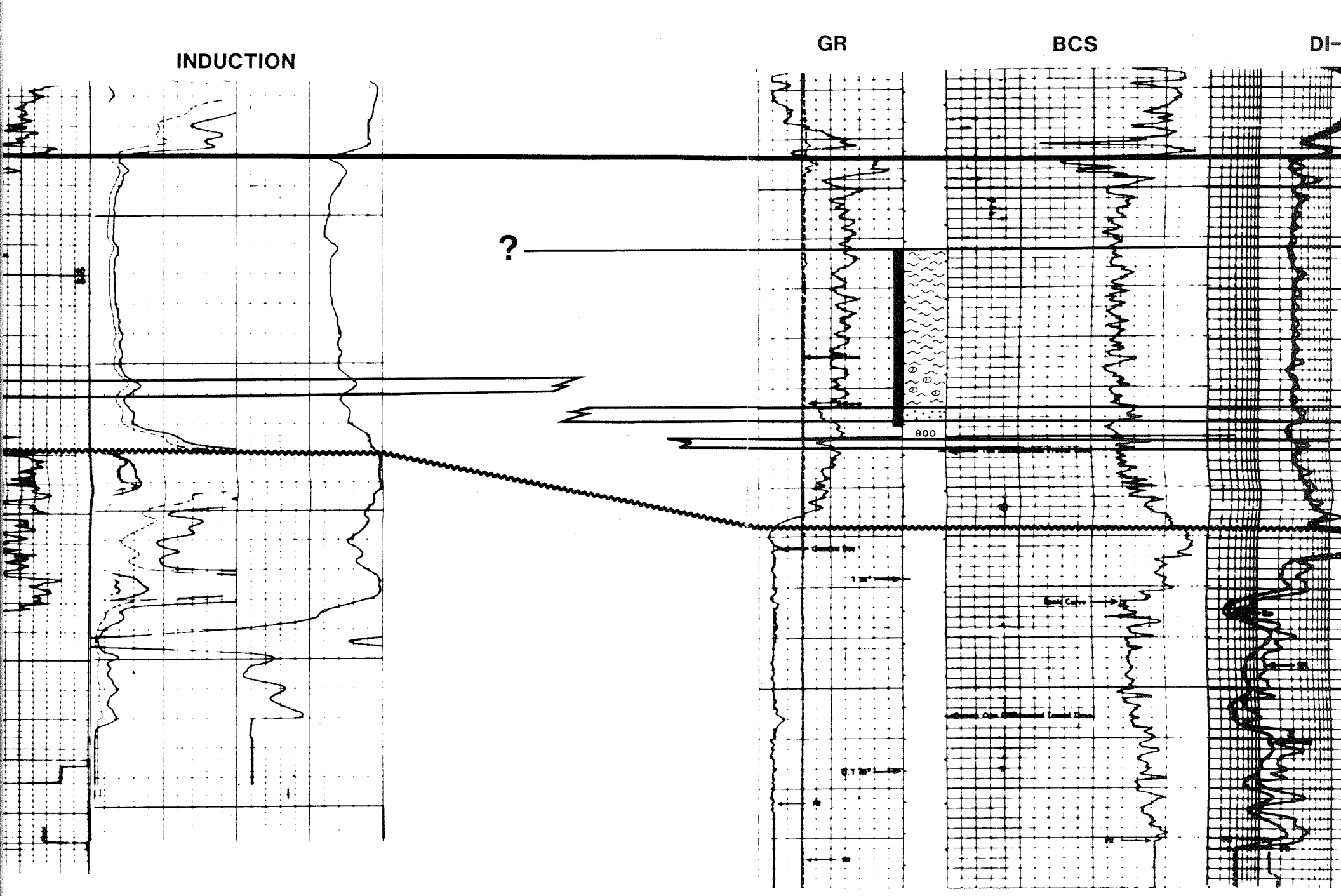

REPORTED

NO DST

NO PERFS RECORDED

6.9mi
11Km

DI-SFL

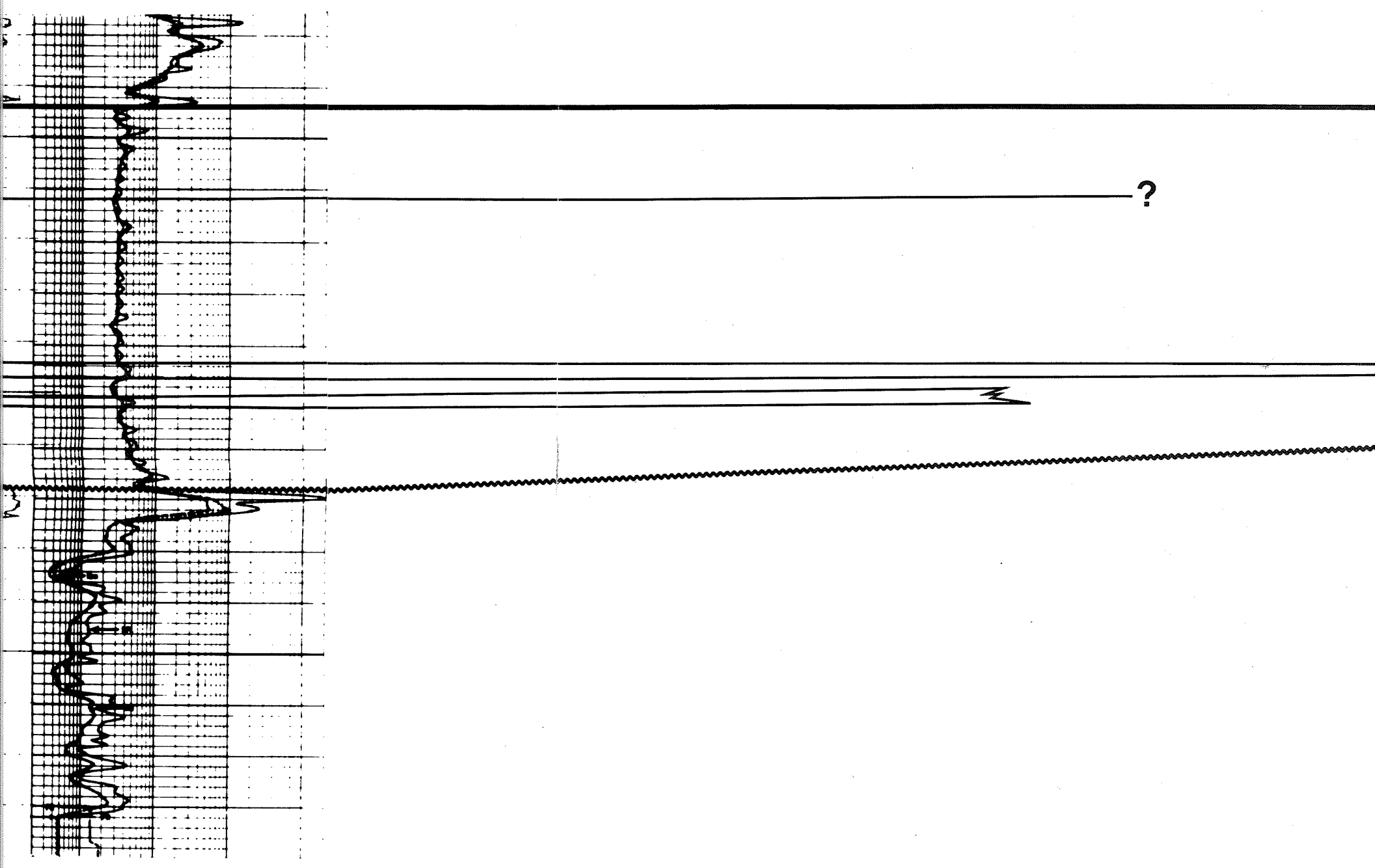

ORDED

L L & E WASKADA
15-20-3-25W1

1970

KB: 468.9m

TD: 1478.0m

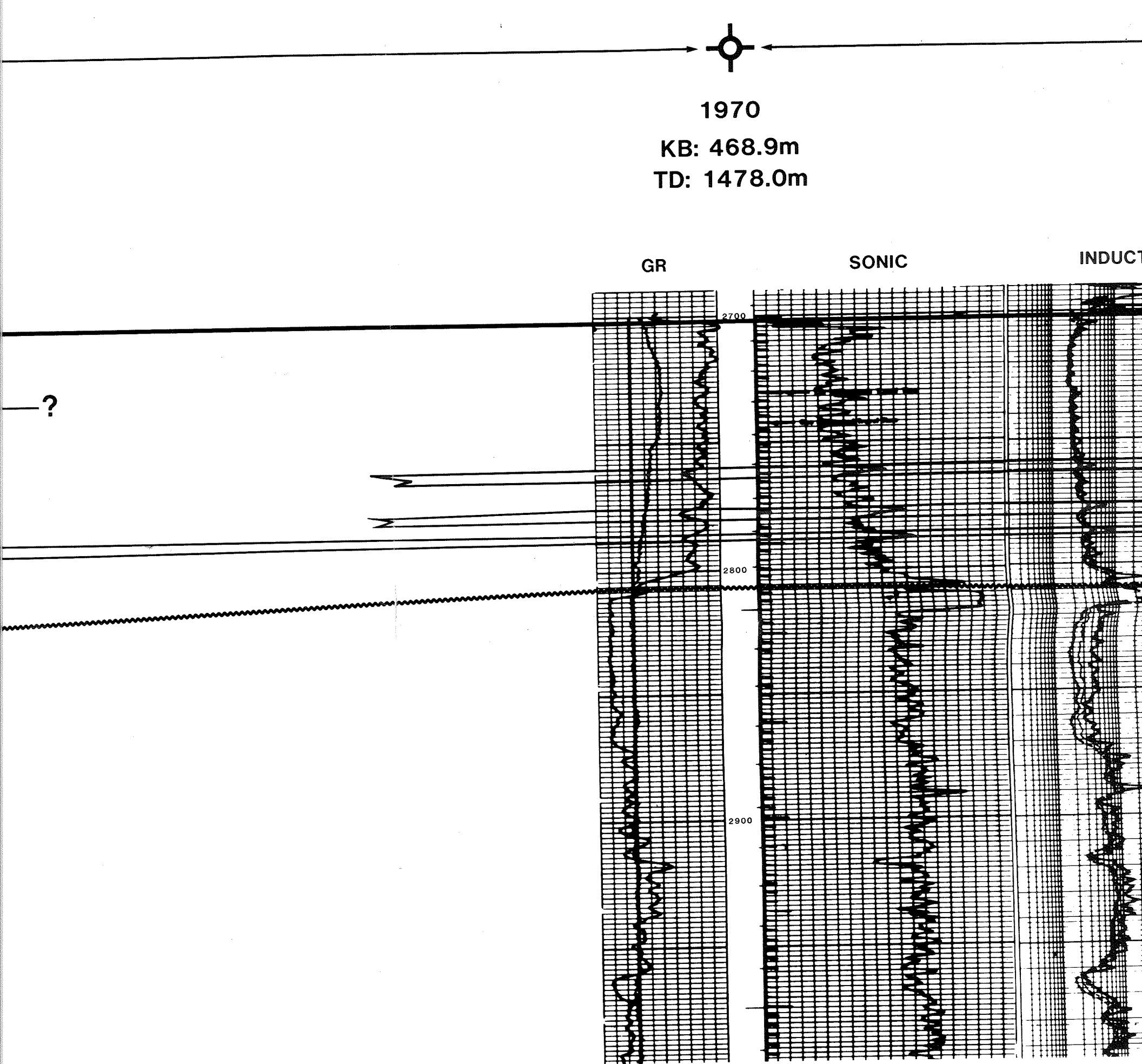

DST #1. 4200-4240 ft. : 940 ft. S. WTR.
#2. 3709-3736 ft. : 20 ft. MUD

NO PERFS REPORTED

NO CORE CUT

BARRON KIDD SAMBROOK
15-25-3-25W1

4.2mi
6.8Km

1961
KB: 475.2m
TD: 857.1m

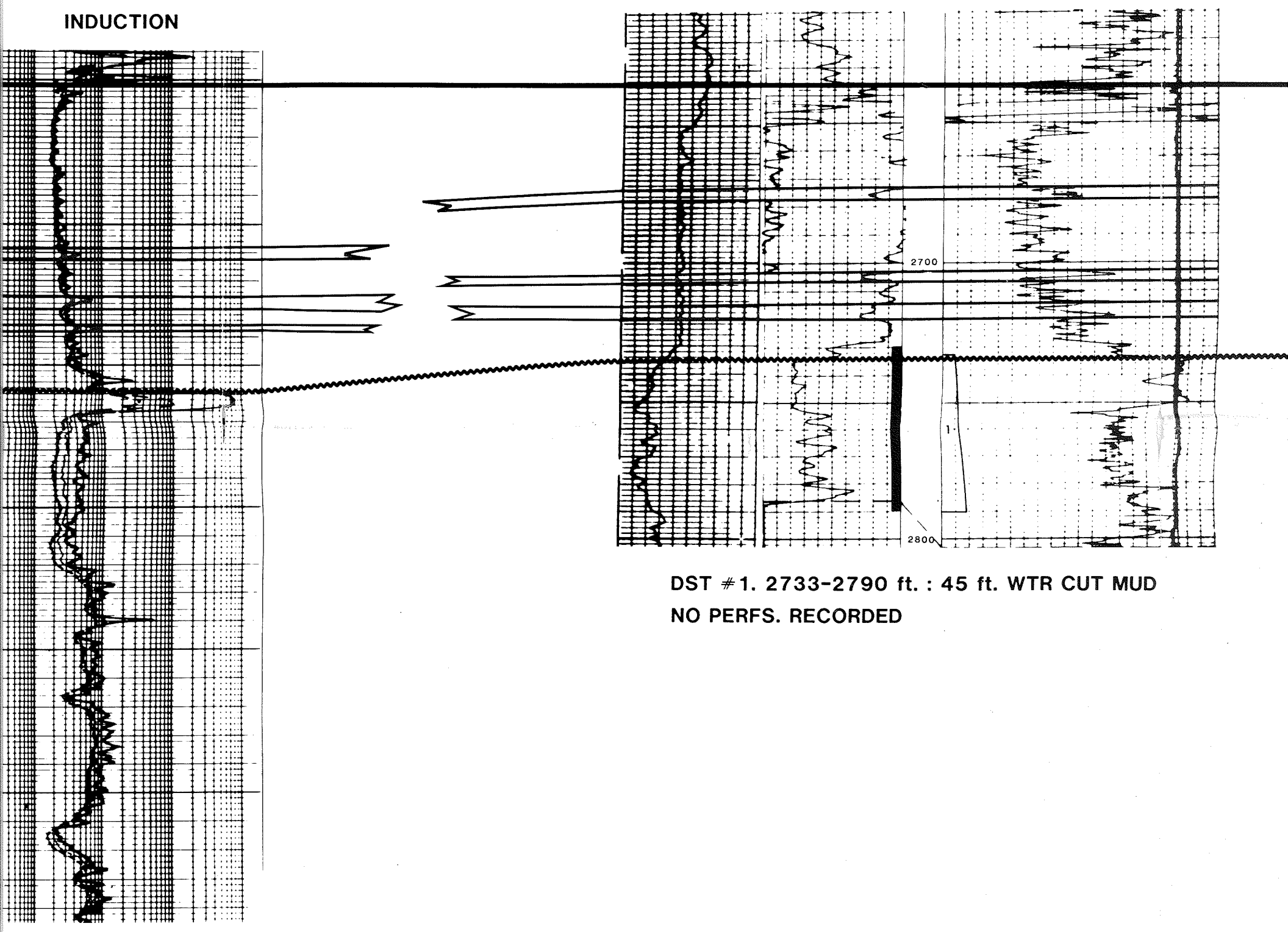

DST #1. 2733-2790 ft. : 45 ft. WTR CUT MUD
NO PERFS. RECORDED

ft. S. WTR.
t. MUD

STI

FIGU
B. HA

ON KIDD SAMBROOK
15-25-3-25W1

A′

NE

1961
KB: 475.2m
TD: 857.1m

GR SONIC

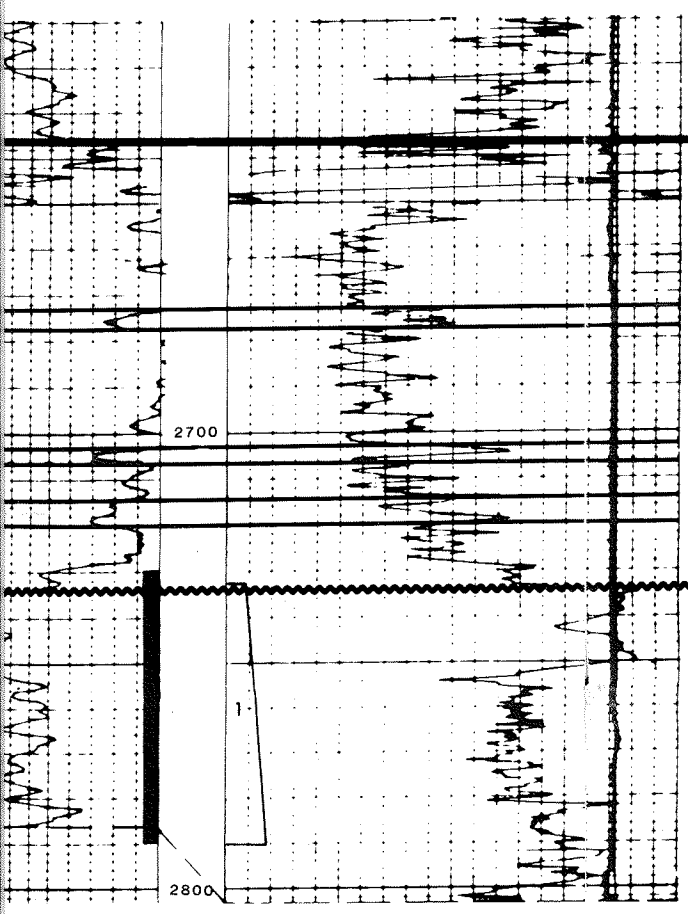

DATUM: TOP
LOWER AMARANTH

PALEOZOIC EROSIONAL
SURFACE

33-2790 ft. : 45 ft. WTR CUT MUD
RECORDED

LITHOLOGY

- REDDISH-BROWN MUDSTONE (LITHOFACES A)
- SILTSTONE (LITHOFACIES B)
- REDDISH-BROWN-WAVY-CONTORTED INTERLAMINATED MUDSTONE/SILTSTONE/SUBARKOSE (LITHOFACIES D)
- MASSIVE TO BEDDED FINE TO MEDIUM GRAINED SILTY SUBARKOSE (LITHOFACIES C,E)
- COARSE GRAINED LITHARENITE (LITHOFACIES F)
- ANHYDRITIC
- NODULAR ANHYDRITE
- MASSIVE ANHYDRITE
- LIMESTONE
- D — DETRITAL ZONE

STRATIGRAPHIC CROSS-SECTION A-A′
LYLETON-NAPINKA
SOUTHWESTERN MANITOBA

FIGURE: 13

B. HANSEN

JUNE, 1986

C

N

SASKO ET AL SOUTH MELITA
12-12-3-27W1

KB: 457.3m

TD: 939m

SP GR BCS

DATUM: TOP

LOWER AMARANTH

PALEOZOIC EROSIONAL

SURFACE

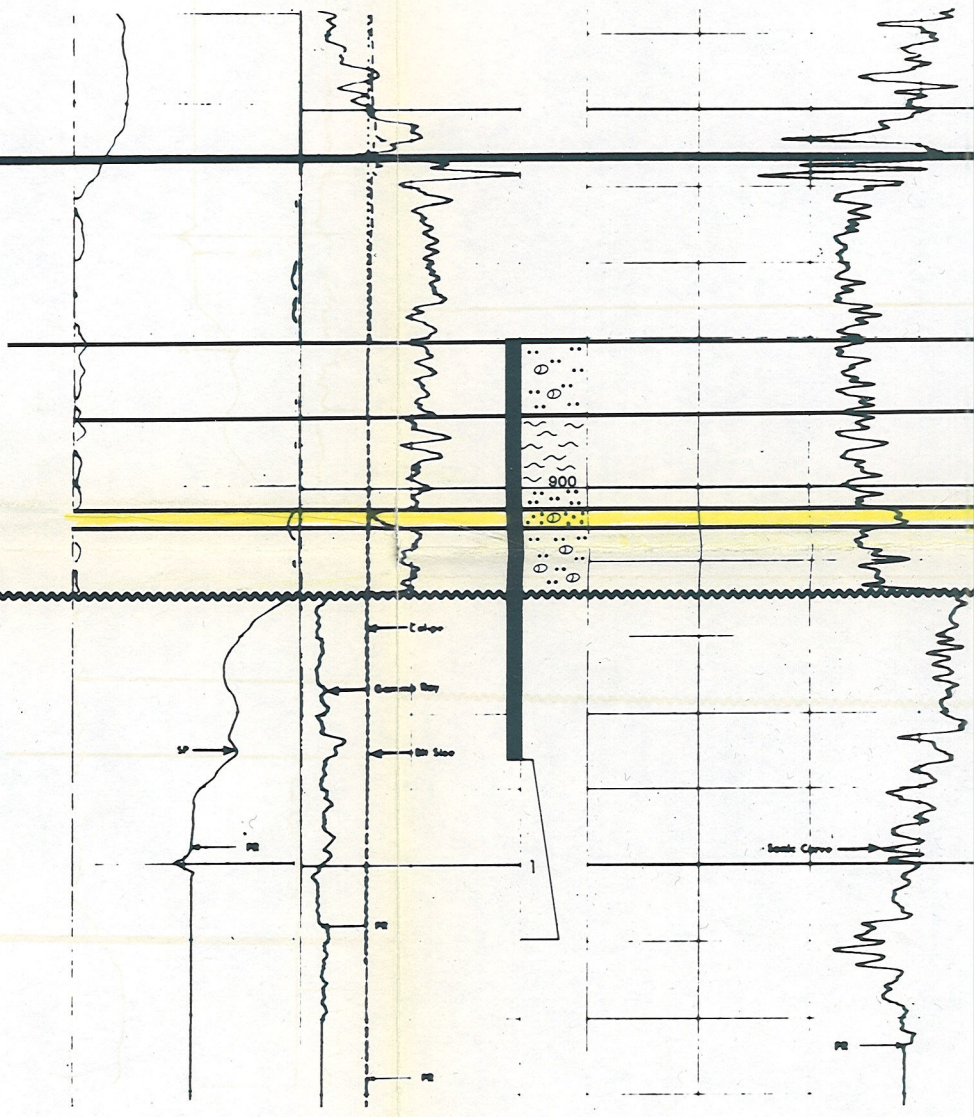

DST #1 : 918-923m : 27

NO PERFS RECORDED

.ITA

3.7mi
6.0Km

CHAUVCO ET AL N. DALNY
13-32-2-26W1

KB: 451.3m

TD: 943.0m

DI-SFL

GR

BCS

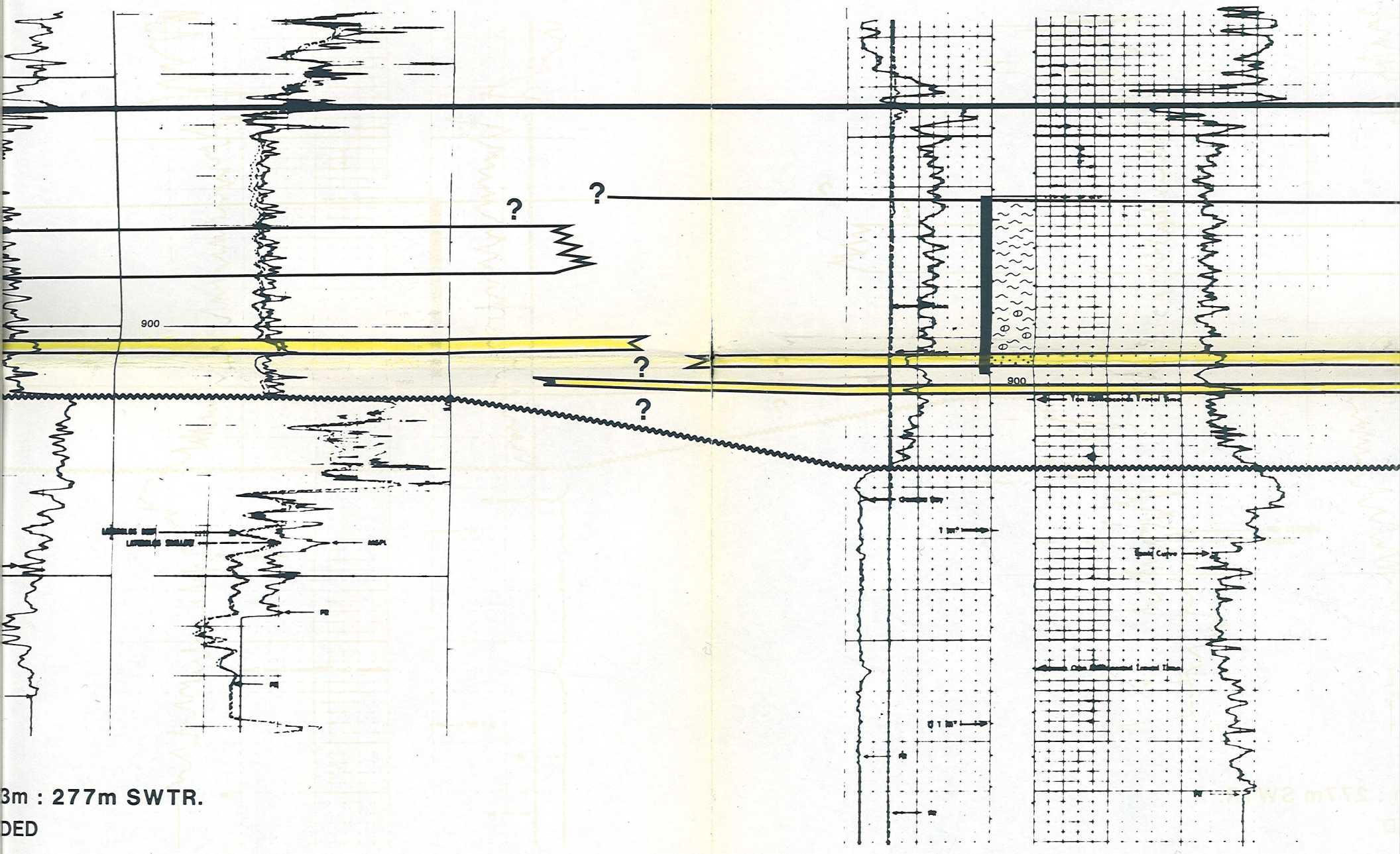

3m : 277m SWTR.

DED

NO DST

NO PERFS LISTED

OMEGA WASKADA PROV

3-14-2-26W1

5.0mi
8.0Km

1982

KB: 471.3m

TD: 955.0m

GR BCS

?

900

950

NO DST

ROXY-ANDEX ET AL WASKADA
16-1-2-26W1

2.0mi
3.2Km

2.1mi
3.4Km

1982

KB: 474.1m

TD: 975m

GR BCS

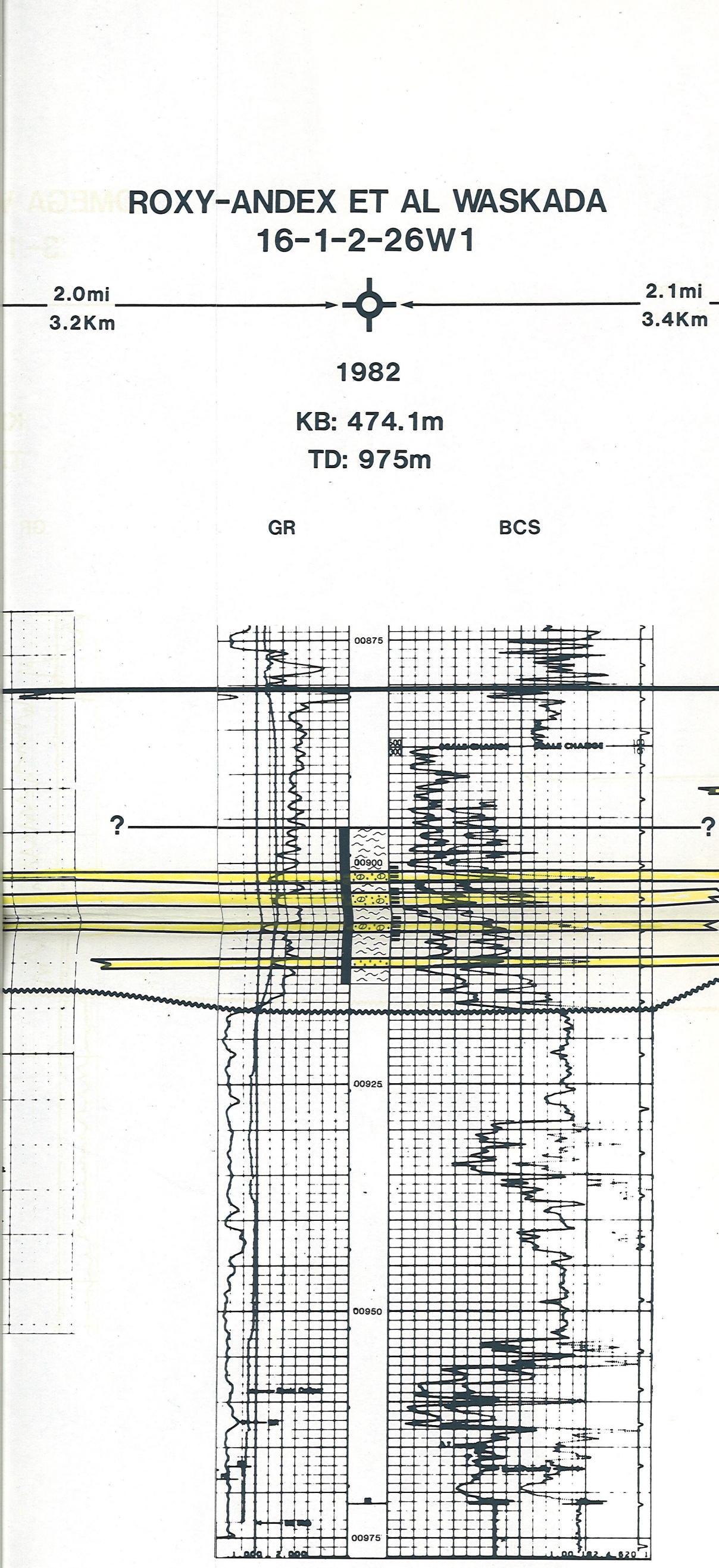

NO DST

OMEGA WASKADA
14-25-1-26W1

1.2mi
1.9Km

1982

KB: 471.2

TD: 936m

GR BCS

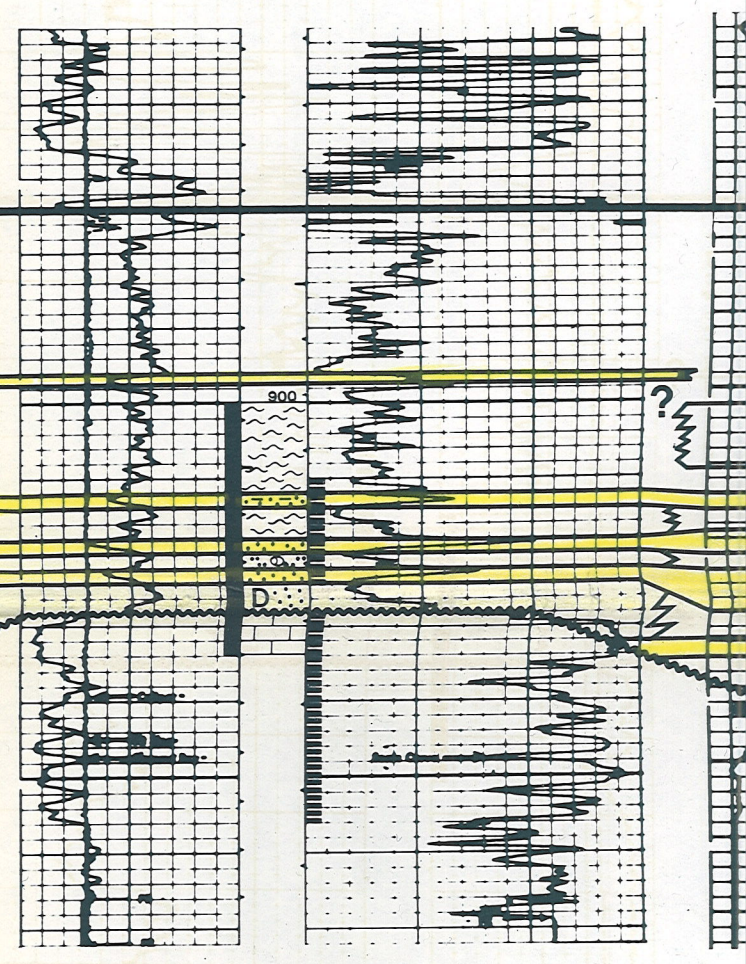

NO DST

OMEGA WASKADA
11-24-1-26W1

1.6mi
2.6Km

1982

KB: 469.8m

TD: 935m

GR BCS

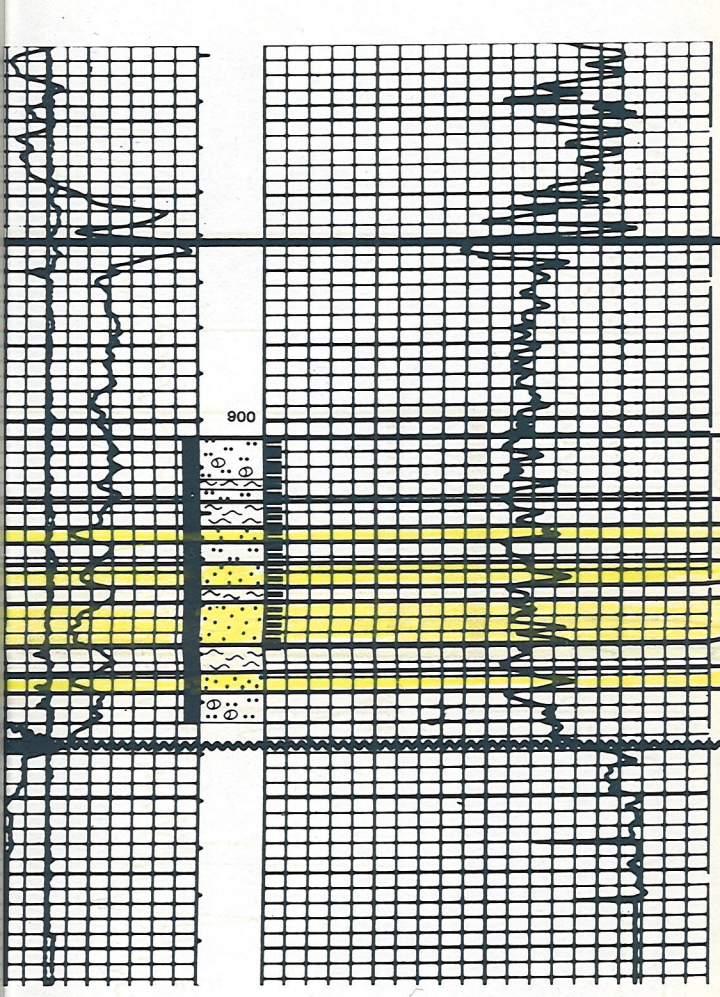

NO DST

OMEGA SOUTH WASKADA
1-13-1-26W1

1.5mi
2.4Km

1982

KB: 470.4m

TD: 945m

GR BCS

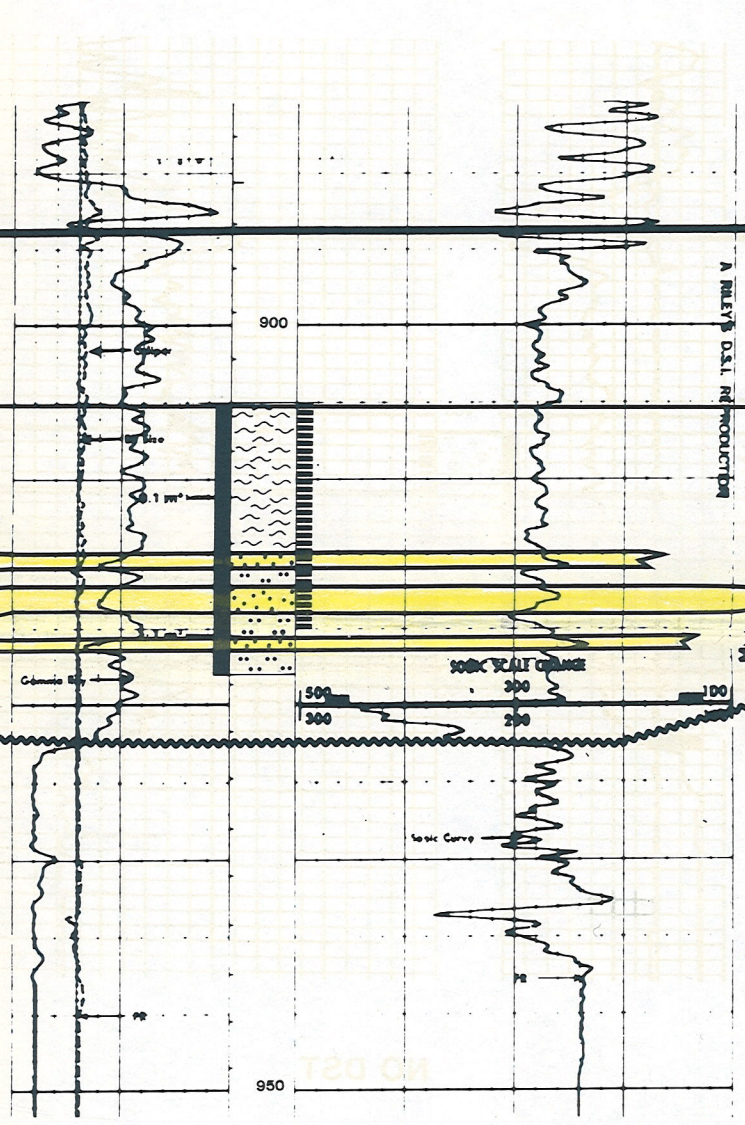

NO DST

CHEVRON WASKADA
9-1-1-26W1

KB: 466.7m

TD: 962m

GR BCS

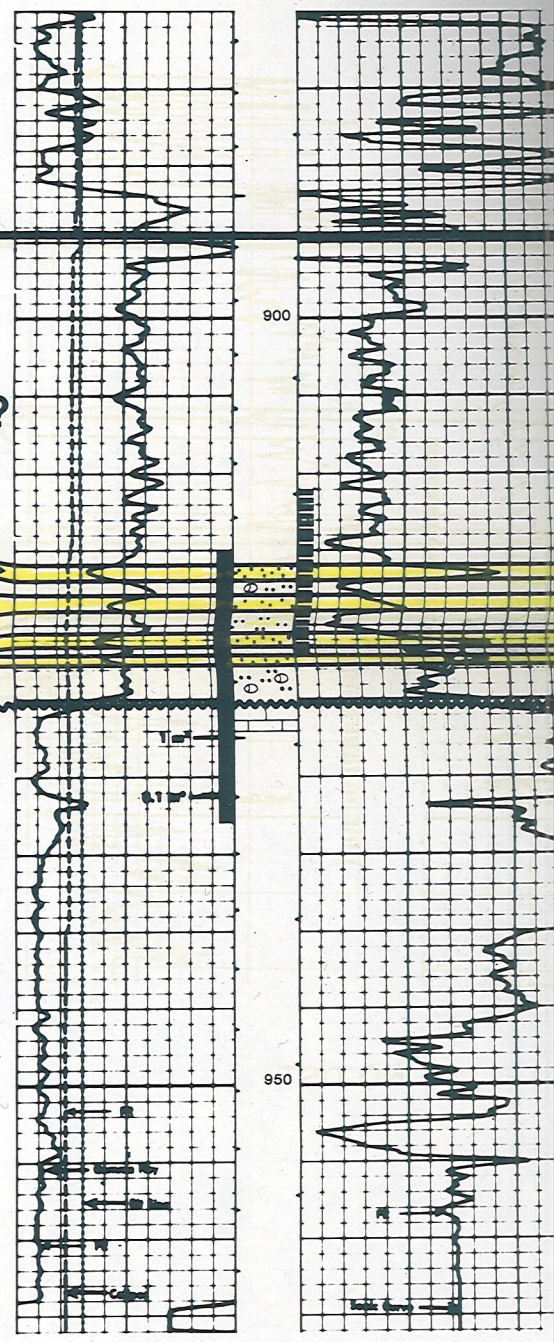

NO DST

RON WASKADA
-1-1-26W1

KB: 466.7m

TD: 962m

BCS

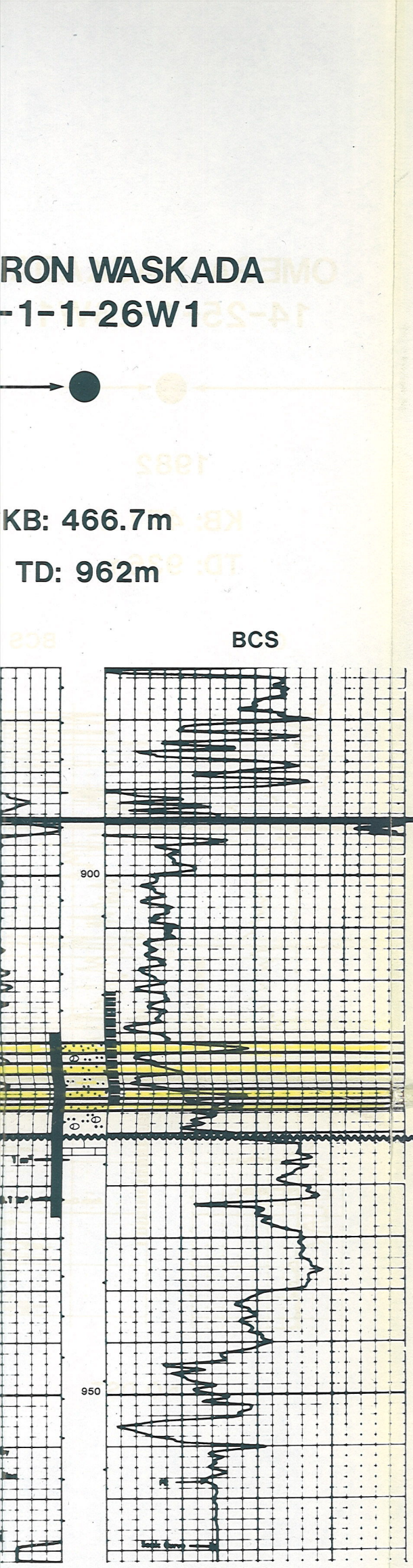

NO DST

C′

S

DATUM: TOP
LOWER AMARANTH

PALEOZOIC EROSIONAL
SURFACE

LITHOLOGY

- REDDISH-BROWN MUDSTONE (LITHOFACES A)
- SILTSTONE (LITHOFACIES B)
- REDDISH-BROWN-WAVY-CONTORTED INTERLAMINATED MUDSTONE/SILTSTONE/SUBARKOSE (LITHOFACIES D)
- MASSIVE TO BEDDED FINE TO MEDIUM GRAINED SILTY SUBARKOSE (LITHOFACIES C,E)
- COARSE GRAINED LITHARENITE (LITHOFACIES F)
- ANHYDRITIC
- NODULAR ANHYDRITE
- MASSIVE ANHYDRITE
- LIMESTONE
- D — DETRITAL ZONE

STRATIGRAPHIC CROSS-SECTION C-C′
MELITA-WASKADA
SOUTHWESTERN MANITOBA

FIGURE: 15

B. HANSEN

JUNE, 1986

D
W

ANGLO ET

TOP
LOWER AMARANTH

DATUM:
515m SUBSEA

PALEOZOIC EROSIONAL
SURFACE

SOURIS VALLEY W ICKS

-8-3-29W1

2.1mi
3.4km

1955

KB: 484.2m

D: 1122.4m

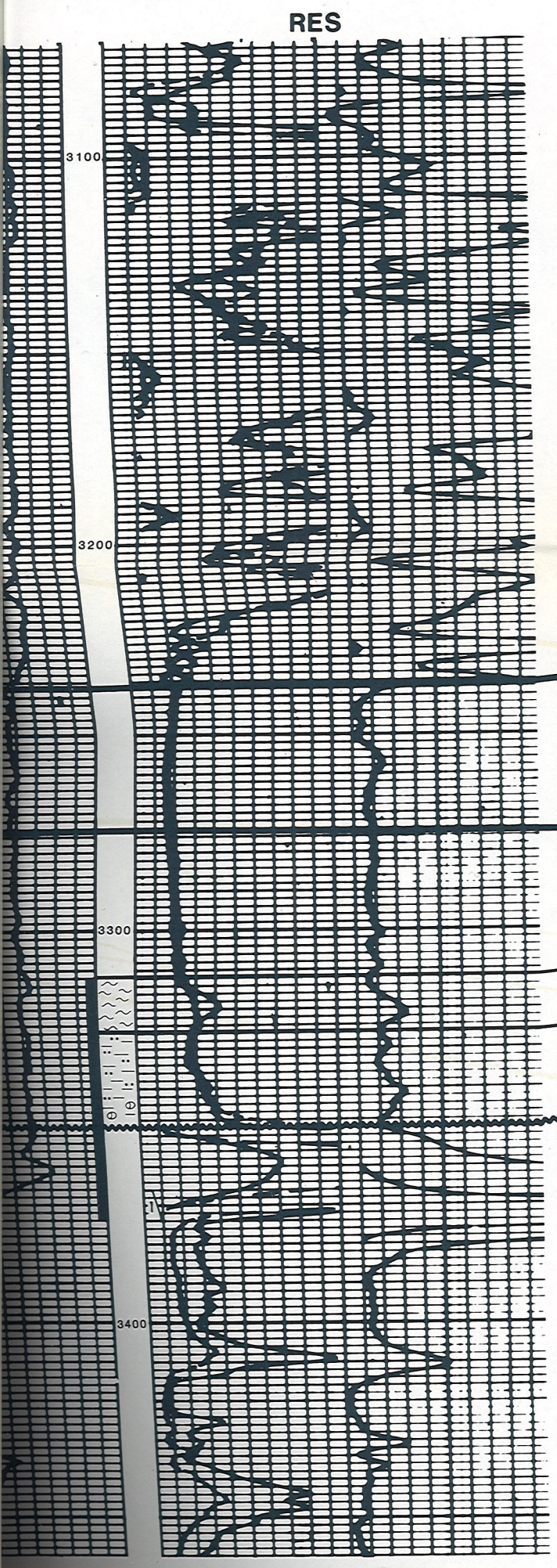

DST #1. 25 ft. GASSY SALT WATER

NO PERFS RECORDED

SWEETGRASS PIERSON
9-10-3-29W1

1956

KB: 478.2m

TD: 1011.3m

0.8mi
1.3km

CALSTAN PIERSON PROV.
10-11-3-29W 1

1977

KB: 475.5m

TD: 1016m

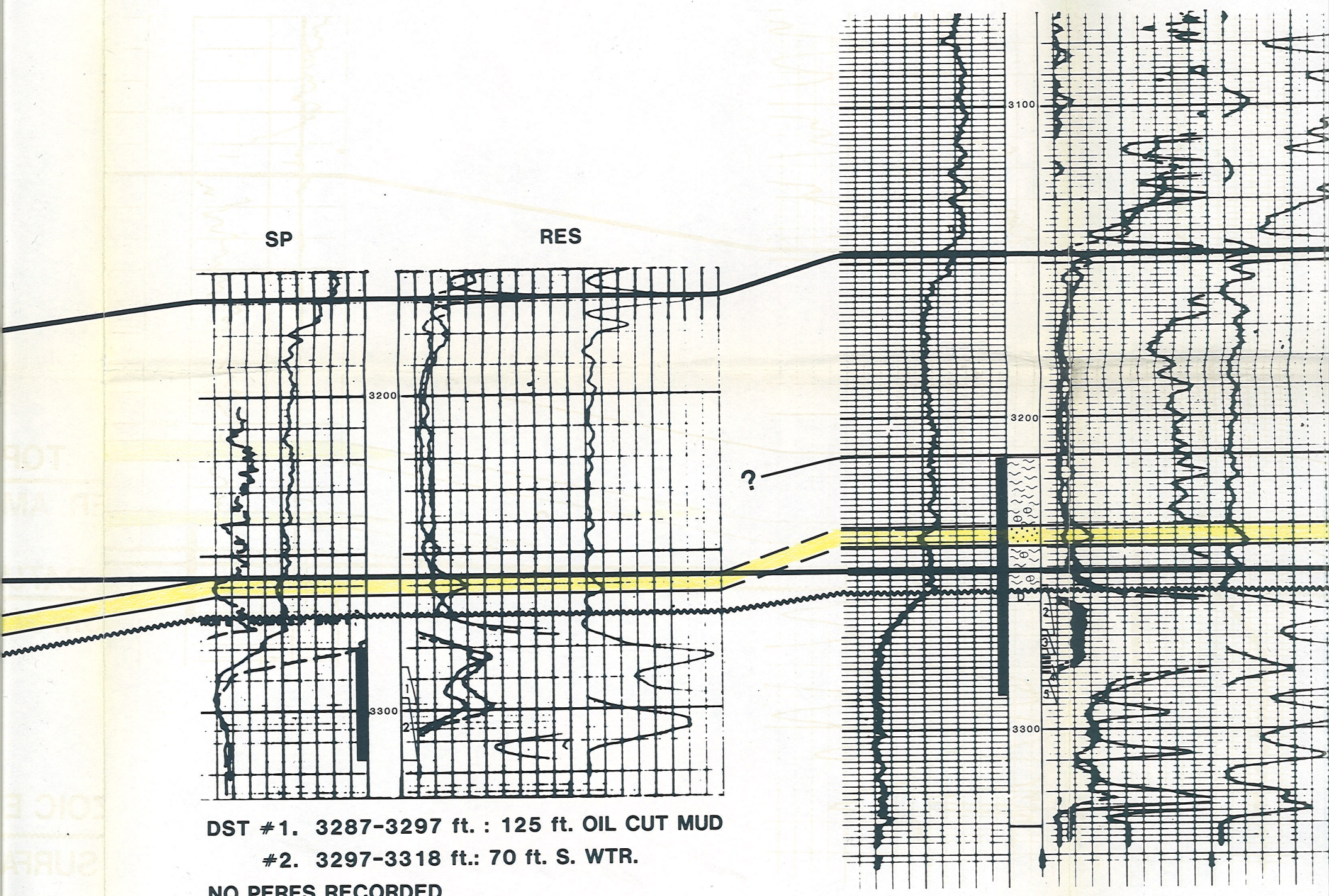

DST #1. 3287-3297 ft. : 125 ft. OIL CUT MUD

#2. 3297-3318 ft.: 70 ft. S. WTR.

NO PERFS RECORDED

DST #2. 3256-3270 ft. : 40 ft. OIL FLK. M

#3. 3270-3275ft. : 10 ft. MUD

#4. 3275.6-3285 ft. : 375 ft. OIL,
45 ft. SALT WTR.

#5. 3285-3290 ft. : 90 ft. MUD
60 ft. SALT WTR.

COPPERHEAD MMR PIERSON
2-13-3-29W 1

1.1mi
1.8km

1.5mi
2.4km

1977

KB: 473.7m

TD: 994.0m

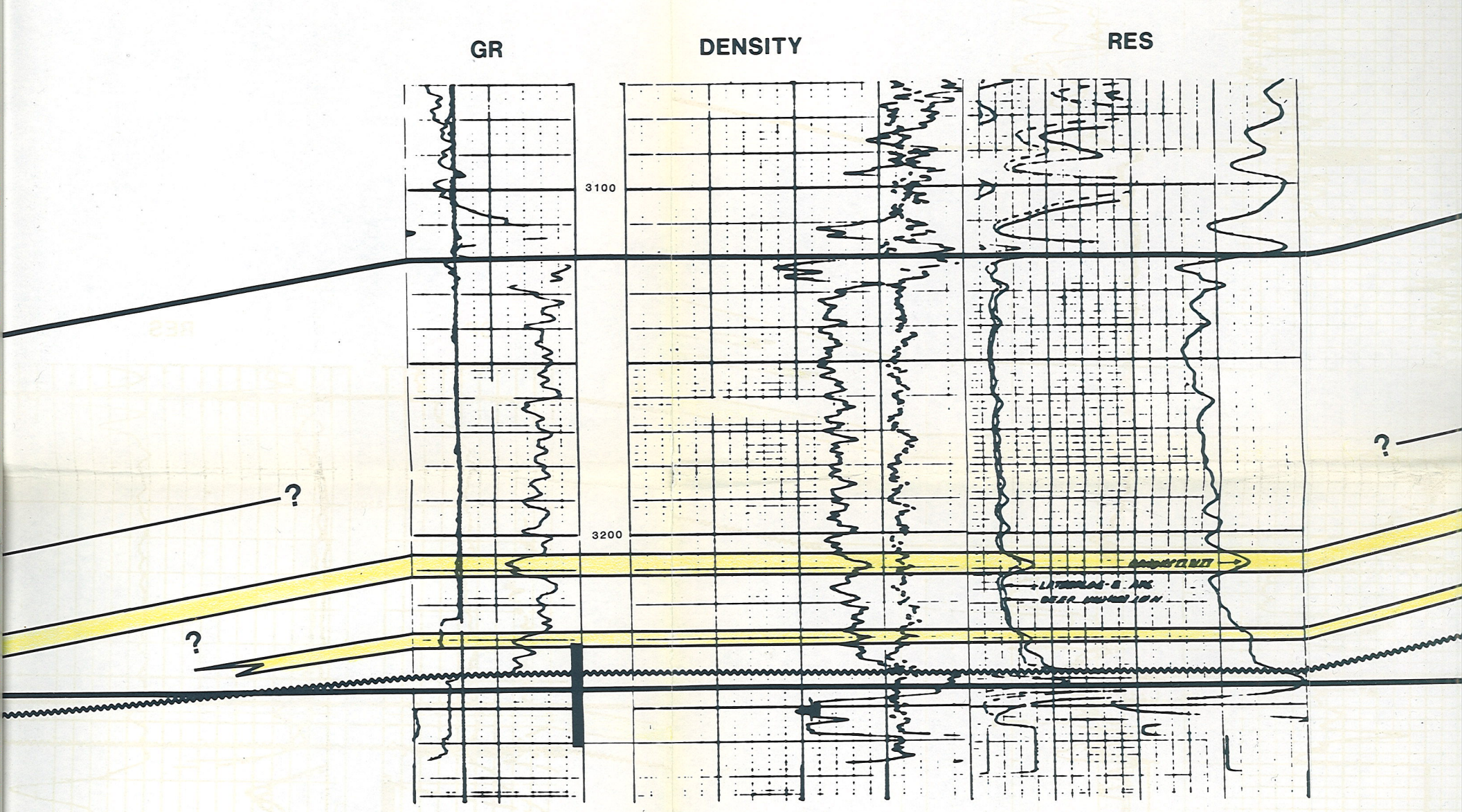

NO DST

NO PERFS RECORDED

TUNDRA ET AL PIERSON
16-18-3-28W1

1.4mi
2.3km

TACOMA
4A-2

KB: 472.8m
TD: 1007m

KB:
TD:

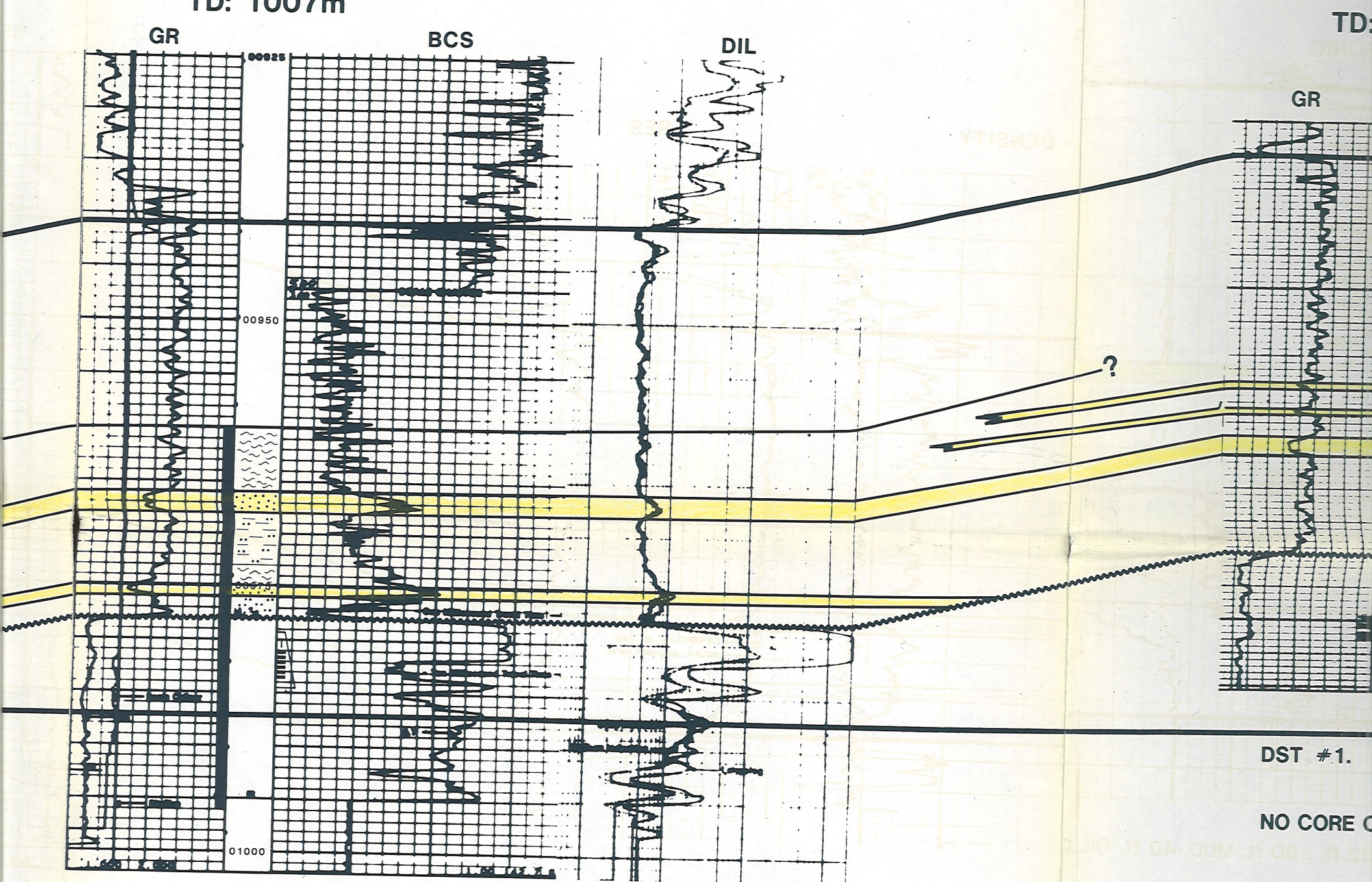

DST #1.

NO CORE C

DST #1. 980-984m : 5 m OIL CUT MUD,
19m GASSY MUD CUT OIL,
43m CLEAN GASSY OIL,
38m SLIGHTLY MUD CUT OIL.

QUEST PIERSON
4A-22-3-28W1

KB: 469.2m
TD: 1014m

SP | RES

950

1000

DST #1. 966-979.5m : 28m OIL CUT MUD.

0.6mi
1.0km

K.R. CANSO EAST PIERSON
2-22-3-28W1

1965

KB: 471.5m
TD: 987.9m

GR | SONIC | RES

3100

3200

DST #1. 3168-3182 ft. : 80 ft. MUD, 40 ft. OIL CUT MUD.

NO PERFS RECORDED

RED MUD (LIT

SILT (LIT

RED INT MUD (LIT

MAS FINE SILT (LIT

PAL

STRUCTUR

SOUTH

FIGURE: 16
B. HANSEN

ST PIERSON
8W1

D´

NE

5m
0m

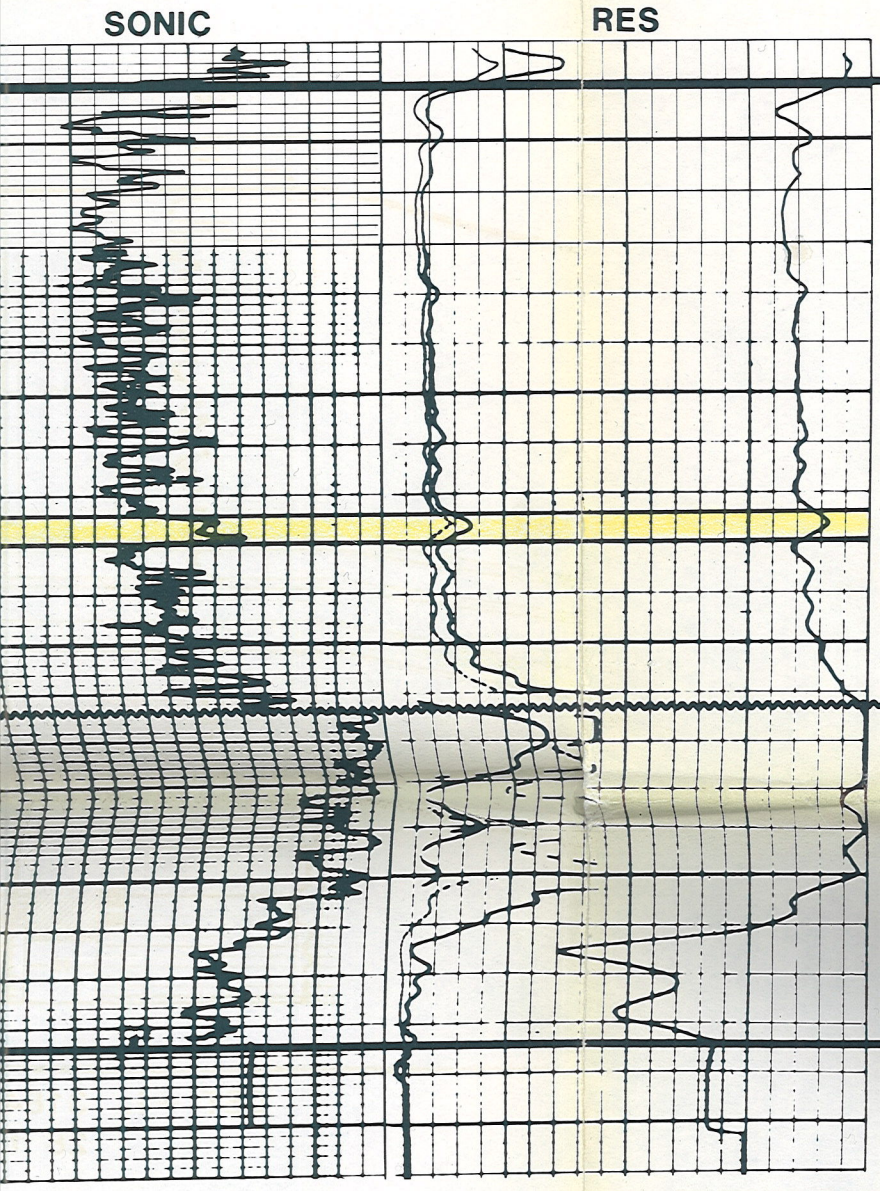

TOP
LOWER AMARANTH

PALEOZOIC EROSIONAL
SURFACE

DATUM:
515m SUBSEA

8-3182 ft. : 80 ft. MUD, 40 ft. OIL CUT MUD.

PERFS RECORDED

LITHOLOGY

- REDDISH-BROWN MUDSTONE (LITHOFACES A)
- SILTSTONE (LITHOFACIES B)
- REDDISH-BROWN-WAVY-CONTORTED INTERLAMINATED MUDSTONE/SILTSTONE/SUBARKOSE (LITHOFACIES D)
- MASSIVE TO BEDDED FINE TO MEDIUM GRAINED SILTY SUBARKOSE (LITHOFACIES C,E)
- COARSE GRAINED LITHARENITE (LITHOFACIES F)
- ANHYDRITIC
- NODULAR ANHYDRITE
- MASSIVE ANHYDRITE
- LIMESTONE
- D — DETRITAL ZONE

STRUCTURAL CROSS-SECTION D-D´
PIERSON FIELD
SOUTHWESTERN MANITOBA

FIGURE: 16

B. HANSEN

JUNE, 1986

E
N

COPPERHEAD PIERSON PROV.
4-30-3-28W1

1.5mi
2.4km

KB: 475.8m
TD: 987.7m

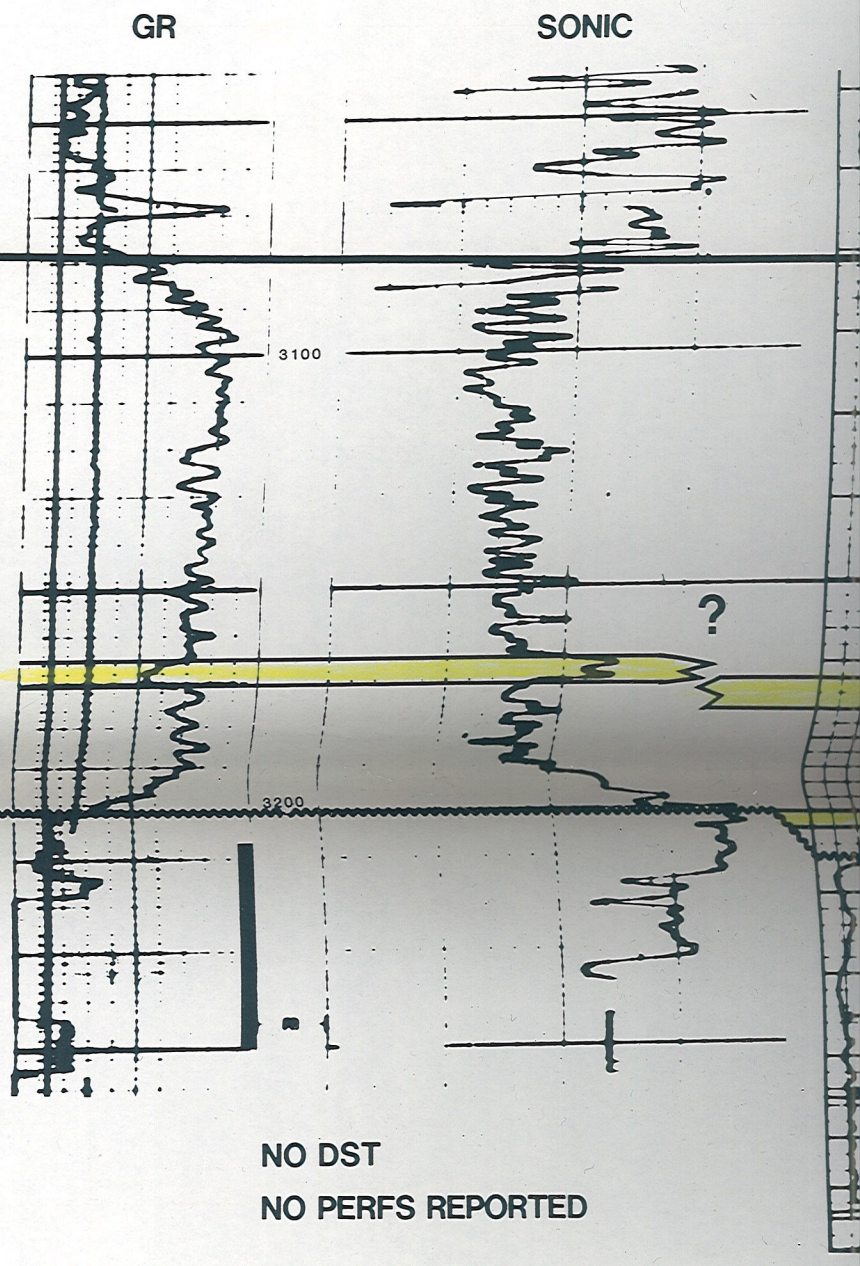

DATUM: TOP
LOWER AMARANTH

PALEOZOIC EROSIONAL
SURFACE

NO DST
NO PERFS REPORTED

ORA ET AL PIERSON
6-18-3-28W1

COLUMBIA ET AL PIERSON
10-12-3-29W1

1.8mi
2.9km

2.4mi
3.9km

1984

KB: 472.5m
TD: 1007.0m

KB: 474.9m
TD: 1036.5m

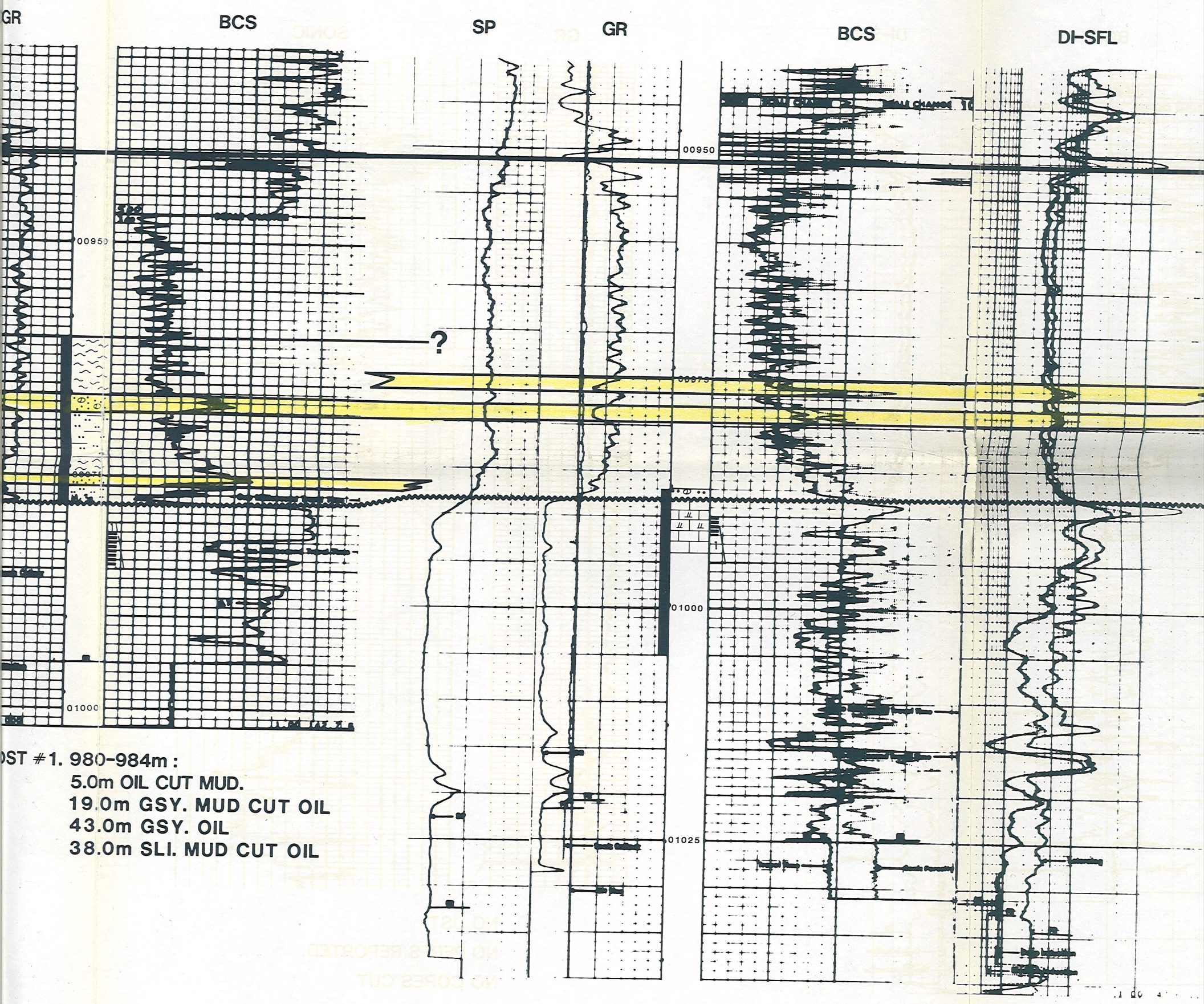

DST #1. 980-984m :
5.0m OIL CUT MUD.
19.0m GSY. MUD CUT OIL
43.0m GSY. OIL
38.0m SLI. MUD CUT OIL

DST #1. 991.5-995.5m : 531.0m OIL

CHANDLER EAST PIERSON
5-36-2-29W1

1.9mi
3.1km

KB: 468.8m
TD: 1036.6m

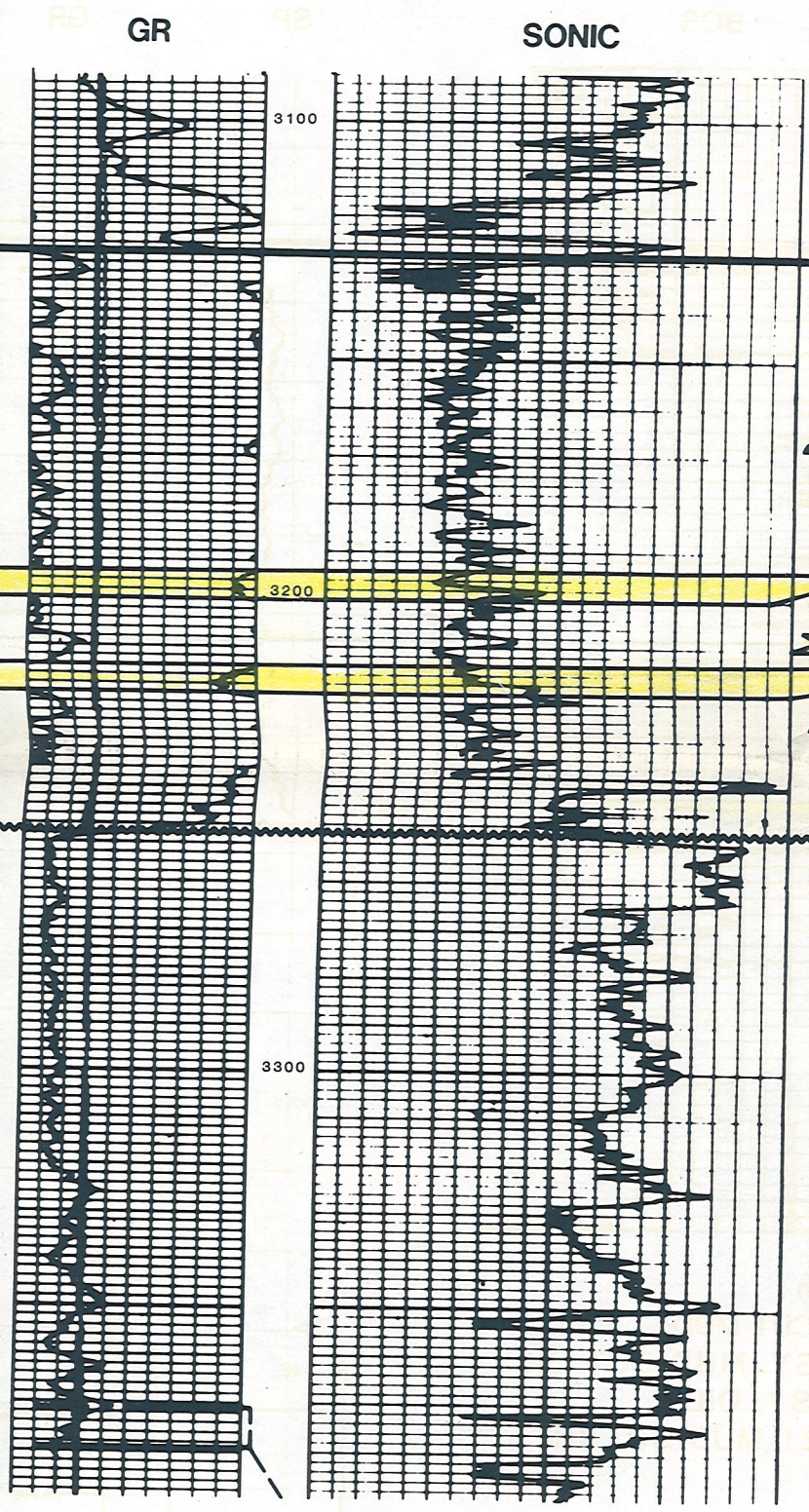

NO DST
NO PERFS REPORTED
NO CORES CUT

COBRA ET AL S. PIERSON
9-24-2-29W1

KB: 465.9m
TD: 1036.0m

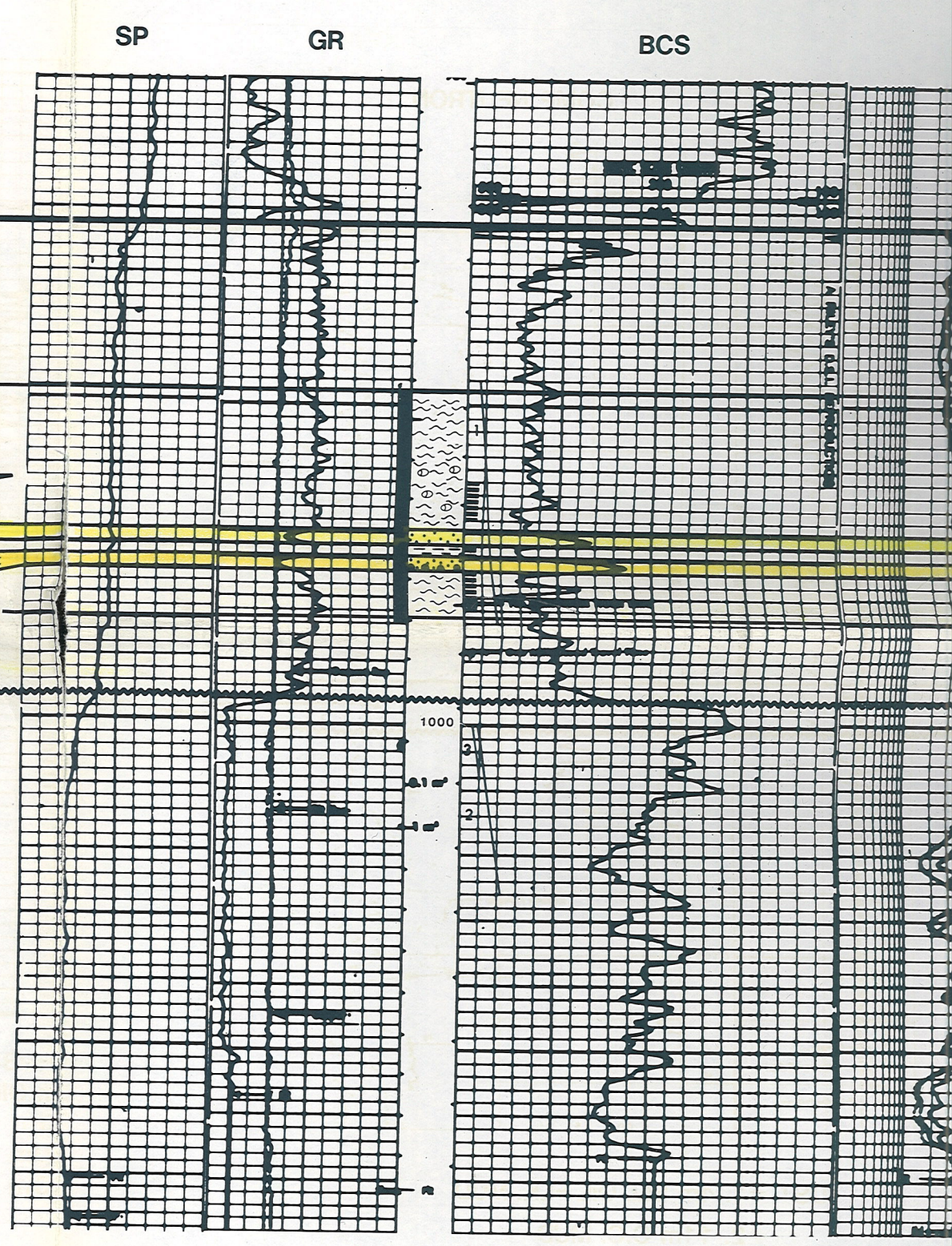

DST # 1. 973.54-992.0m R. 153m MUD, 73m GASSY OIL CUT MUD
34m VERY GASSY FROTHY MUD CUT OIL

#2. 1000-1013m R. 364m MUD, 55m GASSY SL. OIL STAINE
75m MUD CUT WTR.

#3. 1000-1004m R. 35m DRILLING MUD

COBRA SHELL LYLETON
14-5-2-28W1

2.3mi
3.7km

KB: 466.4m
TD: 1033.0m

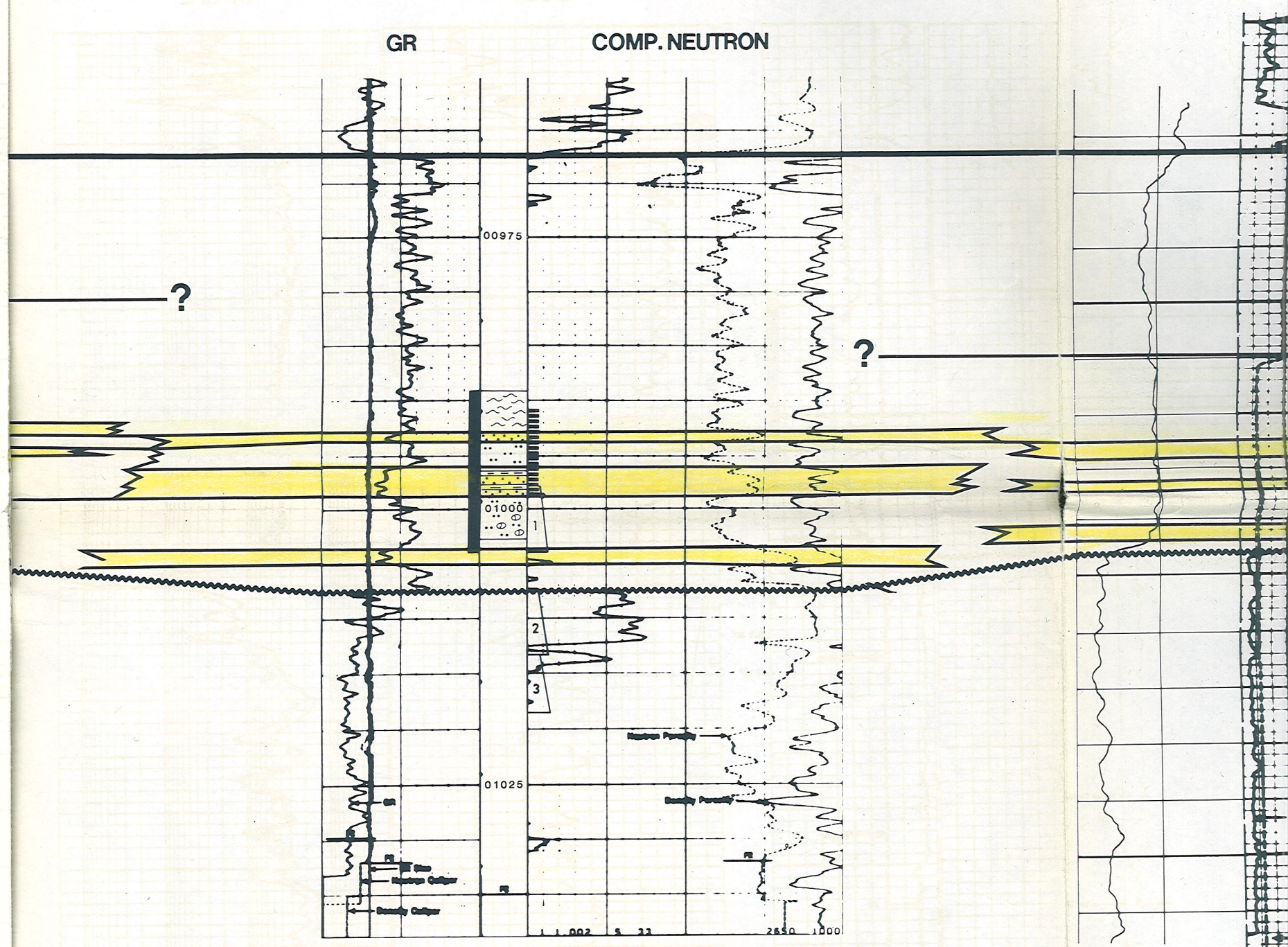

DST #1. 4m SLI. OIL FLK. MUD
#2. 11m O.C. MUD
#3. 65m GSY. OIL

PIPESTONE LYLETON
5-34-1-28W1

1.6mi
2.6km

KB: 461.3m
TD: 1035.0m

GR BCS

950

1000

NO DST

AMERAN ET AL LYLETON
15-26-1-28W1

3.0mi
4.8km

KB: 458.7m
TD: 1031.0m

GR DI-SFL

950

1000

NO DST

PE ET AL COULTER
-20-1-27W1

1.4mi
2.3km

KB: 457.69m
TD: 1017.0m

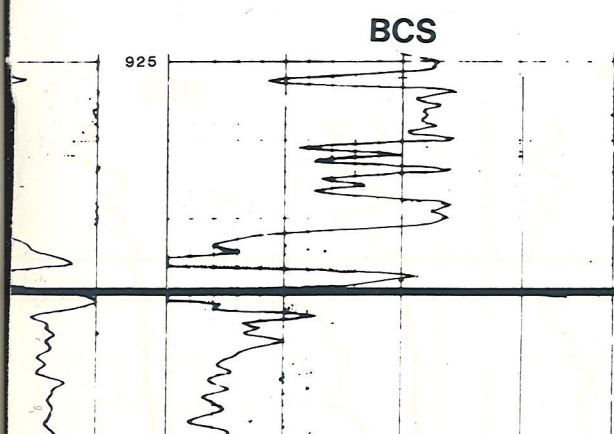

NO DST

VOYAGER BLACKROCK COULTER
5-16-1-27W1

2.9mi
4.7km

KB: 458.1m
TD: 1055.0m

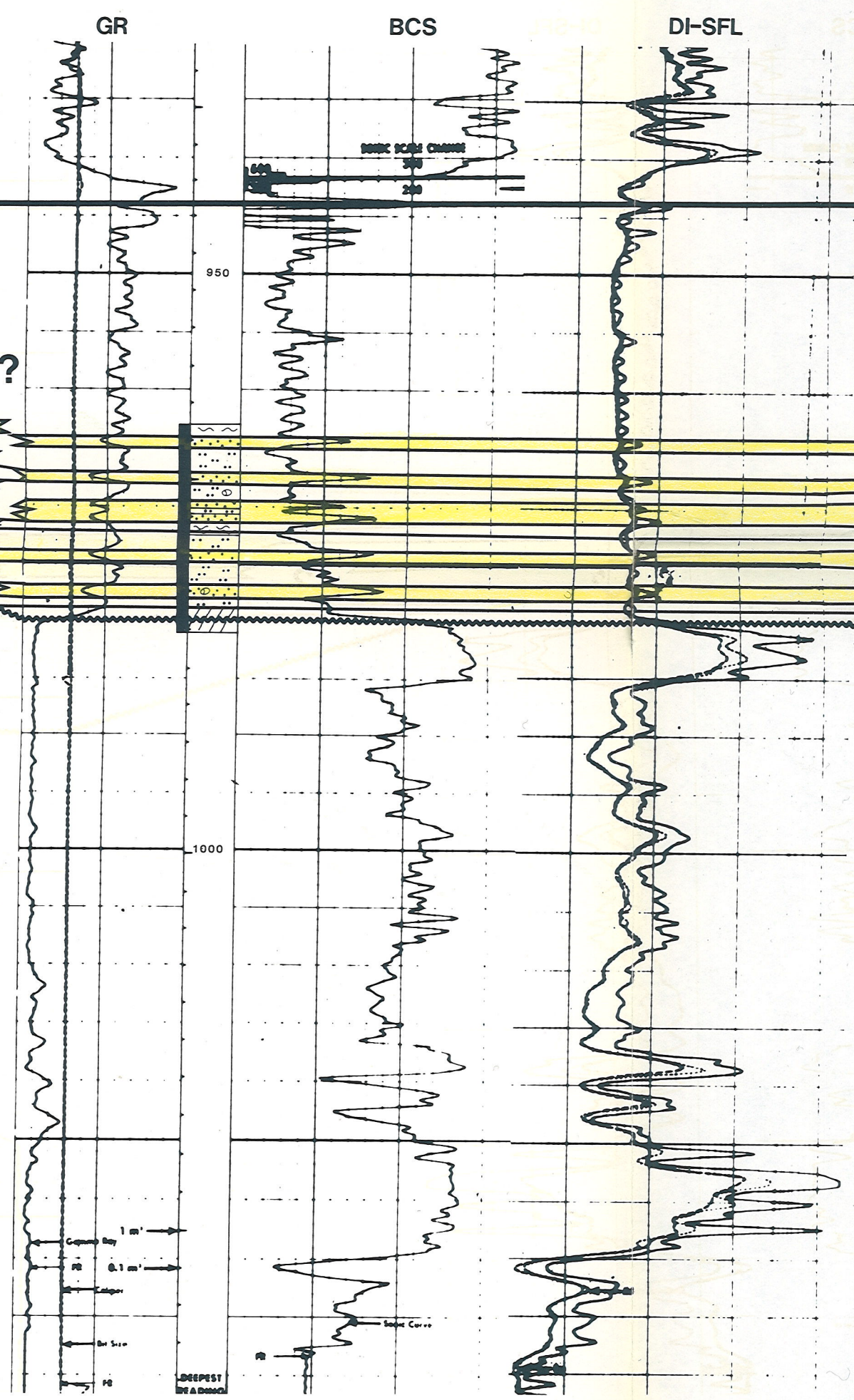

NO DST

NO PERFS REPORTED

E´
s

WARD COULTERVALE
1-3-1-27W1

KB: 455.7m
TD: 1083.6m

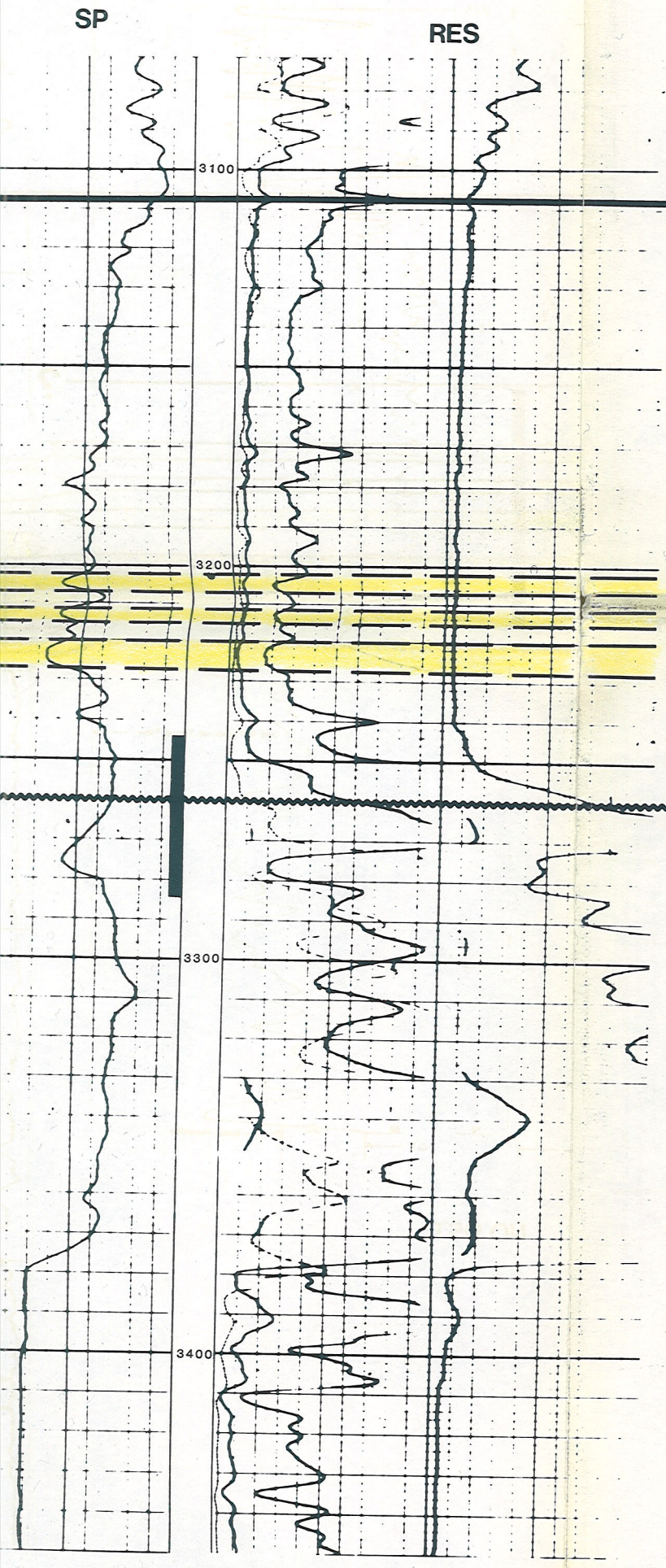

NO DST
NO PERFS REPORTED

DATUM: TOP
LOWER AMARANTH

PALEOZOIC EROSIONAL
SURFACE

LITHOLOGY

- REDDISH-BROWN MUDSTONE (LITHOFACES A)
- SILTSTONE (LITHOFACIES B)
- REDDISH-BROWN-WAVY-CONTORTED INTERLAMINATED MUDSTONE/SILTSTONE/SUBARKOSE (LITHOFACIES D)
- MASSIVE TO BEDDED FINE TO MEDIUM GRAINED SILTY SUBARKOSE (LITHOFACIES C,E)
- COARSE GRAINED LITHARENITE (LITHOFACIES F)
- ANHYDRITIC
- NODULAR ANHYDRITE
- MASSIVE ANHYDRITE
- LIMESTONE
- D — DETRITAL ZONE

STRATIGRAPHIC CROSS-SECTION E-E´
PIERSON-COULTER
SOUTHWESTERN MANITOBA

FIGURE: 17

B. HANSEN

JUNE, 1986

TER VOYAGER BLACKROCK COULTER

5-16-1-27W1

WARD

1-

1.4mi
2.3km

2.9mi
4.7km

KB: 458.1m

TD: 1055.0m

K

T

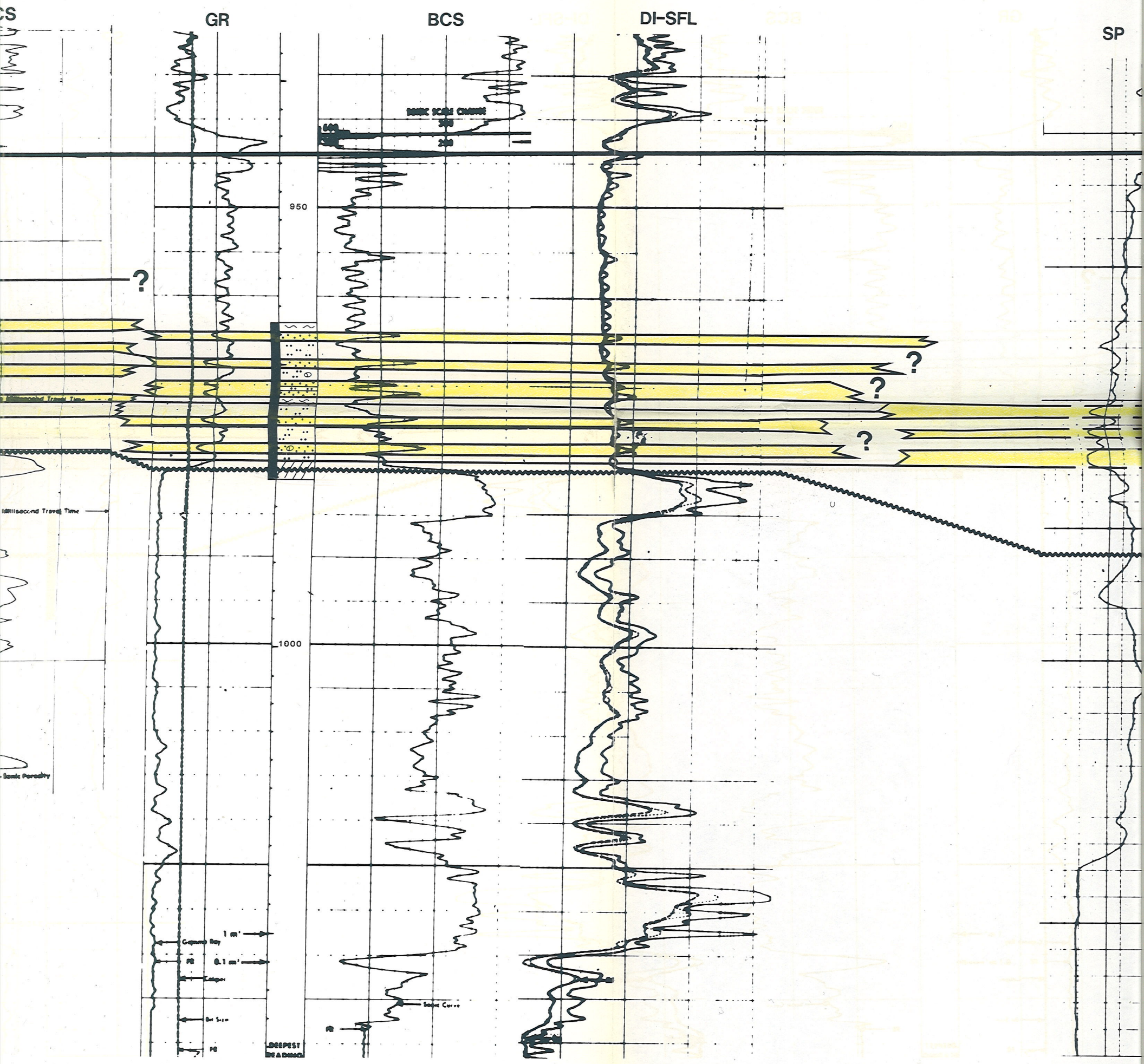

NO DST

NO PERFS REPORTED